Using Quantum Mechanics to Investigate the Location and Diffusion of Hydrogen and its Isotopes in Metals

Matthew Stephen Dyer

Peterhouse

University of Cambridge

This dissertation is submitted for the degree of Doctor of Philosophy.

Declaration

This dissertation is my own work and contains nothing which is the outcome of work done in collaboration with others, except as specified in the text and Acknowledgements.

This dissertation does not exceed 60,000 words in length.

Using Quantum Mechanics to Investigate the Location and Diffusion of Hydrogen and its Isotopes in Metals

Matthew Stephen Dyer

The wave functions and energies of hydrogen and its isotopes, deuterium and tritium, were calculated in stoichiometric palladium hydride (PdH), stoichiometric niobium hydride (NbH), lithium imide (Li_2NH) and model potentials. They were used to investigate the importance in including quantum effects in determining the location of hydrogen in these systems.

The relative stability of the two potential sites for hydrogen in palladium hydride, was found to have a large dependence on the zero point energy of the hydrogen atom. Hydrogen in lithium imide was found to be delocalised in sites around the nitrogen atom. The quantum tunnelling rate between these sites was calculated to be many times larger than the classical rate.

An expression for the diffusion coefficient in terms of the wave functions and energies of a system, derived from Kubo theory, was used to calculate the diffusion coefficients of hydrogen and its isotopes in these systems. The different processes which contribute to hydrogen diffusion were studied. It was found that it is necessary to include quantum effects when considering the diffusion of hydrogen though materials.

Processes at energies lower than the classical barrier to diffusion were found to be important in all of the systems investigated. In palladium hydride, these processes usually involved tunnelling from the octahedral to the tetrahedral site. In niobium hydride tunnelling between the ground states in neighbouring wells was found to contribute strongly to diffusion.

Calculation of the diffusion coefficient in a model system of a one-dimensional potential coupled to a harmonic oscillator showed that both coherent and incoherent tunnelling processes contributed to diffusion. Coherent processes occurred without a change in in the harmonic oscillator quantum state, whereas incoherent processes involved gaining or losing phonons during the transition.

Contents

Chapter 1

Classical and Quantum Mechanical Approaches to Calculating Diffusion Coefficients

1.1 An Introduction to Diffusion

Much of the content of this thesis concerns the phenomenon of diffusion. This section gives a brief overview of the subject, both from a classical and a quantum mechanical perspective. Hansen and McDonald's book, *Theory of Simple Liquids*[1] and Atkin's book, *Physical Chemistry*[2] have been used for reference material throughout this introduction.

From a macroscopic perspective, diffusion is observed as the transport of matter along a concentration gradient. Fick's law states that the flux of matter, $\mathbf{j}(\mathbf{r},t)$, due to diffusion is proportional to concentration gradient, $\nabla\rho(\mathbf{r},t)$, where $\rho(\mathbf{r},t)$ is the particle density at position $\mathbf{r}$ and time t.

$$\mathbf{j}(\mathbf{r},t) = -D\nabla\rho(\mathbf{r},t) \tag{1.1}$$

The constant of proportionality, D, is called the diffusion constant or diffusion coefficient. It is a measure of the rate at which matter will flow along a given concentration gradient.

The continuity equation expresses the conservation of matter during diffusion

$$\dot{\rho}(\mathbf{r},t) + \nabla.\mathbf{j}(\mathbf{r},t) = 0 \tag{1.2}$$

where $\dot{\rho} = \frac{\partial \rho}{\partial t}$. It can be combined with equation 1.1 expressing Fick's Law, to give the diffusion equation

$$\dot{\rho}\left(\mathbf{r}, t\right) = D\nabla^2 \rho\left(\mathbf{r}, t\right) \tag{1.3}$$

1.1.1 Einstein's Diffusion Coefficient

Einstein[3] showed that, in a system of diffusing independent classical particles, the solution of the diffusion equation gives the following relation for the diffusion coefficient, in terms of the mean square displacement of the particles at time, t:

$$D = \lim_{t\to\infty} \frac{1}{6t} \left\langle \left|\mathbf{r}(t) - \mathbf{r}\left(0\right)\right|^2 \right\rangle \tag{1.4}$$

where $\langle\rangle$ represents a statistical average. This expression allows the diffusion coefficient to be calculated very simply from a classical molecular dynamics simulation in which the positions of the particles, $\mathbf{r}(t)$, are calculated at each time step.

In a system with finite volume equation 1.4 will always give a diffusion coefficient of zero if the limit is taken to infinity, since the mean square displacement cannot grow larger than the size of the system. In general, however, the ratio $\left\langle \left|\mathbf{r}(t) - \mathbf{r}\left(0\right)\right|^2 \right\rangle / 6t$ will reach a plateau value before the sides of the boxes are reached. It is this plateau value which provides the definition of D for a finite system.

The displacement of a particle from its initial position $\mathbf{r}\left(0\right)$ can be expressed as an integral over the particle's velocity, $\mathbf{u}(t)$.

$$\mathbf{r}(t) - \mathbf{r}\left(0\right) = \int_0^t \mathbf{u}\left(t'\right) dt' \tag{1.5}$$

Einstein's expression for the diffusion coefficient can then be used to give a relation between the diffusion coefficient and the velocity autocorrelation function.

The classical time-correlation function between two variables, $A(t)$ and $B(t)$ is $\langle A(t)B\left(0\right)\rangle$. If A and B are the same variable then the corresponding quantity is known as the autocorrelation function $\langle A(t)A\left(0\right)\rangle$. In an isotropic system, the velocity autocorrelation function is $\langle u_x(t)u_x\left(0\right)\rangle = \frac{1}{3}\left\langle \mathbf{u}(t).\mathbf{u}\left(0\right)\right\rangle$.

Starting from equation 1.4 and using equation 1.5:

$$D = \lim_{t\to\infty} \frac{1}{6t} \left\langle |\mathbf{r}(t) - \mathbf{r}(0)|^2 \right\rangle \tag{1.6}$$

$$= \lim_{t\to\infty} \frac{1}{6t} \int_0^t dt' \int_0^{t'} dt'' \left\langle \mathbf{u}(t'') . \mathbf{u}(t') \right\rangle \tag{1.7}$$

On changing variables t', t'' to t', $s = t' - t''$ and integrating by parts this gives:

$$D = \frac{1}{3} \int_0^\infty dt \left\langle \mathbf{u}(t) . \mathbf{u}(0) \right\rangle \tag{1.8}$$

This expression is an example of a group of relations known as Green-Kubo relations. They are derived by considering the statistical mechanics of non-equilibrium systems (also called fluctuation-dissipation theory) and relate a macroscopic quantity to the time integral over a time-correlation function of microscopic quantities. They will be discussed in more detail in section 1.2.

1.1.2 Transition State Theory

The diffusion of particles in the condensed phase can often be successfully modelled as a collection of particles jumping from one stable site to a neighbouring site via an energy barrier.

Eyring[4] proposed that, for a system in which particles moved between equivalent sites, the diffusion coefficient, D, could be related to the rate constant for the activated process, k, and the distance between the sites, l, by the expression $D = l^2 k$.

This relationship can be demonstrated by considering a simple one-dimensional system of identical sites, separated by a distance l. The rate of change of concentration at site i is given by

$$\dot{\rho}_i = \sum_j \rho_j K_{ji} - \rho_i K_{ij} \tag{1.9}$$

where the sum over j is over all other sites and K_{ji} is the rate constant for the process of a particle jumping from site j to site i. Assuming that jumps only occur between neighbouring sites and that the rate constants for these jumps is constant, $K_{ji} = k$ for $j = i \pm 1$ and zero otherwise. The expression for $\dot{\rho}_i$ then becomes

$$\dot{\rho}_i = \rho_{i-1} k - 2\rho_i k + \rho_{i+1} k \tag{1.10}$$

The diffusion equation gives

$$\dot{\rho}_i = D\frac{\partial^2 \rho_i}{\partial x^2} = D\frac{\rho_{i-1} - 2\rho_i + \rho_{i+1}}{l^2} \tag{1.11}$$

where the second derivative is found using finite differences. The expression $D = l^2 k$ is then obtained by comparing equations 1.10 and 1.11.

The rate constant, k, can be estimated using the relation proposed by Eyring[5]:

$$k = \kappa \frac{k_B T}{h} \frac{Q^{\ddagger}}{Q^0} e^{-\frac{E_a}{k_B T}} \tag{1.12}$$

where T is the temperature, k_B is Boltzmann's constant and h is Planck's constant. Q^0 is the partition function with the particle in the stable site, whereas $Q^{\ddagger}$ is the partition function with the particle at the top of the barrier, neglecting the degree of freedom along the path that the particle is moving. κ is the transmission coefficient and gives a measure of the probability of the particle remaining in the new site rather than re-crossing the barrier.

Assuming that barrier re-crossings do not occur during diffusion this gives the following equation for the diffusion coefficient:

$$D = \frac{l^2 k_B T}{h} \frac{Q^{\ddagger}}{Q^0} e^{-\frac{E_a}{k_B T}} \tag{1.13}$$

This expression gives a semi-classical method to calculate the diffusion coefficient. It takes into account the quantised energy levels of the diffusing particles, but does not include any effects due to quantum tunnelling or transitions between different quantum states during diffusion. It is assumed that the motion of the particle can be accurately described by classical motion on a potential energy surface.

1.1.3 Quantum Diffusion

The diffusion of particles with small mass through a medium cannot always be described by purely classical or semi-classical techniques. Quantum tunnelling at energies below the classical barrier to diffusion can contribute significantly to diffusion. There are different types of tunnelling processes which can contribute to the diffusion of quantum particles.

Tunnelling can occur between the ground states of two neighbouring wells. No activation

energy is required and the resulting diffusion is largely temperature independent. Ground state tunnelling often only becomes important at low temperatures.

Diffusion can also occur due to tunnelling between two excited states, or between an excited state in one well and a ground state in a different well. These are activated processes, but the activation energy may be well below that predicted by classical theories. Energy and momentum must be conserved in these transitions. Coherent tunnelling occurs when the particle states in the two wells are coincident in energy. If the quantum states in the two wells are not coincident then the energy difference can made up by transferring energy to or from the lattice phonons in the system. This process is known as incoherent tunnelling. These processes are summarised in figure 1.1

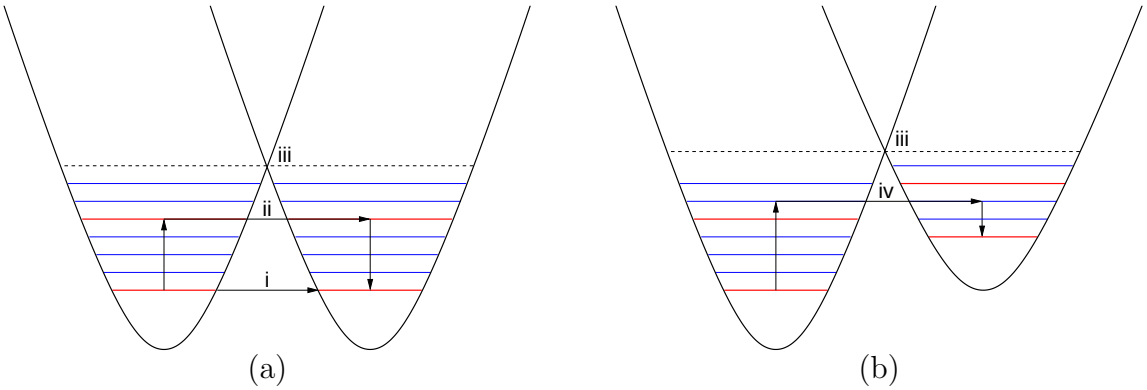

Figure 1.1: Diagrams showing (a) coherent and (b) incoherent tunnelling processes. The red lines represent particle energy levels and the blue lines lattice phonon energy levels. The figures show (i) ground state tunnelling, (ii) activated coherent tunnelling, (iii) the classical barrier to diffusion and (iv) activated incoherent tunnelling

A fully quantum mechanical expression for the calculation of the diffusion coefficient can be derived by considering the statistical mechanics of systems which are not in equilibrium.

1.1.4 Coupling to Other Nuclear Degrees of Freedom

The calculation of diffusion or reaction rates through a static one-dimensional potential is often not sufficient to correctly describe the dynamics of a system with many nuclear degrees of freedom. Coupling between the motion of the diffusing particle and the motion of its surroundings can have a large effect on diffusion rates calculated both classically and quantum mechanically.

In their book *Chemical Dynamics at Low Temperature*, Benderskii *et al*[6] review some of the techniques used to include the coupling to other nuclear degrees of freedom in an

approximate way.

It is not usually possible to include all of the nuclear degrees of freedom explicitly in a calculation of a rate constant or diffusion coefficient, especially in the condensed phase. A calculation including the full 3N nuclear degrees of freedom is likely to be too large to be computationally feasible for all but the smallest of molecular reactions. In general it is necessary to divide the system into one or more reaction coordinates which are treated explicitly, and find some way to model the interaction of the remaining nuclear degrees of freedom.

It is sometimes a sufficiently good approximation to treat all modes except the reaction coordinate as a bath of oscillators which only act to modify the one-dimensional potential through which the particle diffuses or the reaction progresses. In such an approximation the bath of oscillators introduces a frictional force acting on the particle moving in the one-dimensional potential. The study of this system is known as the dissipative tunnelling problem and is described at length in Caldeira and Leggett's paper[7].

If the conditions are such that only the lowest eigenstates in the initial and final positions are occupied then the dissipative tunnelling problem can be reduced to that of a two-level system[8]. Under the two-level system approximation the diffusing particle is assumed to tunnel instantaneously with respect to low frequency oscillations in the bath, but with a tunnelling matrix element which is modified by coupling to the high frequency bath modes.

The dissipative tunnelling model is known to accurately represent the reduction in transport rates due to coupling with other degrees of freedom. In extreme cases this coupling can fully localise a particle in one well. However, it is also the case that strong coupling with degrees of freedom outside the reaction coordinate can lower the reaction barrier or reduce its width and hence promote transitions from one well to a neighbouring well. Coupling to these modes is not well represented in the dissipative tunnelling model and if important must be included in a different way.

Inclusion of the promoting vibrational modes can be included by introducing an exponential decay in the tunnelling matrix element, Δ, which depends on the promoting vibration's coordinate, q_p, and a constant, γ, where γ^{-1} is small compared to the tunnelling distance.

$$\Delta = \Delta_0 e^{-\gamma q_p} \tag{1.14}$$

The above approximation was used by Borgis *et al*[9][10] to include coupling effects when calculating proton and hydrogen transfer rates in solution. Their method allows the calculation of hydrogen transfer rates in weak or moderate strength hydrogen bonded systems across a double well potential, and includes the effects of interactions with a polar solvent and the molecular vibrations which cause the barrier to fluctuate. The transfer reaction rate is calculated by integrating over correlation functions available in a molecular dynamics simulation.

In the field of hydrogen transfer in metals, Flynn and Stoneham[11] proposed a method for calculating diffusion rates of hydrogen in 1970 which includes coupling to phonon modes in the metal lattice.

After using the Born-Oppenheimer approximation to separate out the electronic degrees of freedom, the eigenstates of the nuclei are expressed as products of orthogonal hydrogen wavefunctions, which are localised at a particular interstitial site in the lattice, and a lattice wavefunction describing the motion of the host lattice.

Expressions for the jump rate between two neighbouring wells are then derived starting from the perturbation theory expression for the transition probability between two eigenstates. The resulting expressions for the jump rates at low temperatures depend on the tunnelling matrix element between states in neighbouring interstitial sites and the energy cost of distorting the host lattice during the transition. Some attempt was also made to include the effects of lattice-activated diffusion by considering the dependence of the tunnelling matrix element on the lattice coordinates.

In 2004 Sundell and Wahnström[12] performed calculations on the niobium hydride and tantalum hydride systems. Parameters for Flynn and Stoneham's expression were calculated by constructing a three-dimensional potential energy surface for hydrogen in these systems using density functional theory, and then finding the hydrogen ground state wavefunctions and energies on this surface.

Although Sundell and Wahnström's results were in fair agreement with experiment, they were only able to calculate rates over a very restricted temperature range. Their use of Flynn and Stoneham's expression restricts the validity of their calculations to temperatures low enough to assume that the only the hydrogen ground state wavefunction is occupied, but high enough to treat the lattice phonon modes classically.

In chapter 6 it is shown that the expression used in this thesis to calculate diffusion coefficients can be extended to include the effects of coupling to a fully quantum mechanical

harmonic oscillator. In some cases it is not possible to separate out the other nuclear degrees of freedom on the grounds of having much slower or faster dynamics than hydrogen, and it is hoped that this method will allow a more accurate calculation of the effect of coupling between the motion of hydrogen atoms and other nuclei in these cases.

1.2 Statistical Mechanics of Non-Equilibrium Systems

The theories of classical statistical-mechanics of systems in equilibrium were formulated many years ago by scientists such as Gibbs and Boltzmann.

During the mid-twentieth century several studies were made into the statistical mechanics of irreversible processes, and particularly into transport processes such as diffusion, heat transfer, and fluid flow. It was shown that transport properties, such as conductivity and susceptibility, can be calculated by considering the linear response of a system to a perturbation due an external applied field or force [13][14][15][16][17].

The theory results in expressions which relate macroscopically measurable quantities to the infinite time integral over an autocorrelation function.

Kubo[14] begins by considering a system, characterised by a Hamiltonian, $\hat{\mathcal{H}}$, which has been perturbed away from equilibrium by a time-dependent external force, $F(t)$. From $t = -\infty$ to $t = 0$ the system is assumed to be in equilibrium with an equilibrium density matrix ρ_0. The external force is applied to the system at $t = 0$.

It is assumed that the perturbation is small, as the force is weak, and that the change in the Hamiltonian is given by $\hat{\mathcal{H}}'(t) = -AF(t)$. He then looks for the response to the system in the linear approximation. This response, expressed in the change in the physical quantity B, $\Delta B(t)$, is then expressed in terms of the natural motion of the system.

The deviation of the density matrix at time t away from its equilibrium value is $\Delta\rho(t)$, such that $\rho(t) = \rho_0 + \Delta\rho(t)$. The time-dependence of the density matrix, ρ, is given by the equation of motion:

$$\frac{d\rho(t)}{dt} = \frac{1}{i\hbar}\left[\hat{\mathcal{H}} + \hat{\mathcal{H}}'(t), \rho(t)\right] \tag{1.15}$$

$$= \frac{1}{i\hbar}\left[\hat{\mathcal{H}}, \rho(t)\right] + \frac{1}{i\hbar}\left[\hat{\mathcal{H}}'(t), \rho_0\right] \tag{1.16}$$

where $[A, B] = AB - BA$ and only linear terms have been kept. The deviation of the

density matrix at time t can be calculated by solving the previous expression:

$$\Delta\rho(t) = -\frac{1}{i\hbar}\int_{-\infty}^{t} e^{-\frac{i(t-t')\hat{\mathcal{H}}}{\hbar}}\left[A,\rho_0\right]e^{\frac{i(t-t')\hat{\mathcal{H}}}{\hbar}}F(t')dt' \tag{1.17}$$

The response $\Delta B(t)$ of the quantity B is statistically calculated as a trace over B and the change in the density matrix:

$$\begin{aligned}\Delta B(t) &= Tr\left(\Delta\rho(t)B\right) &(1.18)\\ &= -\frac{1}{i\hbar}Tr\int_{-\infty}^{t} e^{-\frac{i(t-t')\hat{\mathcal{H}}}{\hbar}}\left[A,\rho_0\right]e^{\frac{i(t-t')\hat{\mathcal{H}}}{\hbar}}BF(t')dt' &(1.19)\\ &= -\frac{1}{i\hbar}Tr\int_{-\infty}^{t}\left[A,\rho_0\right]B(t-t')F(t')dt' &(1.20)\end{aligned}$$

where $B(t)$ is the solution to $\dot{B}(t) = -\frac{1}{i\hbar}\left[B(t),\hat{\mathcal{H}}\right], B(0) = B$.

The expression above for $\Delta B(t)$ can be considered in terms of an integral over a response function $\phi_{BA}(t)$, the response of the system over an infinitesimal time period:

$$\begin{aligned}\Delta B(t) &= \int_{-\infty}^{t}\phi_{BA}(t-t')F(t')dt' &(1.21)\\ \phi_{BA}(t) &= -\frac{1}{i\hbar}Tr\left[A,\rho_0\right]B(t) &(1.22)\end{aligned}$$

The response of current in the μ-th direction when a pulse of electric field is applied in the ν-th direction at $t = 0$ is

$$\begin{aligned}\phi_{\mu\nu}(t) &= \frac{1}{i\hbar}Tr\left(\left[qx_\nu,\rho_0\right]q\dot{x}_\mu(t)\right) &(1.23)\\ &= \frac{1}{i\hbar}Tr\left(\rho_0\left[q\hat{x}_\nu, q\dot{\hat{x}}_\mu(t)\right]\right) &(1.24)\end{aligned}$$

where q is the charge of a particle, and $\hat{x}_\nu$ is the position operator in the ν direction.

The last expression was obtained by cyclic interchange inside the trace:

$$\begin{aligned}Tr\left(\left[A,\rho_0\right]B\right) &= \sum_{n,m,l}\langle n|A|m\rangle\langle m|\rho_0|l\rangle\langle l|B|n\rangle - \langle n|\rho_0|m\rangle\langle m|A|l\rangle\langle l|B|n\rangle &(1.25)\\ &= \sum_{n,m,l}\langle m|\rho_0|l\rangle\langle l|B|n\rangle\langle n|A|m\rangle - \sum_{n,m,l}\langle n|\rho_0|m\rangle\langle m|A|l\rangle\langle l|B|n\rangle &(1.26)\\ &= \sum_{n,m,l}\langle n|\rho_0|m\rangle\langle m|B|l\rangle\langle l|A|n\rangle - \langle n|\rho_0|m\rangle\langle m|A|l\rangle\langle l|B|n\rangle &(1.27)\\ &= Tr\left(\rho_0\left[A,B\right]\right) &(1.28)\end{aligned}$$

If the applied electric field is oscillatory, with an angular frequency ω, then the electrical conductivity, $\sigma_{\mu\nu}(\omega)$, is given by

$$\sigma_{\mu\nu}(\omega) = \frac{1}{V}\int_0^\infty \phi_{\mu\nu}(t)e^{-i\omega t}dt \tag{1.29}$$

$$= \frac{1}{i\hbar V}\int_0^\infty Tr\left(\rho_0\left[q\hat{x}_\nu, q\dot{\hat{x}}_\mu(t)\right]\right)e^{-i\omega t}dt \tag{1.30}$$

where V is the volume of the system. The quantum mechanical current operator, $\hat{j}_\mu = q\dot{\hat{x}}_\mu$, is related to $\hat{x}_\mu$ such that $q\hat{x}_\mu e^{-i\omega t}$ can be replaced with $\frac{i}{\omega}\hat{j}_\mu e^{-i\omega t}$. The previous expression can then be rewritten in terms of the current operator rather than the position operator:

$$\sigma_{\mu\nu}(\omega) = \frac{1}{\hbar\omega V}\int_0^\infty Tr\left(\rho_0\left[\hat{j}_\nu, \hat{j}_\mu(t)\right]\right)e^{-i\omega t}dt \tag{1.31}$$

Assuming Boltzmann statistics, the equilibrium density matrix, $\rho_0 = e^{-\beta\hat{\mathcal{H}}}/Tr\left(e^{-\beta\hat{\mathcal{H}}}\right)$ where $\beta = 1/k_BT$.

The static eigenvectors of the time-independent Hamiltonian, $\hat{\mathcal{H}}$, are given by solving the time-independent Schrödinger equation $\hat{\mathcal{H}}\left|n\right\rangle = E_n\left|n\right\rangle$. Working in this basis the expression for the electrical conductivity becomes

$$\sigma_{\mu\nu}(\omega) = \frac{1}{\hbar\omega VQ}\int_0^\infty \sum_n \left\langle n|e^{-\beta\hat{\mathcal{H}}}\left[\hat{j}_\nu, \hat{j}_\mu(t)\right]|n\right\rangle e^{-i\omega t}dt \tag{1.32}$$

where Q is the quantum mechanical partition function given by $\sum_n \left\langle n|e^{-\beta\hat{\mathcal{H}}}|n\right\rangle$. Introducing the fact that $\hat{j}_\mu(t) = e^{\frac{i\hat{\mathcal{H}}t}{\hbar}}\hat{j}_\mu e^{\frac{-i\hat{\mathcal{H}}t}{\hbar}}$ this becomes

$$\sigma_{\mu\nu}(\omega) = \frac{1}{\hbar\omega VQ}\int_0^\infty \sum_{n,m} e^{-\beta E_n}e^{-i\omega t}\left(e^{-\frac{i}{\hbar}(E_n-E_m)t}\left\langle n|\hat{j}_\nu|m\right\rangle\left\langle m|\hat{j}_\mu|n\right\rangle - \right.$$
$$\left. e^{\frac{i}{\hbar}(E_n-E_m)t}\left\langle n|\hat{j}_\mu|m\right\rangle\left\langle m|\hat{j}_\nu|n\right\rangle\right)dt \tag{1.33}$$

Terms where $m = n$ evidently do not contribute to the sum and can be removed.

Greenwood [18] obtained a similar expression for the conductivity in metallic systems by solving the Boltzmann equation for a system of randomly placed scattering centres in a crystal.

The time integral can be carried out analytically since $\int_0^\infty e^{-i\omega t}dt = \frac{i}{\omega+i0} = \pi\delta(\omega)$. The diagonal elements of the conductivity are then

$$\begin{aligned}\sigma_{\mu\mu}(\omega) &= \frac{\pi}{\hbar\omega VQ}\sum_{n,m\neq n} e^{-\beta E_n}|\langle n|\hat{j}_\mu|m\rangle|^2 \times \\ &\left(\delta\left(\frac{E_n}{\hbar}-\frac{E_m}{\hbar}+\omega\right)+\delta\left(\frac{E_n}{\hbar}-\frac{E_m}{\hbar}-\omega\right)\right) \end{aligned} \tag{1.34}$$

The δ-functions mean that contributions can only come when $\hbar\omega = \pm E_n - E_m$ which means that we can rewrite the expression

$$\begin{aligned}\sigma_{\mu\mu}(\omega) &= \frac{\pi}{\hbar\omega VQ}\sum_{n,m\neq n} e^{-\frac{\beta}{2}(E_n+E_m)}|\langle n|\hat{j}_\mu|m\rangle|^2 \times \\ &\left(e^{\frac{\beta}{2}\hbar\omega}\delta\left(\frac{E_n}{\hbar}-\frac{E_m}{\hbar}+\omega\right)+e^{-\frac{\beta}{2}\hbar\omega}\delta\left(\frac{E_n}{\hbar}-\frac{E_m}{\hbar}-\omega\right)\right) \end{aligned} \tag{1.35}$$

The static electrical conductivity is found in the zero-frequency limit, $\omega \to 0$. The diffusion coefficient is related to the static electrical conductivity by the Nernst-Einstein relation,

$$D = \frac{k_B TV}{Nq^2}\sum_\mu \lim_{\omega\to 0}\sigma_{\mu\mu}(\omega) \tag{1.36}$$

where N is the number of conducting particles in volume V. This expression is valid for conducting particles in which the motion of different types of particles is uncorrelated. Using the Nernst-Einstein relation the previously calculated expression for the electrical conductivity can be changed to an expression for the diffusion coefficient, D:

$$D = \frac{k_B T\pi}{NQ\hbar q^2}\lim_{\omega\to 0}\frac{1}{\omega}\left(e^{\frac{\beta}{2}\hbar\omega}-e^{-\frac{\beta}{2}\hbar\omega}\right)\sum_{n,m\neq n} e^{-\beta E_n}|\langle n|\hat{j}_\mu|m\rangle|^2\delta\left(\frac{E_n}{\hbar}-\frac{E_m}{\hbar}\right) \tag{1.37}$$

Taking the limit that $\omega \to 0$ this gives:

$$D = \frac{\pi}{NQq^2}\sum_{n,m\neq n} e^{-\beta E_n}|\langle n|\hat{j}_\mu|m\rangle|^2\delta\left(\frac{E_n}{\hbar}-\frac{E_m}{\hbar}\right) \tag{1.38}$$

The current operator is simply related to the quantum mechanical momentum operator, $\hat{p}_\mu$, by $\hat{j}_\mu = q\dot{\hat{x}}_\mu = \frac{q}{m}\hat{p}_\mu$ where m is the mass of a particle. This gives a final expression for the diffusion coefficient of

$$D = \frac{\pi}{NQm^2}\sum_{n,m\neq n} e^{-\beta E_n}|\langle n|\hat{p}_\mu|m\rangle|^2\delta\left(\frac{E_n}{\hbar}-\frac{E_m}{\hbar}\right) \tag{1.39}$$

Equation 1.39 gives an expression that allows the calculation of diffusion coefficients once the eigenstates of a system are known. Rather than working in the space of the full Hamiltonian of the system, it will be necessary to make approximations by only considering certain degrees of freedom with quantum mechanics and to assume that good results can still be obtained using single-particle wave functions and energies.

Although the time integral was performed to infinity, it should only be performed to a large enough upper limit to average out microscopic fluctuations but before macroscopic equilibrium is reached [13][15][16]. Introducing an upper limit to the time integral would produce sinc-like functions with a finite width. The δ-function in equation 1.39 will be replaced with a Gaussian function in the calculations which follow.

Chapter 2

Theoretical Methods

2.1 Density Functional Theory

The electronic structure calculations described in the following sections were carried out using the Car-Parrinello molecular dynamics (CPMD)[19] and CASTEP[20] packages. The packages use density functional theory (DFT) in a plane-wave basis to calculate the electronic wave functions and energies of a system, given the nuclear coordinates.

In quantum mechanics the properties of a system are described by a Hamiltonian for the system, $\hat{\mathcal{H}}$, and the corresponding set of many-body wave functions, $\{\Psi_N\}$, which satisfy the time-independent Schrödinger equation, $\hat{\mathcal{H}}\Psi_N = E_N\Psi_N$. In the Born-Oppenheimer approximation[21] the many-body wave function is assumed to take the form

$$\Psi_N\left(\{\mathbf{R}_I\},\{\mathbf{r}_i\}\right) = \phi_N\left(\{\mathbf{R}_I\}\right)\psi_n\left(\{\mathbf{r}_i\};\{\mathbf{R}_I\}\right) \tag{2.1}$$

where $\phi_N\left(\{\mathbf{R}_I\}\right)$ depends only on the nuclear coordinates, $\{\mathbf{R}_I\}$ and $\psi_n\left(\{\mathbf{r}_i\};\{\mathbf{R}_I\}\right)$ depends on the electronic coordinates, $\{\mathbf{r}_i\}$, and only parametrically on $\{\mathbf{R}_I\}$. This tends to be a good approximation due to the large difference in mass between nuclei and electrons.

The electronic wave functions, $\{\psi_n\}$ are found by solving the time-independent Schrödinger equation with an effective Hamiltonian, $\hat{\mathcal{H}}_{elec}$, which depends parametrically on $\{\mathbf{R}_I\}$ to obtain an electronic energy, E_n, which also depends parametrically on $\{\mathbf{R}_I\}$; $\hat{\mathcal{H}}_{elec}\psi_n = E_n\left(\{\mathbf{R}_I\}\right)\psi_n$.

The electronic coordinates are then integrated out and the energy of the entire system can be calculated using a Hamiltonian which only depends on the nuclear coordinates, $\{\mathbf{R}_I\}$.

Within DFT the electronic energy of a system is expressed in terms of the electron density, $n(\mathbf{r})$, rather than the electronic wave function. Following Kohn and Sham[22], the electron density can be expanded in a set of one-electron orbitals, the so-called Kohn-Sham (KS) orbitals: $n(\mathbf{r}) = \sum_i |\psi_i(\mathbf{r}))|^2$. A functional of the density is then used to calculate the energy. The KS orbitals can be expanded in any suitable set of basis functions. A basis of plane-waves is usually chosen if the calculations are performed for a periodic system.

In general the functional will include a term for the kinetic energy of a non-interacting system of electrons, T, a simple Coulombic term, E_H, given by the Hartree energy functional, a term due to any external potential, E_{ext}, and a term containing the corrections necessary due to approximations in the kinetic energy and Coulomb functionals, known as the exchange-correlation functional, E_{xc}:

$$E[n] = T[n] + E_H[n] + E_{ext}[n] + E_{xc}[n] \tag{2.2}$$

The exchange-correlation energy functional is in general not known exactly, and an approximation to it must be made. It is often approximated with a functional based on the exchange-correlation functional for an homogeneous electron gas, with extra terms involving the local density (local density approximation (LDA) functionals) and optionally the local gradient of the density (generalised gradient approximation (GGA) functionals). The approximation used in this study is a GGA functional proposed by Perdew, Burke and Ernzerhof (PBE)[23] which has been shown to give accurate energies and geometries of systems in the condensed phase.

Once the energy functional is known, the electronic energy is then found by minimising the functional with respect to the KS orbitals. The problem can be formulated as a set of KS equations which can be solved for the KS orbitals:

$$\left(\hat{\mathcal{T}} + V_H + V_{ext} + V_{xc}\right)\psi_i(\mathbf{r}) = \varepsilon_i\psi_i(\mathbf{r}) \tag{2.3}$$

where V_H, V_{ext}, and V_{xc} are the functional derivatives of E_H, E_{ext}, and E_{xc} respectively. If the potential is periodic then the equations can be solved using Bloch theory as described in section 2.3. Alternatively, conventional CPMD performs minimisation of the energy functional by applying dynamical simulated annealing to fictional dynamics of the KS

orbitals. This method treats the electron density adiabatically on the zero temperature Born-Oppenheimer surface.

2.1.1 Free Energy Molecular Dynamics

The conventional CPMD method is unable to correctly model metallic systems at finite temperatures. Fractionally occupied states cannot be treated and the time steps needed to accurately integrate the equations of motion are prohibitively small in metallic systems, due to the fast dynamics of the electronic degrees of freedom.

The introduction of a free energy functional [24] allows for the fractional occupation of states, and the functional can be efficiently calculated using an iterative diagonalisation technique. This method has been included for all the CPMD calculations described in this study.

Free energy molecular dynamics (FEMD) is based on the work of Mermin[25], who extended Hohenberg and Kohn's[26] theory of a variational functional for the ground state of a system to a finite temperature electron gas. Mermin showed the existence of a grand potential functional which is minimal for the density of an electron gas in thermal equilibrium, and that for this density, the functional gives the free energy of the system.

In FEMD a free energy functional, $\mathcal{F}$, is introduced, which is stationary at the same density as the Mermin functional, and allows this density to be computed,

$$\mathcal{F} = \Omega + \mu N + E_{II} \tag{2.4}$$

where μ is the chemical potential, E_{II} is the ion-ion Coulomb energy, and Ω is the grand potential for an interacting electron gas within DFT:

$$\Omega\left[n(\mathbf{r}), R_I\right] = -\frac{2}{\beta}\ln\det\left(1+e^{-\beta(\hat{\mathcal{H}}-\mu)}\right) - \frac{1}{2}\int d\mathbf{r}d\mathbf{r}'\frac{n(\mathbf{r})n\left(\mathbf{r}'\right)}{|\mathbf{r}-\mathbf{r}'|} - \int d\mathbf{r}n(\mathbf{r})\frac{\delta\Omega_{xc}}{\delta n(\mathbf{r})} + \Omega_{xc} \tag{2.5}$$

Ω_{xc} is the exchange correlation grand potential functional, $\beta = 1/k_B T_e$ where T_e is an electronic temperature parameter, and $\hat{\mathcal{H}}$ is the one-electron Hamiltonian from the usual Kohn-Sham theory,

$$\hat{\mathcal{H}} = -\frac{1}{2}\nabla^2 + V_{eff}(\mathbf{r}) \tag{2.6}$$

where atomic units have been used and where

$$V_{eff}(\mathbf{r}) = \sum_I V_{eI}\left(\mathbf{r} - R_I\right) + \int d\mathbf{r}' \frac{n\left(\mathbf{r}'\right)}{|\mathbf{r} - \mathbf{r}'|} + \frac{\delta\Omega_{xc}}{\delta n(\mathbf{r})} \tag{2.7}$$

For a given effective potential, V_{eff}, the resulting density, $n_{out}(\mathbf{r})$, is given by:

$$\frac{\delta\Omega\left[n(\mathbf{r})\right]}{\delta V_{eff}(\mathbf{r})} = n_{out}(\mathbf{r}) \tag{2.8}$$

and can be defined in terms of the one-electron states which are eigenstates of $\hat{\mathcal{H}}$, ψ_i:

$$n_{out}(\mathbf{r}) = \sum_i f_i \psi_i^*(\mathbf{r})\psi_i(\mathbf{r}) \tag{2.9}$$

where f_i are the thermal Fermi-Dirac occupation numbers given by $f_i = 1/(1 + e^{\beta(\varepsilon_i - \mu)})$.

Using 2.8 and the thermodynamic relation $(\partial\Omega/\partial\mu)_{n(\mathbf{r})} = -N$ the functional derivative of $\mathcal{F}$ can be calculated as:

$$\frac{\delta\mathcal{F}}{\delta n(\mathbf{r})} = \int d\mathbf{r}\left[n_{out}(\mathbf{r}) - n(\mathbf{r})\right]\left(\frac{1}{|\mathbf{r} - \mathbf{r}'|} + \frac{\delta^2\Omega_{xc}}{\delta n(\mathbf{r}) n\left(\mathbf{r}'\right)}\right) \tag{2.10}$$

The stationary point in $\mathcal{F}$ and the Mermin functional is found when self-consistency is reached in the density (i.e. $n_{out}(\mathbf{r}) = n(\mathbf{r})$). To solve this problem $\mathcal{F}$ must be evaluated. This evaluation is carried out by diagonalisation of the density matrix, $\rho_{ij} = \left\langle \mathbf{r}_i \left| e^{-\frac{\beta}{p}\hat{\mathcal{H}}} \right| \mathbf{r}_j \right\rangle$, using Trotter factorisation to simplify the density matrix and the Krylov-space (Lanczos) iterative diagonalisation method, allowing mixing of input and output densities between iterations to prevent unstable charge oscillations arising.

2.2 Pseudopotentials

Due to the rapid oscillations of the electronic wave function in the the region of a nuclear core, and the high kinetic energy of the tightly bound core electrons, a plane-wave basis set is poorly suited to describing the electronic wave function in the region of nuclear cores. Performing an all-electron calculation would require a prohibitively high energy cutoff for the plane-wave basis set.

Since the physical properties of solids are mainly dependent on the valence electrons, the core electrons and ionic potential can be replaced with one alternative weaker potential. This potential is known as a pseudopotential. It is also helpful to remove the oscillatory nature of the wave functions in the core region, and a pseudopotential is constructed so that this is the case. The new smoothed wave functions are known as pseudo-wave functions. The pseudo-wave functions and pseuodopotentials are constructed so that they match the real wave functions and potentials exactly beyond a certain cutoff radius, r_c (see figure 2.1).

The pseudopotentials used with CPMD were norm-conserving potentials, that is the pseudo-wave functions and real-wave functions have identical charge densities in the core region. They were generated according to the method suggested by Troullier and Martins[27]. The calculations using CASTEP used the ultrasoft pseudopotentials proposed by Vanderbilt [28].

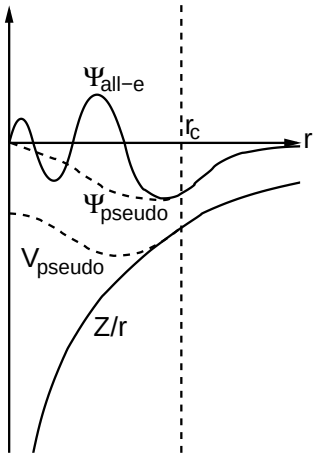

Figure 2.1: A schematic diagram of all-electron (solid) and pseudo (dashed) wave functions and potentials

2.3 Bloch Theory

In a periodic potential where a_α is the periodicity in the x_α direction, the single particle density, $|\psi(\mathbf{x})|^2$ must also have the same periodicity.

$$V(\mathbf{x}+\mathbf{a}) = V(\mathbf{x}) \Rightarrow |\psi(\mathbf{x}+\mathbf{a})|^2 = |\psi(\mathbf{x})|^2 \tag{2.11}$$

Thus a relationship between $\psi(\mathbf{x}+\mathbf{a})$ and $\psi(\mathbf{x})$ can be obtained by splitting $\psi(\mathbf{x})$ into a part $u(\mathbf{x})$ which has the same periodicity as the lattice and a remaining phase factor.

$$\begin{aligned}
\psi(\mathbf{x}) &= e^{-i\mathbf{k}.\mathbf{x}}u(\mathbf{x}) && (2.12)\\
|\psi(\mathbf{x}+\mathbf{a})|^2 &= \psi^*(\mathbf{x}+\mathbf{a})\,\psi(\mathbf{x}+\mathbf{a}) && (2.13)\\
&= e^{i\mathbf{k}.\mathbf{x}+i\mathbf{k}.\mathbf{a}}e^{-i\mathbf{k}.\mathbf{x}-i\mathbf{k}.\mathbf{a}}u^*(\mathbf{x}+\mathbf{a})\,u(\mathbf{x}+\mathbf{a}) && (2.14)\\
&= e^{i\mathbf{k}.\mathbf{x}}e^{-i\mathbf{k}.\mathbf{x}}u^*(\mathbf{x})u(\mathbf{x}) && (2.15)\\
&= \psi^*(\mathbf{x})\psi(\mathbf{x}) = |\psi(\mathbf{x})|^2 && (2.16)
\end{aligned}$$

This is a statement of Bloch's theorem [29]. The part of the wave function with periodicity $\mathbf{a}$ is known as the Bloch function. The vector $\mathbf{k}$ must be a vector in the reciprocal space of the system and can be used to label each wave function without loss of generality.

$$\psi_{\mathbf{k}}(\mathbf{x}) = e^{-i\mathbf{k}.\mathbf{x}}u_{\mathbf{k}}(\mathbf{x}) \tag{2.17}$$

It is often useful to further divide the vector $\mathbf{k}$ into the sum of the vector pointing to the closest point on the reciprocal lattice, $\mathbf{g}$, (defined by $g_\alpha = \frac{2\pi G_\alpha}{a_\alpha}$ where G_α is an integer) and then a remainder which lies within the first Brillouin zone, $\mathbf{k}'$. The wave function is then labelled by $\mathbf{g}$ and $\mathbf{k}'$. As $e^{-i\mathbf{g}.\mathbf{x}}$ is periodic in $\mathbf{a}$ this part can be absorbed into the Bloch function. A deeper discussion of vectors in the reciprocal lattice of a system is given in Brillouin's book on *Wave Propagation in Periodic Structures*[30].

$$\psi_{\mathbf{k},\mathbf{g}}(\mathbf{x}) = e^{-i\mathbf{k}'.\mathbf{x}}e^{-i\mathbf{g}.\mathbf{x}}u_{\mathbf{k}',\mathbf{g}}(\mathbf{x}) = e^{-i\mathbf{k}'.\mathbf{x}}u'_{\mathbf{k}',\mathbf{g}}(\mathbf{x}) \tag{2.18}$$

After this point the vector $\mathbf{k}'$ shall be re-labelled $\mathbf{k}$, and u' re-labelled as u in order to keep the notation as uncluttered as possible.

The Bloch function and the corresponding single particle energy level can be found using

the single particle time-independent Schrödinger equation.

$$-\frac{1}{2m}\nabla^2 e^{-i\mathbf{k}.\mathbf{x}}u_{\mathbf{k},\mathbf{g}}(\mathbf{x}) + \left(V(\mathbf{x}) - \varepsilon_{\mathbf{k},\mathbf{g}}\right)e^{-i\mathbf{k}.\mathbf{x}}u_{\mathbf{k},\mathbf{g}}(\mathbf{x}) = 0 \quad (2.19)$$

$$\frac{1}{2m}e^{-i\mathbf{k}.\mathbf{x}}\left(i\nabla + \mathbf{k}\right)^2 u_{\mathbf{k},\mathbf{g}}(\mathbf{x}) + \left(V(\mathbf{x}) - \varepsilon_{\mathbf{k},\mathbf{g}}\right)e^{-i\mathbf{k}.\mathbf{x}}u_{\mathbf{k},\mathbf{g}}(\mathbf{x}) = 0 \quad (2.20)$$

$$\frac{1}{2m}\left(-i\nabla - \mathbf{k}\right)^2 u_{\mathbf{k},\mathbf{g}}(\mathbf{x}) + \left(V(\mathbf{x}) - \varepsilon_{\mathbf{k},\mathbf{g}}\right)u_{\mathbf{k},\mathbf{g}}(\mathbf{x}) = 0 \quad (2.21)$$

At each point in the first Brillouin zone (i.e. each k-point) a set of Bloch equations can be solved to obtain the wave functions and energies of the single particle states labelled by the reciprocal lattice vector $\mathbf{g}$ or equivalently the quantum number $\mathbf{n}$.

$$\frac{1}{2m}\left(-i\nabla - \mathbf{k}\right)^2 u_{\mathbf{k},\mathbf{n}}(\mathbf{x}) + \left(V(\mathbf{x}) - \varepsilon_{\mathbf{k},\mathbf{n}}\right)u_{\mathbf{k},\mathbf{n}}(\mathbf{x}) = 0 \quad (2.22)$$

The potential and the Bloch functions have periodicity $\mathbf{a}$ and can be expressed in a basis of plane-waves with the same periodicity by a Fourier transform. These plane-waves have wave-vectors which are the reciprocal lattice vectors, $\mathbf{g}$.

$$u_{\mathbf{k},\mathbf{n}}(\mathbf{x}) = \sum_{\mathbf{g}} \tilde{u}_{\mathbf{k},\mathbf{n}}(\mathbf{g})e^{-i\mathbf{g}.\mathbf{x}} \quad (2.23)$$

$$V(\mathbf{x}) = \sum_{\mathbf{g}} \tilde{V}(\mathbf{g})e^{-i\mathbf{g}.\mathbf{x}} \quad (2.24)$$

Entering these expressions into the Bloch equation for $u_{\mathbf{k},\mathbf{n}}(\mathbf{x})$, equation 2.22, gives a set of new equations to solve for the Fourier coefficients of the Bloch functions:

$$\frac{1}{2m}\left(-i\nabla - \mathbf{k}\right)^2 \sum_{\mathbf{g}} \tilde{u}_{\mathbf{k},\mathbf{n}}(\mathbf{g})e^{-i\mathbf{g}.\mathbf{x}} + \left(\sum_{\mathbf{g}'} \tilde{V}\left(\mathbf{g}'\right)e^{-i\mathbf{g}'.\mathbf{x}} - \varepsilon_{\mathbf{k},\mathbf{n}}\right)\sum_{\mathbf{g}} \tilde{u}_{\mathbf{k},\mathbf{n}}(\mathbf{g})e^{-i\mathbf{g}.\mathbf{x}} = 0 \quad (2.25)$$

$$\sum_{\mathbf{g}}\left(\frac{1}{2m}\left|\mathbf{g} + \mathbf{k}\right|^2 - \varepsilon_{\mathbf{k},\mathbf{n}}\right)\tilde{u}_{\mathbf{k},\mathbf{n}}(\mathbf{g})e^{-i\mathbf{g}.\mathbf{x}} + \sum_{\mathbf{g}}\sum_{\mathbf{g}'} \tilde{V}\left(\mathbf{g}'\right)e^{-i\mathbf{g}'.\mathbf{x}}\tilde{u}_{\mathbf{k},\mathbf{n}}(\mathbf{g})e^{-i\mathbf{g}.\mathbf{x}} = 0 \quad (2.26)$$

These equations can be simplified by multiplying by a plane-wave with arbitrary momen-

tum, $e^{i\mathbf{g}''.\mathbf{x}}$ and integrating over $\mathbf{x}$. Taking the first term in the equations:

$$\begin{aligned}
&\int_0^a d\mathbf{x} e^{i\mathbf{g}''.\mathbf{x}} \sum_{\mathbf{g}} \left(\frac{1}{2m} |\mathbf{g}+\mathbf{k}|^2 - \varepsilon_{\mathbf{k},\mathbf{n}} \right) \tilde{u}_{\mathbf{k},\mathbf{n}}(\mathbf{g}) e^{-i\mathbf{g}.\mathbf{x}} \\
&= \sum_{\mathbf{g}} \left(\frac{1}{2m} |\mathbf{g}+\mathbf{k}|^2 - \varepsilon_{\mathbf{k},\mathbf{n}} \right) \tilde{u}_{\mathbf{k},\mathbf{n}}(\mathbf{g}) \delta(\mathbf{g}-\mathbf{g}'') \qquad (2.27) \\
&= \left(\frac{1}{2m} |\mathbf{g}''+\mathbf{k}|^2 - \varepsilon_{\mathbf{k},\mathbf{n}} \right) \tilde{u}_{\mathbf{k},\mathbf{n}}(\mathbf{g}'') \qquad (2.28)
\end{aligned}$$

The second term can be treated in the same way:

$$\begin{aligned}
&\int_0^a d\mathbf{x} e^{i\mathbf{g}''.\mathbf{x}} \sum_{\mathbf{g}} \sum_{\mathbf{g}'} \tilde{V}(\mathbf{g}') \tilde{u}_{\mathbf{k},\mathbf{n}}(\mathbf{g}) e^{-i(\mathbf{g}+\mathbf{g}').\mathbf{x}} \qquad (2.29) \\
&= \int_0^a d\mathbf{x} \sum_{\mathbf{g}} \sum_{\mathbf{g}'} \tilde{V}(\mathbf{g}') \tilde{u}_{\mathbf{k},\mathbf{n}}(\mathbf{g}) e^{-i(\mathbf{g}+\mathbf{g}'-\mathbf{g}'').\mathbf{x}} \qquad (2.30) \\
&= \sum_{\mathbf{g}} \tilde{V}(\mathbf{g}''-\mathbf{g}) \tilde{u}_{\mathbf{k},\mathbf{n}}(\mathbf{g}) \qquad (2.31)
\end{aligned}$$

In reality the Fourier transforms are carried out as finite sums over the reciprocal lattice vectors, $\mathbf{g}$. Usually an upper limit to the kinetic energy is chosen such that the sum is performed over n_{max} g-vectors. A cutoff energy is chosen and a spherical cutoff applied such that:

$$\frac{1}{2m} |\mathbf{g}_{max}+\mathbf{k}|^2 < E_{cutoff} \qquad (2.32)$$

In general, a much higher energy cutoff is required for convergence of electronic wave functions than hydrogen wave functions, due to the mass dependence of the kinetic energy.

Combining the two terms back together gives the n_{max} equations:

$$\left(\frac{1}{2m} |\mathbf{g}''+\mathbf{k}|^2 - \varepsilon_{\mathbf{k},\mathbf{n}} \right) \tilde{u}_{\mathbf{k},\mathbf{n}}(\mathbf{g}'') + \sum_{\mathbf{g}} \tilde{V}(\mathbf{g}''-\mathbf{g}) \tilde{u}_{\mathbf{k},\mathbf{n}}(\mathbf{g}) = 0 \qquad (2.33)$$

and can be solved by diagonalising the $n_{max} \times n_{max}$ matrix whose elements are given by:

$$U_{\mathbf{g},\mathbf{g}'} = \frac{1}{2m} |\mathbf{g}+\mathbf{k}|^2 \delta_{\mathbf{g},\mathbf{g}'} + \tilde{V}(\mathbf{g}-\mathbf{g}') \qquad (2.34)$$

This gives the Fourier coefficients for the n_{max} Bloch functions, $u_{\mathbf{k},\mathbf{n}}$, and their corresponding energies, $\varepsilon_{\mathbf{k},\mathbf{n}}$.

Once the Bloch functions and energies have been calculated, the momentum matrix element necessary for the calculation of the diffusion coefficient using equation 1.39 can be obtained by integration in Fourier space:

$$\langle \psi_{\mathbf{k}',\mathbf{n}'} | \hat{p}_{\mathbf{x}} | \psi_{\mathbf{k},\mathbf{n}} \rangle = -i \int \sum_{\mathbf{g}} \tilde{u}^*_{\mathbf{k}',\mathbf{n}'}(\mathbf{g})\, e^{i(\mathbf{g}'+\mathbf{k}').\mathbf{x}} \nabla_{\mathbf{x}} \sum_{\mathbf{g}'} \tilde{u}_{\mathbf{k},\mathbf{n}}(\mathbf{g}) e^{-i(\mathbf{g}+\mathbf{k}).\mathbf{x}} d\mathbf{x} \quad (2.35)$$

$$= -\int \sum_{\mathbf{g},\mathbf{g}'} \tilde{u}^*_{\mathbf{k}',\mathbf{n}'}(\mathbf{g}')\, \tilde{u}_{\mathbf{k},\mathbf{n}}(\mathbf{g})\, (\mathbf{g}+\mathbf{k})\, e^{i(\mathbf{g}'-\mathbf{g}+\mathbf{k}'-\mathbf{k}).\mathbf{x}} d\mathbf{x} \quad (2.36)$$

$$= -\sum_{\mathbf{g}} \tilde{u}^*_{\mathbf{k}',\mathbf{n}'}(\mathbf{g})\, (\mathbf{g}+\mathbf{k}')\, \tilde{u}_{\mathbf{k},\mathbf{n}}(\mathbf{g}) \delta_{\mathbf{k}',\mathbf{k}} \quad (2.37)$$

Chapter 3

Palladium Hydride

Palladium hydride has been the subject of many experimental and theoretical studies over the past 100 years. Extensive academic interest in the subject has arisen from its unusual properties and connected technological applications.

In many other metals, addition of hydrogen causes severe embrittlement and the loss of electrical conductivity. This is not the case with palladium. The high diffusion rates of hydrogen through palladium, and the large volumes of hydrogen that palladium is able to absorb, allow palladium hydride to be used as a hydrogen diffusion membrane and a potential hydrogen storage medium. Palladium is also used extensively as a hydrogenation catalyst.

An extensive review of early experimental work on palladium hydride is presented in Lewis' *The Palladium Hydrogen System*[31]. More information can be found in Völkl and Alefeld's book *Hydrogen in Metals*[32], and a more recent review was published by Flanagan and Oates in 1991[33].

The palladium atoms in both bulk palladium and palladium hydride have been shown to have a face centred cubic (FCC) structure. Two main interstitial sites exist in the FCC structure, one with tetrahedral symmetry and one with octahedral symmetry. The FCC unit cell with the interstitial sites marked can be seen in figure 3.1.

Palladium hydride has been shown to exist in two concentration dependent phases. The α phase occurs at low hydrogen concentrations (PdH_x $x < 0.1$) in which the hydrogen atoms are randomly distributed in the octahedral interstitial sites within the palladium lattice and are well separated from each other. At higher concentrations ($x > 0.6$) the β phase

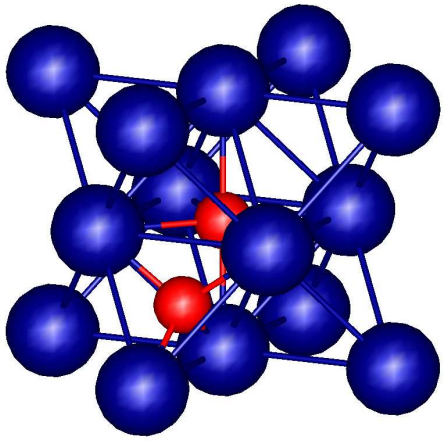

Figure 3.1: The unit cell of a face centred cubic lattice with the tetrahedral and octahedral interstitial sites marked by red spheres.

is formed in which near stoichiometric ($x = 1$) regions are formed in which the hydrogen atoms occupy the octahedral interstitial sites forming a rock salt (NaCl) structure. The two phases coexist at intermediate concentrations.

Bulk palladium has a lattice constant, a, of 3.891 Å at room temperature [34] which expands with the addition of hydrogen to roughly 3.9 Å in the α phase and between 4.0 Å and 4.1 Å in the β phase[35]. Ross *et al* measured the lattice constant of $PdH_{0.99}$ at 100K to be 4.095 Å[36].

3.1 Preliminary Studies

Bulk palladium and stoichiometric palladium hydride (PdH) were studied using the CPMD package[19] to perform electronic structure calculations using density functional theory (DFT) in a plane-wave basis set. Calculations were performed using a norm-conserving Troullier-Martins [27] pseudopotential for the palladium atoms. The density functional proposed by Perdew, Burke, and Ernzerhof (PBE)[23] within the generalised gradient approximation (GGA) was used. In addition a free energy functional [24] was included to allow the accurate calculation of metallic states.

3.1.1 Bulk Palladium

The lattice constant and bulk modulus of bulk palladium in an FCC lattice were calculated by performing single point calculations of the system with different values of the lattice constant, a, and fitting the results to a polynomial curve. The calculations were found to be converged with a plane-wave cutoff of 50 Ryd (680 eV) and were performed on a 16^3 k-point grid.

The lattice constant was calculated to be 3.97 Å and the bulk modulus 171 GPa in reasonable agreement with experimental values of 3.89 Å[34] and 180–195 GPa[37][38][39]. Density functionals using generalised gradient approximations are known to overestimate the lattice constants of transition metals and underestimate their bulk moduli.

3.1.2 Palladium Hydride

Similar calculations were carried out using stoichiometric palladium hydride with the hydrogen atom in the octahedral and tetrahedral interstitial sites. In both cases a plane-wave cutoff of 60 Ryd (820 eV) and a k-point mesh of 12^3 points was found to be sufficient to obtain converged results.

With the hydrogen atom in the octahedral site the lattice constant, a, was calculated to be 4.15 Å and with the hydrogen in the alternative tetrahedral site it was found to be 4.26 Å. Experimentally the lattice constant of almost stoichiometric PdH was found to be 4.095 Å at 100K[36] and predicted to be 4.09 Å for PdH_1 by Schirber and Morosin[40].

The DFT calculations show that the most stable configuration is found with the hydrogen in the tetrahedral site at a = 4.26 Å. This configuration was found to be 70 meV lower in energy than that with the hydrogen in the octahedral site at a = 4.15 Å. Even at a = 4.15 Å the tetrahedral site is found to be more stable by 11 meV.

The relative stabilities of the octahedral and tetrahedral sites are reversed when the zero point energy (ZPE) of the hydrogen atom is included. The ZPE was estimated by shifting the hydrogen atom away from a site and recalculating the energies using DFT. The curvature of the resulting potential was estimated using finite differences and the ZPE of the hydrogen atom calculated using the harmonic approximation.

The ZPE of the hydrogen at the octahedral site, with a = 4.15 Å, was calculated to be 68 meV, the ZPE of hydrogen in the tetrahedral site at the same lattice constant

was calculated to be 194 meV. Including the ZPE of the hydrogen atom, the octahedral site becomes the most stable, as suggested by experiment[41]. At the equilibrium lattice constant of 4.26 Å the ZPE of the hydrogen atom in the tetrahedral site drops to 169 meV.

The bulk modulus of PdH with the hydrogen in the octahedral site was calculated to be 179 GPa, close to the experimental value of 183 GPa obtained for $PdH_{0.76}$ by Nygren and Leisure [38].

3.2 Hydrogen Energy Levels

Several investigations have been made into the excitation energies between hydrogen and deuterium vibrational states using inelastic neutron scattering (INS)[42][36][43]. The vibration spectra were measured for both the α and β phases of PdH_x and PdD_x. The spectra were interpreted by fitting to results calculated using a three-dimensional oscillator. The potential in the direction of the nearest palladium atoms was found to be strongly anharmonic.

Alongside the experimental studies, Elsässer *et al* performed calculations of the vibrational energy levels of hydrogen and deuterium in palladium using *ab initio* techniques [44][45].

A mixed basis of plane-waves and localised functions was used to calculate the total energy of the system with the hydrogen atom at different positions within the super-cell. The calculations used DFT within the local-density-functional approximation (LDA). The core electrons of the palladium atom were replaced by a norm-conserving pseudopotential and calculations were made over a suitably large k-point grid. The equilibrium lattice constant was calculated to be 4.07 Å.

The Fourier components of a three-dimensional adiabatic potential for the hydrogen atom were fitted to the points calculated using DFT, and the hydrogen states were calculated by solving Bloch equations as described in section 2.3.

The resulting energy levels were compared with those calculated using a harmonic approximation to the potential, and a potential in which anharmonicity was included perturbatively. The Fourier technique was found to better reproduce experimental values and the calculated energy levels were used to interpret the available date from INS studies.

Using a similar procedure to that employed by Elsässer *et al*, a potential was built by repeatedly carrying out single point electronic structure calculations, with the hydrogen atom at different locations within the FCC unit cell with a lattice constant of 4.16 Å. The hydrogen atom was placed at the points on a 32^3 cubic grid which are unrelated by symmetry, and the total energy of the system calculated in a plane-wave basis using DFT with the PBE GGA functional, a free energy functional, and a Troullier-Martins pseudopotential for the Pd atoms. The calculations were carried out over a 12^3 k-point mesh with a plane-wave cutoff of 60 Ryd (820 meV). A contour plot of the potential in the 110 plane of the lattice can be seen in figure 3.2.

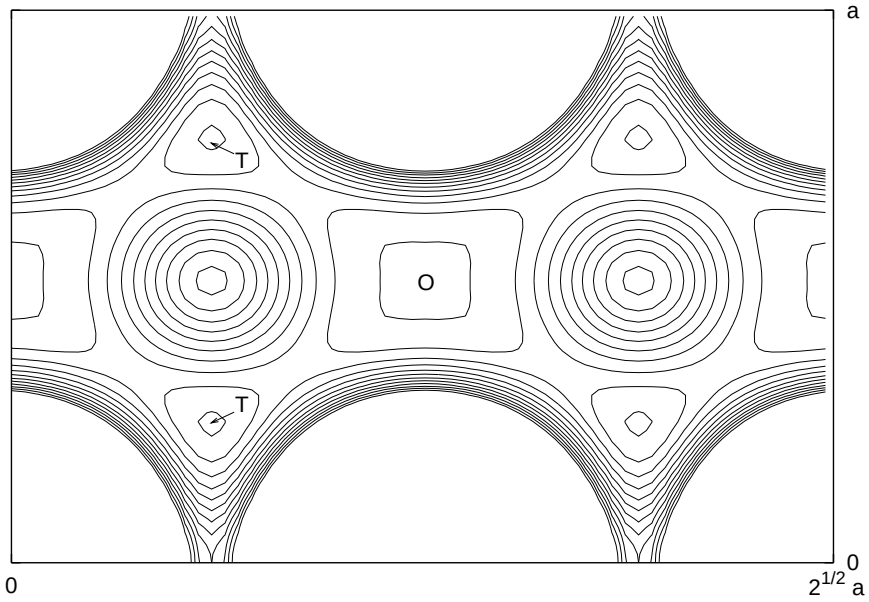

Figure 3.2: A contour plot of the potential in the 110 plane of the PdH lattice. The positions of some tetrahedral (T) and octahedral (O) sites are labelled, the others can be inferred by symmetry. Palladium atoms are located at the corners of the plot and at the centre of the upper and lower borders. Contours are placed at intervals of 140 meV.

Once the potential for the hydrogen atom was obtained on the real space grid, a Fourier transform was taken and the hydrogen wave functions and energy levels calculated using Bloch theory. Where it was necessary to represent the wave function on a more dense grid than the potential, the extra points were interpolated from the original potential on the 32^3 grid. The wave functions and energies were calculated at the Γ-point (k=0).

It is assumed that interactions between different hydrogen atoms are included in the potential calculated using DFT. There are no other hydrogen interaction terms in the Bloch equations solved for the wave functions and energies.

The ground state energies ($E_{0,|000\rangle}$) for ^{1}H and ^{2}D in the octahedral and tetrahedral sites, and the excitation energies in each well ($e_{M,|\mu\rangle}$) are shown in tables 3.1 and 3.2. The states are labelled according to the scheme used by Elsässer *et al*, in which M is the number of energy quanta involved in the excitation and $|\mu\rangle$ shows the eigenfunctions into which the quanta are placed. The tables show results from INS studies, the work of Elsässer *et al*, and the energies calculated using the method described above. The energies were calculated both at the experimentally determined lattice constant of 4.095 Å and 4.16 Å, close to the calculated value.

The states $|A\rangle$, $|B\rangle$, $|C\rangle$ are defined by Elsässer *et al* as follows:

$$|A\rangle = \left(1/\sqrt{2}\right)(|200\rangle - |020\rangle) \tag{3.1}$$

$$|B\rangle = \left(1/\sqrt{6}\right)(|200\rangle + |020\rangle - 2\,|002\rangle) \tag{3.2}$$

$$|C\rangle = \left(1/\sqrt{3}\right)(|200\rangle + |020\rangle + |002\rangle) \tag{3.3}$$

The ground state energies and excitation energies calculated in this study are lower than those calculated by Elsässer *et al* which is consistent with the use of a larger lattice constant, and hence a shallower potential. As in the study of Elsässer *et al* excitation energies involving double excitation in any one direction (for example $e_{2,|200\rangle}$) are found to be higher than predicted using a harmonic potential (i.e. greater than twice $e_{1,|100\rangle}$). This is due to the anharmonicity of the potential in the direction of the surrounding palladium atoms which has a shallow well which becomes very steep.

The different states can be identified by their degeneracies and by viewing real space plots of the related wave functions. Plots of relevant wave functions can be seen in figure 3.3. The states labelled $E_{0,|000\rangle}$, $e_{1,|100\rangle}$, $e_{2,|110\rangle}$ and $e_{3,|111\rangle}$ have s, p, d and f-like symmetries respectively. As predicted, the state labelled $e_{2,|C\rangle}$ is the in-phase combination of three different 2p-like states.

Table 3.1: Zero-point energies and excitation energies for ^{1}H, ^{2}D and ^{3}T in the octahedral site in meV

	^{1}H	^{2}D	^{3}T
$E_{0,\|000\rangle}$			
a = 4.16 Å	61	39	28
a = 4.095 Å	79		
Calc.[45]	78	51	40
$e_{1,\|100\rangle}$			
a = 4.16 Å	54	34	25
a = 4.095 Å	64		
Calc.[45]	62	40	32
Expt. (β phase)	60[42], 56[36], 57[43]	40[42]	
Expt. (α phase)	69[42]	46.5[42]	
$e_{2,\|110\rangle}$			
a = 4.16 Å	104	65	50
a = 4.095 Å	123		
Calc.[45]	117	78	61
Expt. (β phase)	110[36], 115.5[43]		
Expt. (α phase)	115[42]		
$e_{2,\|C\rangle}$			
a = 4.16 Å	123	78	60
a = 4.095 Å	142		
Calc.[45]	132	88	69
Expt. (β phase)	135[36], 139[43]		
Expt. (α phase)	137[42]		
$e_{2,\|A\rangle} = e_{2,\|B\rangle}$			
a = 4.16 Å	133	82	62
a = 4.095 Å	151		
Calc.[45]	147	94	73
Expt. (β phase)	148[36], 155[43]		
Expt. (α phase)	156[42]		
$e_{3,\|111\rangle}$			
a = 4.16 Å	148	95	73
a = 4.095 Å	178		
Expt. (β phase)	$\approx$ 170 [43]		

Table 3.2: Zero-point energies and excitation energies for ^{1}H, ^{2}D and ^{3}T in the tetrahedral site in meV

	^{1}H	^{2}D	^{3}T
$E_{0,\|000\rangle}$			
a = 4.16 Å	171	114	109
a = 4.095 Å	207		
Calc.[45]	213	150	123
$e_{1,\|100\rangle}$			
a = 4.16 Å	121	86	71
a = 4.095 Å	128		
Calc.[45]		92	77

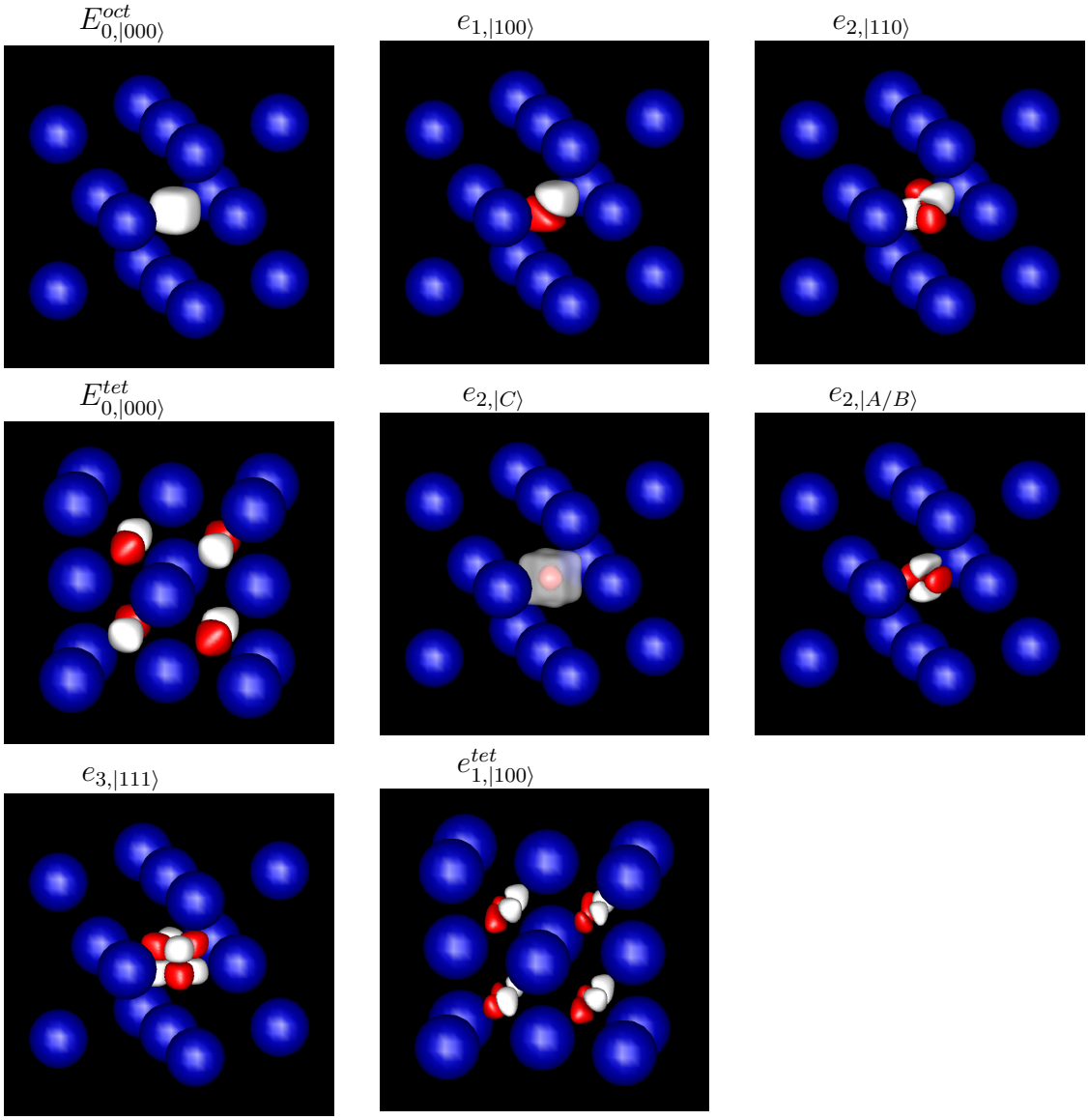

Figure 3.3: The real part of some ^{1}H wave functions labelled in a similar way to table 3.1

3.3 Hydrogen Diffusion

3.3.1 Experimental Studies

The temperature dependence of the diffusivity of hydrogen and its heavier isotopes in palladium has been studied extensively using many different techniques. A review of many of the earlier studies is provided by Völkl and Alefeld[46].

Hydrogen and its isotopes are found to diffuse with Arrhenius behaviour in the temperature regions investigated and the diffusion coefficients can then be fitted with an expression of the form:

$$D\left(T\right) = D_0 e^{-\frac{E_a}{k_B T}} \tag{3.4}$$

A collection of values of D_0 and E_a for fits of experimentally determined diffusion coefficients at temperatures above 200 K is given in table 3.3.

In all cases in which the diffusion of the two isotopes have been compared the activation energy of deuterium is less than that of hydrogen. This leads to an inverse isotope effect in which the heavier isotope, deuterium, diffuses faster than the lighter, hydrogen. There is currently insufficient evidence to comment on the relative diffusion rate of tritium, although Völkl and Alefeld[46] suggest that tritium has a lower rate of diffusion than the other two isotopes, and the activation energy given by Sicking and Buchold[47] is high compared to that obtained for the other isotopes in other studies.

There is some evidence from NMR studies that at low temperatures (< 200 K), hydrogen diffuses with a much reduced activation energy. Cornell and Seymour [48] find an activation energy of 100±20 meV between 100 K and 195 K in $PdH_{0.7}$, although it is stressed that this data is not as reliable as that recorded at higher temperatures.

There has been much discussion over the mechanism of hydrogen diffusion in palladium. Bohmholdt and Wicke's work[49] suggests two possible mechanisms. The first is a simple transition from one octahedral site to the neighbouring site. The second is a similar transition involving the hydrogen atom moving through the tetrahedral site in-between the two octahedral sites, but not getting trapped there.

Relaxation times calculated in NMR studies suggest that only one process is important. A model considering only jumps between neighbouring octahedral sites fits the data well[48][50]. Studies using other methods have suggested that the diffusion mechanism

may be more complicated. Beg and Ross[51] suggest that in the β-phase diffusion is modelled more accurately by considering other processes alongside jumps between nearest neighbour octahedral sites, such as non-nearest neighbour jumps and jumps involving the tetrahedral sites. Similar comments have been made by Rowe *et al*[41], Kuballa and Baranowksi[52] and Majorowski and Baranowski[53].

Two paths for motion in-between two octahedral sites are shown in figure 3.4. One involves direct motion from one site to the next, the other involves passage through an intervening tetrahedral site. The hydrogen atom may or may not be trapped in the tetrahedral site as it passes through.

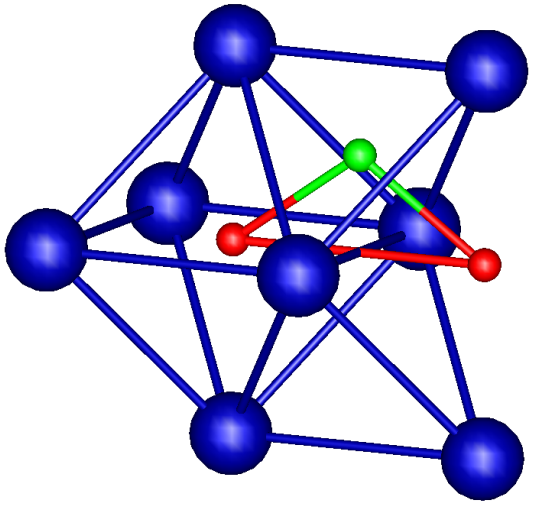

Figure 3.4: Two paths between neighbouring octahedral sites (red) The tetrahedral site is marked in green.

Table 3.3: D_0 in $\times 10^{-3}$ $cm^2 s^{-1}$ and E_a in meV for fits of the diffusion coefficient of hydrogen isotopes in palladium to Arrhenius behaviour from experimental studies. x is the molar fraction of the hydrogen isotope and palladium.

Reference	^{1}H			^{2}D			^{3}T		
	x	D_0	E_a	x	D_0	E_a	x	D_0	E_a
Bohmholdt and Wicke, 1967[49]	0.743	5.7±1.4	249±6.5	0.708	3.5±0.9	230±6.5			
Holleck and Wicke, 1967[54]	0.695	11±3.9	265±11	0.665	8±2.8	247±11			
Beg and Ross, 1970[51]	β-phase	1.1	147						
Völkl *et al*, 1971[55]	0.2–0.6	2.5±0.5	226±0.6	0.2–0.6	1.7±0.6	206±0.7			
Sicking and Buchold, 1971[47]							V. Low	10.5±3.0	275±13
Seymour *et al*, 1975[50]	0.7	0.9(3)	228(6)						
Katsuta *et al*, 1979[56]	≈0.01	2.83±0.15	225±13						
Majorowski and Baranowski, 1982[53]	0.8–0.98	11.3±0.2	287±4	0.8–0.98	10.5±0.2	268±5			

3.3.2 Simple Estimation of Activation Energies

A simple estimation of the activation energy was made by dragging the hydrogen atom from the octahedral site to a neighbouring tetrahedral site or octahedral site and performing DFT calculations along the path. The palladium atoms were held rigid during the procedure, with a lattice constant of 4.15 Å.

The transition state for the path from the octahedral to tetrahedral site was found at (0.35,0.35,0.35). The barrier from the octahedral site to this point, ignoring ZPE, was calculated as 198 meV, and from the tetrahedral site was 209 meV.

The ZPE of the hydrogen atom at the transition state was estimated by performing a similar calculation to that described in section 3.1.2 and including the ZPE from the two modes perpendicular to the diffusion path. The ZPE at the transition state was calculated as 182 meV. The activation energies including ZPEs are then 312 meV from the octahedral site and 197 meV from the tetrahedral site.

Assuming that the ZPE for a deuterium atom is $\frac{1}{\sqrt{2}}$ times that of the hydrogen atom, a similar calculation gives an activation energy of 279 meV from the octahedral site and 201 meV from the tetrahedral site. Schematic diagrams of these calculations can be seen in figure 3.5.

Although the estimated activation barriers are considerably larger than the experimental values discussed in the previous section, the inverse isotope dependence of the activation energies has been reproduced. The ZPE of the diffusing atom at the transition state is high since the atom must pass between three close palladium atoms. This ZPE is reduced by a much larger amount than the ZPE in the relatively shallow octahedral well when moving to a heavier isotope.

A similar procedure was carried out for the path directly linking two neighbouring octahedral sites. The activation energy for this process, ignoring ZPEs, was calculated to be 1160 meV. This is much higher than the barrier to the tetrahedral site. The hydrogen atom is not at a true transition state at the top of the barrier since motion towards both the octahedral and tetrahedral sites is downhill. Only the mode involving motion towards the neighbouring palladium atoms has positive curvature.

The calculated barriers are in general agreement with the barriers calculated by Elsässer *et al* using a similar method with a LDA functional[45].

The path between two octahedral sites via the tetrahedral site is a much lower energy process. Diffusion is much more likely to occur as a result of a mechanism involving this path than by direct motion between two octahedral sites.

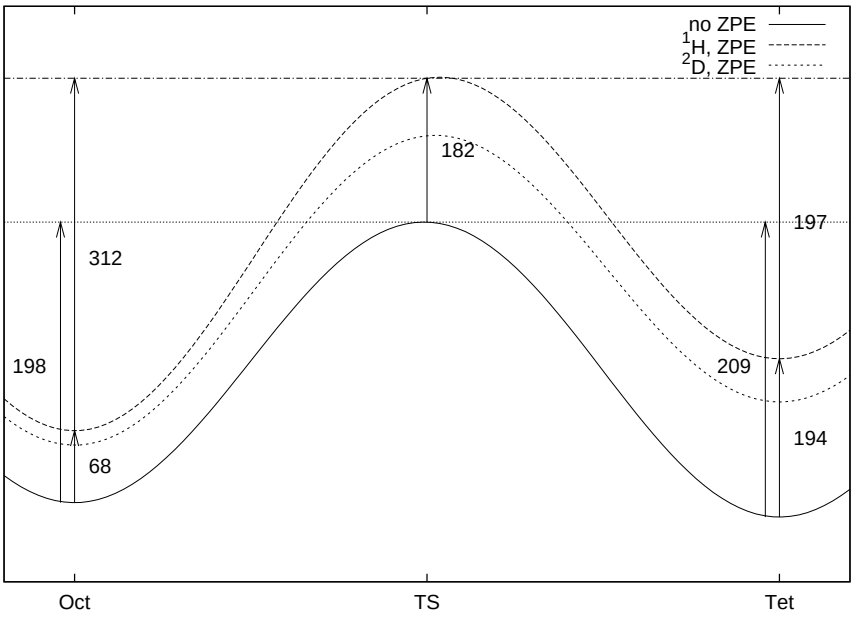

(a)

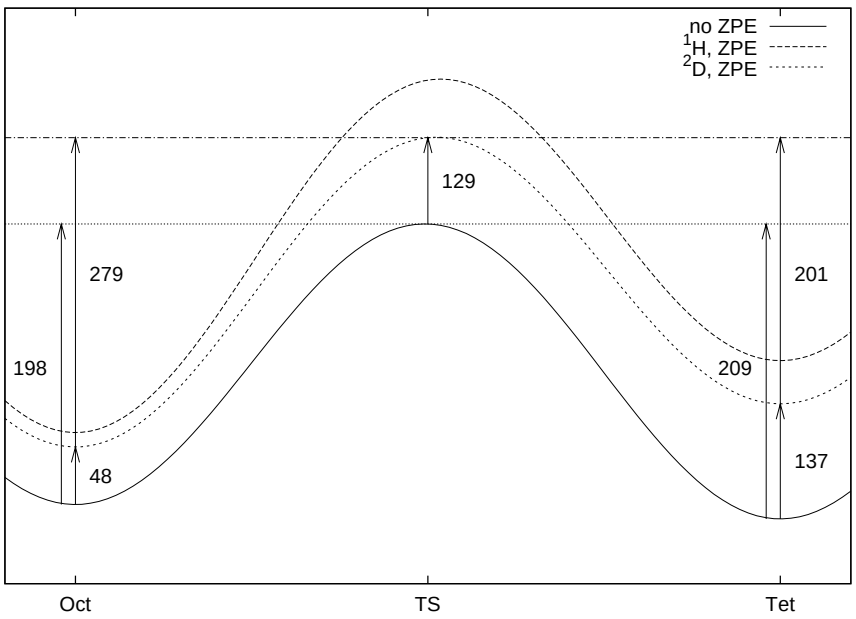

(b)

Figure 3.5: A schematic diagram of the diffusion path for (a) ^{1}H and (b) ^{2}D from the octahedral site to the tetrahedral site. Calculated ZPEs and activation energies are in meV. The curve for the other isotope has been included for comparison.

3.3.3 Kubo Formula

The energies and wave functions for hydrogen and its isotopes calculated in section 3.2 were used in equation 1.39 to calculate diffusion coefficients at different temperatures.

Computational Details

The δ-function in equation 1.39 was replaced with a Gaussian function with finite width.

$$\delta\left(E_N - E_M\right) \approx \frac{1}{\sigma\sqrt{2\pi}}\, e^{\frac{\left(E_N - E_M\right)^2}{2\sigma^2}} \tag{3.5}$$

The width, σ,was chosen by performing calculations with varying widths and choosing a width in the region where the diffusion coefficients varied slowly with respect to changing it. A set of diffusion curves with varying σ can be seen in figure 3.6. In the following calculations the width was chosen to be 1 meV.

The diffusion coefficients calculations were converged with respect to the number of plane-waves used to calculate the energies and wave functions, and the number of states included in the sum over momentum matrix elements in equation 1.39. A summary of the parameters required for convergence is given in table 3.4.

Table 3.4: Converged parameters for diffusion coefficient calculations.

	^{1}H	^{2}D	^{3}T
Size of grid used for wave function	48^3	64^3	80^3
Corresponding plane-wave cutoff [eV]	0.68	0.61	0.63
Number of states included in sum	800	1200	3000

All calculations were carried out at the Γ-point (k=0). The states studied in section 3.2 were well bound and a test calculation on a 6^3 k-point grid showed little difference in the diffusion coefficients when other k-points were included.

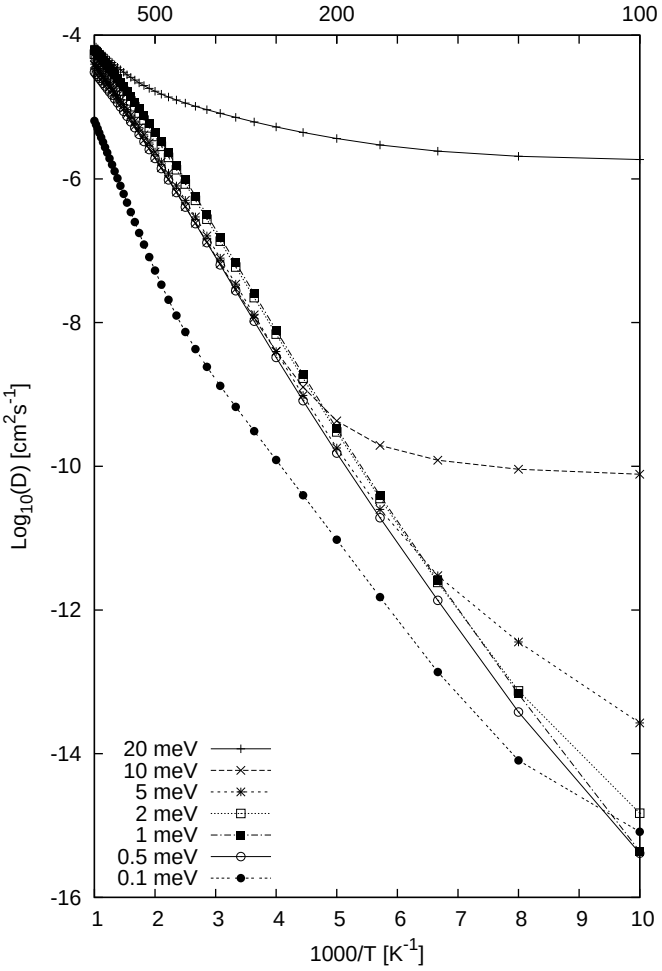

Figure 3.6: The diffusion coefficient of ^{1}H in PdH calculated with varying Gaussian widths, σ.

Results and Discussion

The diffusion coefficients of ^{1}H, ^{2}D and ^{3}T were calculated in stoichiometric palladium hydride over a range of temperatures. The calculations were performed at lattice constant of 4.16 Å close to the theoretically predicted value. The resulting diffusion curves can be seen in figure 3.7.

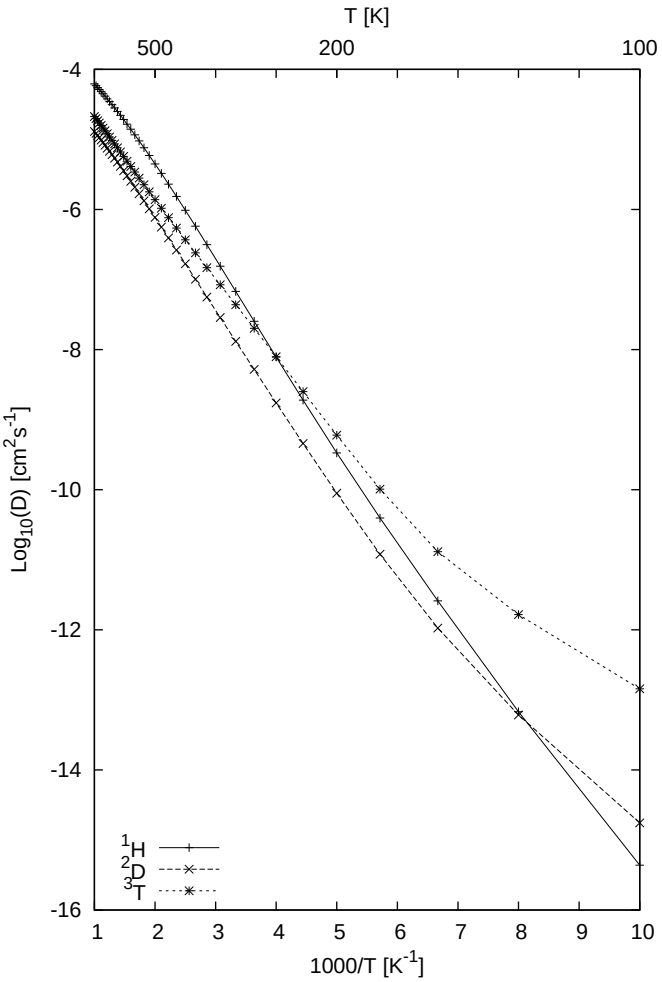

Figure 3.7: The diffusion coefficients of ^{1}H, ^{2}D and ^{3}T over a temperature range of 100 K – 1000 K

The diffusion curves between 250 K and 500 K in figure 3.7 were fitted to Arrhenius expressions for comparison with experiment. The fitted values of D_0 and E_a can be seen in table 3.5.

Table 3.5: Parameters of an Arrhenius fit of diffusion coefficients. between 250 K and 500 K

	^{1}H	^{2}D	^{3}T
D_0 [10^{-3} cm^{2}s^{-1}]	2.7	0.35	0.23
E_a [meV]	274	263	222

The activation energies for ^{1}H and ^{2}D obtained from the Arrhenius fits fall within the range of values obtained by experimental methods (see table 3.4). The inverse isotope effect in the activation energies is reproduced with a ratio $E_a(^1\text{H})/E_a(^2\text{D})$ of 1.04 compared to 1.07–1.10 from the data in table 3.4. The values are closest to those given by Majorowski and Baranowski[53] who used samples near to stoichiometric palladium hydride.

Although the value of D_0 falls roughly within the range of experimental data for ^{1}H it is lower than that obtained by Majorowski and Baranowski and Holleck and Wicke[54], who obtained similar activation energies. The value of D_0 for ^{2}D is lower than would be expected. As a result, the rate of diffusion of both ^{1}H and ^{2}D is underestimated with respect to experiment for temperatures above 250 K and the low value of D_0 for ^{2}D means that there is no inverse isotope effect in the diffusion coefficients themselves, in spite of the one present in the activation energies. An inverse isotope is only seen in figure 3.7 at low temperatures (< 120 K).

The values of D_0 and E_a obtained for ^{3}T are considerably different from those obtained by Sicking and Buchold[47]. Their investigation was performed with a very low concentration of tritium in palladium, as there is little other experimental evidence with which to compare these values. Following a similar argument to that given in the previous section (3.3.2), tritium would be expected to have a lower barrier to diffusion than hydrogen and deuterium as obtained in these calculations, rather than a higher barrier as shown by Sicking and Buchold.

The sum over states in equation 1.39 only contains contributions from states which are close in energy due to the δ-function in the formula. As a result, it is possible to collect contributions from different regions of the energy spectrum and analyse the results in terms of which states contribute to diffusion.

Plots of the contributions from separate regions of the energy spectrum can be seen in figures 3.8 and 3.9. The proportion of each contribution arising from the octahedral and tetrahedral wells is shown alongside the total contribution at each energy.

By integrating each wave function over the octahedral and tetrahedral sites it was possible to identify each state as either predominantly bound in the octahedral site, in the tetrahedral site, or spread over both sites. The proportion of each contribution arising from the octahedral and tetrahedral wells is shown alongside the total contribution at each energy.

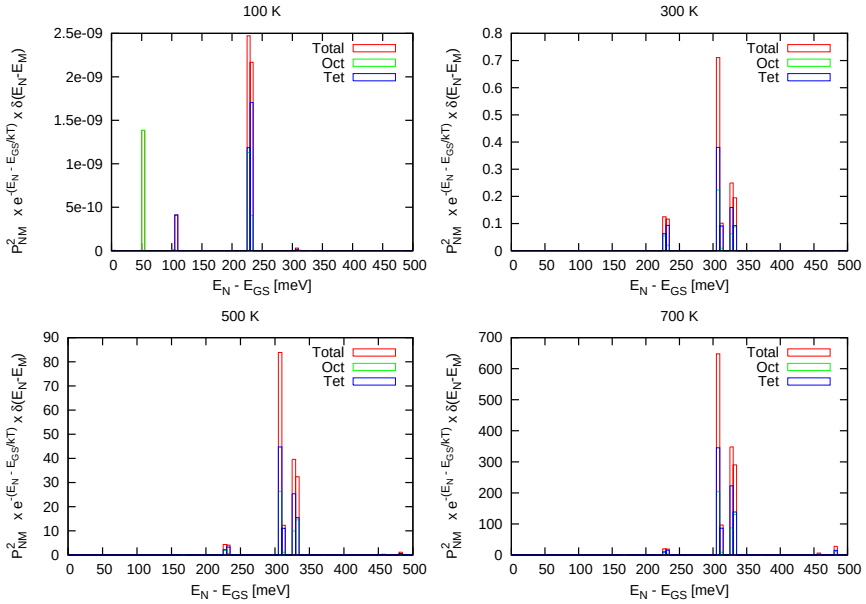

(a)

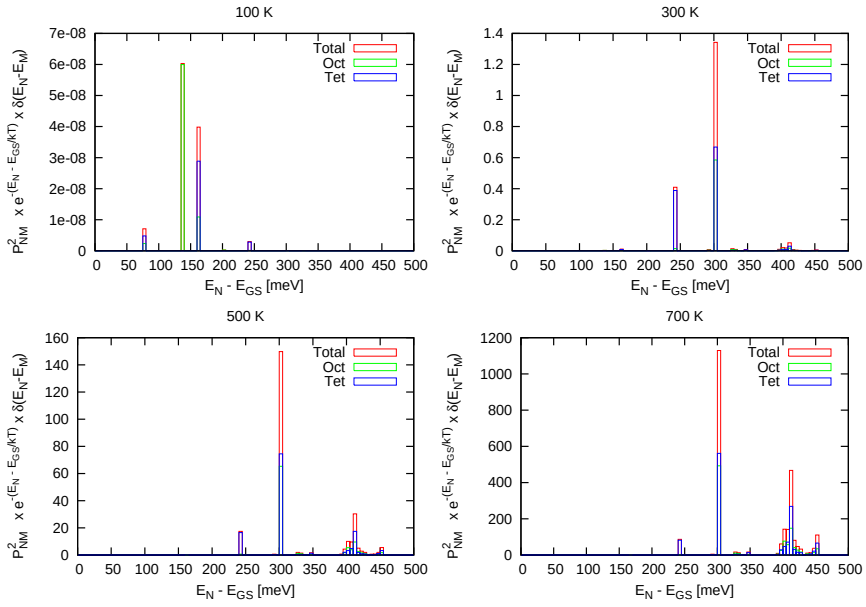

(b)

Figure 3.8: The contributions to the diffusion coefficient from different regions of the eigenspectrum below 500 meV above the ground state for (a) ^{1}H and (b) ^{2}D

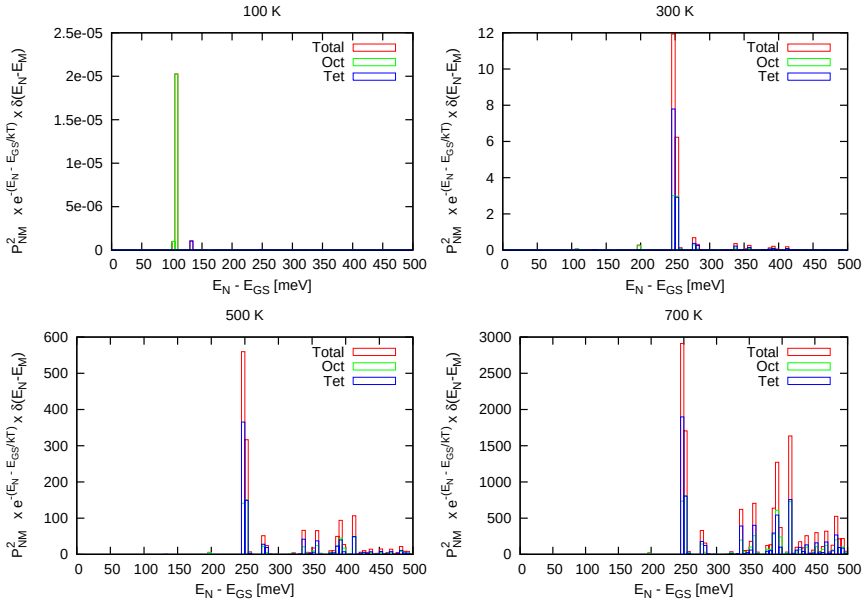

Figure 3.9: The contributions to the diffusion coefficient from different regions of the eigenspectrum below 500 meV above the ground state for ^{3}T

For ^{1}H diffusion above 250K there are three main regions in the energy spectrum which contribute to diffusion. The lowest in energy is at 228 meV above the octahedral ground state. This is considerably below the 312 meV barrier predicted for classical diffusion.

Each contribution involves a pair of states. The largest contributions come from pairs of states of which one state is in the octahedral sites and the other is one of the $e_{1,|100\rangle}$ states in the tetrahedral sites described in section 3.2. There are also contributions involving states in which both sites are occupied, but in which there is no occupation of the barrier region in between the sites. A plot of some of the contributing states in this region is shown in figure 3.10.

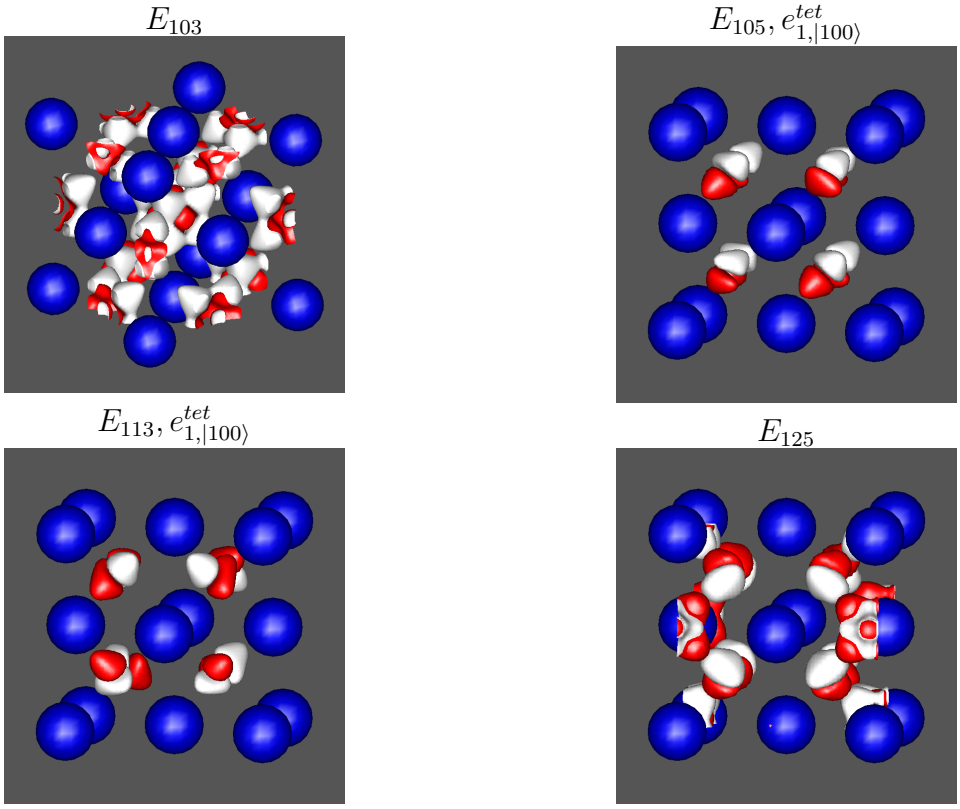

Figure 3.10: The real part of some of the ^{1}H wave functions contributing to diffusion at 228 meV above the ground state. The 103-rd and 105-th states form a contributing pair in which the 103-rd is in the octahedral sites, and the 105-th in the tetrahedral sites. The 113-th and 125-th states form a pair in which the 113-th state is in the tetrahedral well and the 125-th in both.

The next lowest energy contributions come from 305–307 meV and 328 meV in the region of the classical barrier. These contributions arise once again between pairs of states of which one state is predominantly in the tetrahedral sites and the other is either in the octahedral sites or shared between the two sites. The states are now more diffuse and some occupation is seen in the region of the barrier between the octahedral and tetrahedral

sites. Plots of one pair of contributing states in the 307 meV region is shown in figure 3.11.

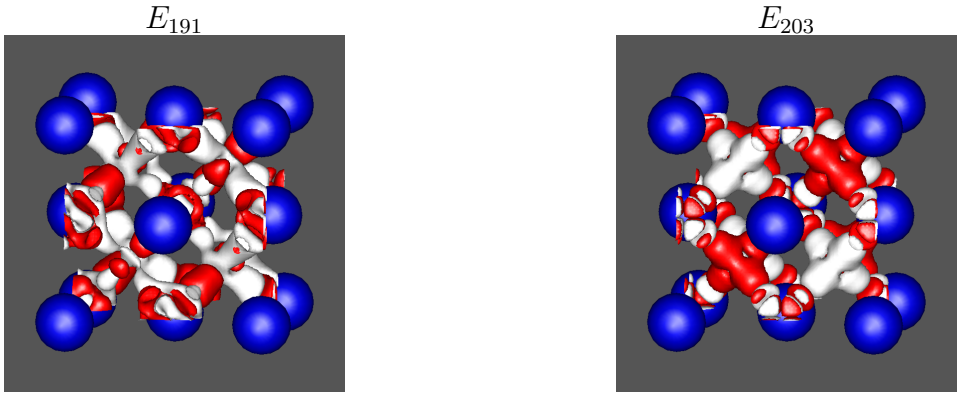

Figure 3.11: The real part of two of the ^{1}H wave functions contributing to diffusion at 307 meV above the ground state. The 191-st and 203-rd states form a contributing pair in which the 203-rd is predominantly in the tetrahedral site, and the 191-st is spread over the two sites.

Hydrogen diffusion occurs when states which are in the octahedral and tetrahedral wells become close in energy. This can occur either below or above the classically allowed barrier, and contributions come from both types of processes. The processes involving diffusion below the barrier are still activated processes. The hydrogen must be excited from the octahedral ground state into an excited state in the octahedral well, from which it can tunnel into the tetrahedral well. Thus diffusion at temperatures above 250 K occurs by paths between the octahedral ground states via paths involving excited states in the tetrahedral well, and not directly between two states in different octahedral wells.

The activation energy seen in the Arrhenius fits to the diffusion curves arises by a weighted average of the contributions from different regions of the energy spectrum.

The contributions to diffusion above 250 K for ^{2}D arise at lower energies than those in ^{1}H. They arise from pairs of states at 243 meV, 292 meV, 305 meV and 420 meV. As a result the activation energy for ^{2}D diffusion is lower than that for ^{1}H. The inverse isotope effect in the activation energies occurs as a result of the increase in density of states at low energies on increasing mass. The same effect also leads to a lower activation energy for ^{3}T.

The pairs of states contributing to ^{2}D and ^{3}T diffusion are similar to those contributing to ^{1}H diffusion. They involve pairs in which one state is predominantly in the tetrahedral site and the other is either in the octahedral site or is a mixture of states in both sites. This suggests that the mechanism for diffusion for all three isotopes is similar.

Diffusion of hydrogen isotopes in palladium hydrides at low temperatures does not follow the Arrhenius law seen above 250 K. The curves in figure 3.7 show considerable deviation from Arrhenius behaviour in the low temperature regions. The diffusion coefficients for ^{1}H and ^{2}D from 10 K to 250 K are shown in figure 3.12. In addition the contributions to the diffusion coefficient at 50K are shown in figure 3.13.

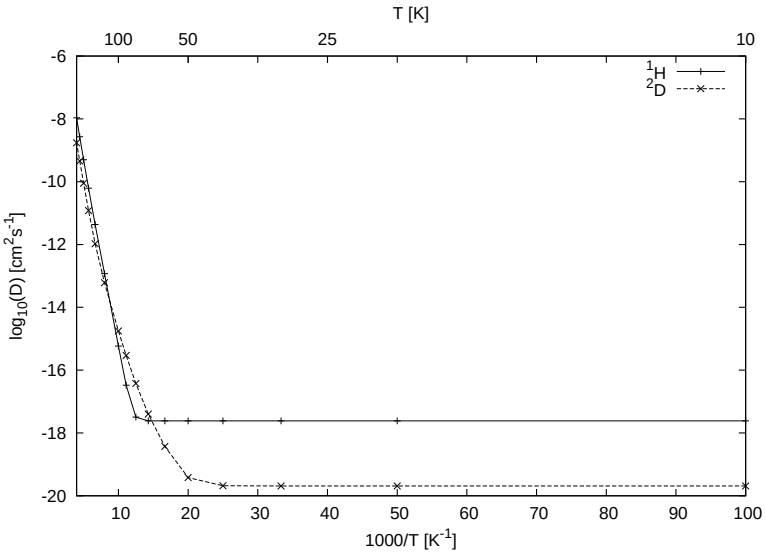

Figure 3.12: The diffusion coefficients of ^{1}H and ^{2}D in the temperature range 10–250 K.

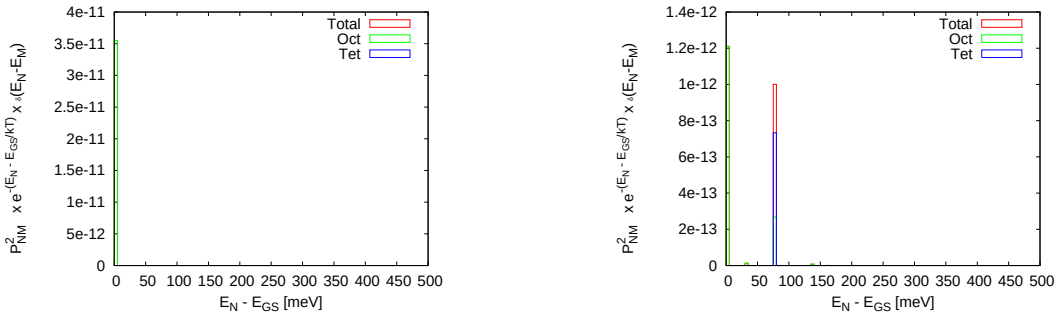

(a) (b)

Figure 3.13: The contributions to (a) ^{1}H and (b) ^{2}D diffusion from different regions of the energy spectrum at 50 K.

The contributions to ^{1}H diffusion at 100 K shown in figure 3.8(a) between pairs of states at 54 meV and 110 meV above the octahedral ground state. These contributions arise due to tunnelling between the first excited states $e_{1,|100\rangle}$ in different octahedral wells (54 meV) and the ground state in different tetrahedral wells (110 mev).

At 50 K the only noticeable contribution occurs due to tunnelling between octahedral ground states. The diffusion process is no longer an activated process and as a result the diffusion coefficient no longer varies with temperature.

^{2}D diffusion at 100 K shows contributions at 76–78 meV, 137 meV and 160–162 meV. The contributions at 76–78 meV arise from pairs of states in which one state is a ground state in the tetrahedral well, and the other is one of the $e_{2,|C\rangle}$ states in the octahedral well which are at a similar energy. The contributions at 137 meV come from tunnelling between excited states in different octahedral wells and those at 160–162 meV from pairs of states in which one is an excited state in the octahedral wells, and the other is one of the first excited states in the tetrahedral wells.

At 50 K only tunnelling between octahedral ground states and the contributions at 76–78 meV are seen for ^{2}D. Below 30 K only the octahedral ground states are occupied and the diffusion coefficient becomes invariant with temperature, as seen in ^{1}H. The ^{2}D ground state wave functions are more tightly bound, and hence have less overlap than the ^{1}H wave functions, leading to slower diffusion for ^{2}D in this temperature range.

The major contribution to ^{3}T diffusion at 100 K is from pairs of excited states in the octahedral wells at 104 mev.

Since at low temperatures the states which contributed strongly to diffusion above 250 K are thermally inaccessible different states contribute to diffusion. As well as contributions due to tunnelling between the octahedral and tetrahedral wells, tunnelling between states which are both in octahedral or both in tetrahedral wells now contributes. At low enough temperatures diffusion is dominated by tunnelling between ground states in the octahedral wells since other states are not accessible.

Lattice Phonons

In the previous calculations it has been assumed that the lattice remains static as the hydrogen atom diffuses from one site to the next. The lattice vibrations have been used as a bath to allow occupation of states according to Boltzmann statistics.

The Debye frequency of palladium (the maximum frequency of phonons in the crystalline solid) is 394.4 cm^{-1}. This gives a maximum separation of phonon energy levels of 49 meV in pure palladium, a similar magnitude to the gaps seen in the vibrational energy levels of the hydrogen isotopes in palladium hydride. It seems likely that coupling between lattice

phonon modes and hydrogen wave functions will have an effect on the rates of diffusion of hydrogen and its isotopes.

The full coupled system is too large a problem to tackle exactly. Consideration of a simple model potential, based on hydrogen transport in a one-dimensional potential coupled to a fully quantum mechanical harmonic oscillator, may give an insight into the effect that coupling to phonons has on diffusion, and how best these effects can be included when calculating diffusion coefficients in more realistic systems.

3.4 Conclusions

A quantum mechanical treatment of hydrogen and its isotopes in palladium gives an insight into both the location of hydrogen in palladium hydride and its diffusion.

The ground states and low lying excited states of hydrogen, deuterium and tritium are all found to be tightly bound in one of two types of sites, octahedral sites or the tetrahedral sites. The ground state in the octahedral site is more stable than that in the tetrahedral site by 110 meV for ^{1}H, 76 meV for ^{2}D and 60 meV for ^{3}T. Assuming Boltzmann statistics this would give an occupation of ≈ 1 % ^{1}H for the tetrahedral ground state, and ≈ 10 % ^{3}T at 298 K.

Density functional theory calculations predict the tetrahedral site to be more stable than the octahedral site. A quantum mechanical approach to hydrogen dynamics is essential, since including the hydrogen zero point energies reverses the relative stabilities of the two sites.

Using the calculated wave functions and energies in a equation 1.39 to calculate diffusion coefficients shows that above 250 K the temperature dependence of the diffusion coefficients is Arrhenius.

At these temperatures diffusion occurs by two types of processes. Diffusion occurs by occupation of diffuse states above the classical barrier, and by tunnelling between pairs of states below the classical barrier, one of which is in based at the octahedral site, and the other at the tetrahedral site. Although this is a quantum tunnelling process, it is nevertheless an activated process since the states involved are not the ground state for the system.

Diffusion is found to become non-Arrhenius at lower temperatures. Other quantum processes are now found to contribute, tunnelling between ground states and excited states in neighbouring octahedral sites and similar processes between states in neighbouring tetrahedral sites. More experimental work needs to be done to investigate the diffusion of hydrogen in β-PdH at low temperatures and discover this non-Arrhenius behaviour.

The relative diffusion rates of the different isotopes depend both on the number of tunnelling processes which contribute and on the amount of diffusion which arises from the processes. In general the heavier isotopes, ^{2}D and ^{3}T have a higher density of states at low energies, so the probability of finding the degenerate or near-degenerate states which contribute to diffusion is higher. However the states of the heavier isotopes tend to be more tightly bound than ^{1}H states, and there is less tunnelling between them.

In palladium hydride these effects lead to an inverse isotope effect in the activation energies to diffusion, since considerably more below the barrier tunnelling occurs with ^{2}D and ^{3}T than with ^{1}H.

Although the methods used in this study reproduced experimental vibrational energies and activation energies of diffusion, the absolute values of the diffusion coefficients were underestimated and deuterium was not found to have a higher diffusion coefficient than hydrogen above room temperature.

It is likely that coupling between hydrogen states and phonon states in the palladium lattice, which is neglected in these calculations, has a large effect on diffusion rates. Further study is needed to investigate the rôle which phonon coupling has in hydrogen diffusion.

Chapter 4

Other Materials

A similar method to that used to study the hydrogen eigenstates and diffusion coefficients in palladium hydride was used to study niobium hydride and lithium imide. This work was carried out in collaboration with Dr Changjun Zhang[57][58].

4.1 Niobium Hydride

Niobium hydride has a complicated phase diagram depending on temperature and hydrogen concentration. Stoichiometric NbH has been shown to be in the ordered β-phase at most temperatures[59][60]. The β-phase has a face centred orthorhombic lattice[61], in which the niobium atoms form a slightly distorted body centred cubic (BCC) lattice and the hydrogen atoms reside in the tetrahedral interstitial sites. Since the distortions away from this ideal structure are very small (≈ 0.01Å in the lattice constant) calculations were made using a simple BCC lattice for the niobium atoms. This structure of β-NbH can be seen in figure 4.1.

The plane-wave based DFT code, CASTEP, was used to perform electronic structure calculations on the NbH system. The core electrons of the niobium atoms were replaced by an ultrasoft pseudopotential and the PBE functional was used to calculate energies. A plane-wave cutoff of 400 eV was sufficient for convergence and calculations were performed over a 12^3 k-point grid.

The niobium atoms were placed in a BCC cell and the hydrogen atoms at tetrahedral interstitial sites. The lattice constant was then varied to find the equilibrium value. The

lattice constant was calculated as 3.47 Å, in excellent agreement with experimentally determined values of 3.45–3.48 Å[61].

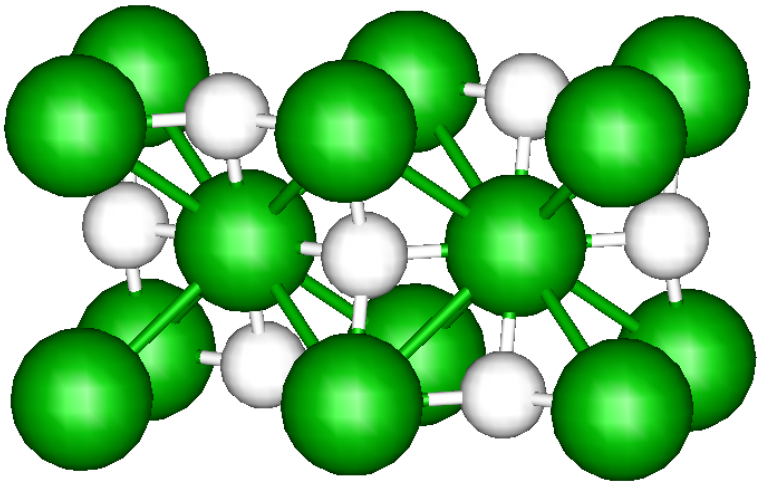

Figure 4.1: An idealised unit cell of the β-NbH system showing the hydrogen atoms in tetrahedral sites

4.1.1 Hydrogen Energy Levels

The vibrational energy spectra of hydrogen and its isotopes in niobium have been studied by inelastic neutron scattering (INS)[62][63][64][65]. These investigations have been carried out on different phases of NbH_x and at different concentrations of hydrogen.

The vibrational energy levels of γ-NbH, were calculated by Tao *et al*[66] using a similar method to that used by Elsässer *et al*[45] when calculating energy levels in β-PdH. The structure of γ-NbH is similar to that of β-NbH, with the hydrogen atoms occupying a different combination of tetrahedral sites. A potential was calculated for the hydrogen atom in a niobium lattice by calculating the energy of the system with the hydrogen at 35 positions in the unit cell. The energy calculations were carried out using DFT with an LDA functional, norm-conserving pseudopotentials and a mixed basis of plane-waves and local functions. The points were fitted to a Fourier series which was used to calculate hydrogen energy levels by expanding the hydrogen wave functions in a plane-wave basis.

Elsässer *et al* showed that these results are close to those calculated using a simple local polynomial potential in the harmonic approximation[45], suggesting that the anharmonicity in NbH is weak.

The energies and wave functions of hydrogen and its isotopes in a BCC lattice of niobium atoms were calculated using the same method described in section 3.2. A potential was calculated on a 32^3 cubic grid in real space, by carrying out single point electronic structure calculations with the hydrogen atom at different locations within the BCC unit cell. The lattice constant was set to the calculated equilibrium value of 3.47 Å.

The single point calculations were carried out using the plane-wave based DFT code, CASTEP, as described in the previous section. A contour plot of the potential in the 100 plane of the lattice can be seen in figure 4.2. The tetrahedral sites were found to be at minima in the potential, but unlike in the PdH system, the octahedral sites were found to be at maxima.

Once the potential was obtained in real space it was transformed into Fourier space and hydrogen wave functions and energies found by solving a set of Bloch equations. The wave functions and energies were calculated at the Γ-point (k=0). The number of plane-waves was increased until the calculations had converged. In order to reach convergence the potential was interpolated onto 48^3, 64^3 and 72^3 grids for ^{1}H, ^{2}D and ^{3}T respectively. This corresponded to imposing spherical cutoffs of 0.98 eV, 0.87 eV and 0.73 eV to the

plane-wave kinetic energies.

The results of these calculations are shown in table 4.1 alongside those obtained experimentally and those calculated by Tao *et al*[66]. In some cases the calculation produced a spread of energies due to mixing between the 12 tetrahedral sites in the cubic BCC unit cell. As in section 3.2 the states have been labelled according to the scheme used by Elsässer *et al*.

The calculated results are close to those observed in experiments and to those calculated by Tao *et al*. However, they underestimate experimental excitation energies by roughly 10%. The difference in energy between the $|100\rangle$ and $|010\rangle$ states, and the $|001\rangle$ states is due to the tetragonal symmetry at the tetrahedral sites.

Table 4.1: Zero-point energies and excitation energies for ^{1}H, ^{2}D and ^{3}T in meV. Experimental data was taken from references [62], [63], and [64].

	^{1}H	^{2}D	^{3}T
$E_{0,\|000\rangle}$			
Calculated	223	158	128
Tao *et al*[66]	237	169	139
$e_{1,\|001\rangle}$			
Calculated	109–112	81	67
Tao *et al*[66]	113	84	70
Expt.	114–122	81–89	72
$e_{1,\|010\rangle} = e_{1,\|100\rangle}$			
Calculated	147–152	109	90
Tao *et al*[66]	161	118	98
Expt.	160–167	111–125	101
$e_{2,\|002\rangle}$			
Calculated	193–217	155–157	131
Tao *et al*[66]	218	161	136
Expt.	227–233	166–170	

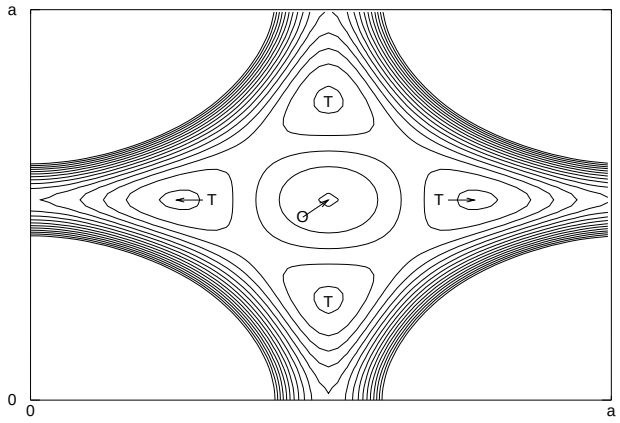

Figure 4.2: A contour plot of the potential in the 100 plane of the NbH lattice. The positions of the tetrahedral (T) and octahedral (O) sites are labelled. The tetrahedral sites are at minima in the potential, and the octahedral site at a maximum. In-plane niobium atoms are located at the corners of the plot, the out-of-plane niobium atoms are located behind the octahedral site. Contours are placed at intervals of 140 meV.

4.1.2 Hydrogen Diffusion

Experimental Results

The diffusion of hydrogen and its isotopes in niobium has been the subject of many experimental studies using a variety of experimental techniques. A comprehensive summary of early results was published by Völkl and Alefeld in 1978[46].

Most studies were made in niobium hydride samples with low hydrogen concentrations ($NbH_{<0.4}$). In these systems, hydrogen is found to have two regions of different Arrhenius behaviour. Above 273 K the temperature dependence of the diffusion coefficient can be fitted to an Arrhenius expression ($D(T) = D_0 e^{-\frac{E_a}{k_B T}}$) with $D_0 = 5.0 \times 10^{-4}$ cm^{2}s^{-1} and $E_a = 106$ meV. Below room temperature the activation energy becomes 68 meV and the pre-exponential, D_0, 0.90×10^{-4} cm^{2}s^{-1}. This behaviour has been observed to continue to temperatures as low as 34 K[67].

The diffusion of the other isotopes, ^{2}D and ^{3}T, follows the expected isotope behaviour at low concentrations. Tritium has the lowest diffusion coefficient and highest activation energy ($D_0 = 4.5 \times 10^{-4}$ cm^{2}s^{-1} and $E_a = 135$ meV) and the diffusion coefficient of deuterium lies between that of hydrogen and tritium ($D_0 = 5.2 \times 10^{-4}$ cm^{2}s^{-1} and $E_a = 127$ meV). Although diffusion with a different activation energy at low temperatures has not been seen for the heavier isotopes, Engelhard's results[67] suggest that deviation from Arrhenius behaviour is present for deuterium at 50 K.

Fewer studies have been made into the diffusion of hydrogen in niobium at higher concentrations. Results published by Völkl and Alefeld[46] suggest that the rate of diffusion is over an order of magnitude slower in β-$NbH_{0.9}$. A rough fit of the diffusion coefficients shown in [46] gives $D_0 \approx 5 \times 10^{-4}$ cm^{2}s^{-1} and $E_a \approx 240$ meV over the temperature range 300–400 K. No data is shown at lower temperatures or for ^{2}D and ^{3}T diffusion at this concentration.

Kubo Formula

The wave functions and energies calculated for β-NbH in section 4.1.1 were used in equation 1.39 to calculate the diffusion coefficients of ^{1}H, ^{2}D and ^{3}T in niobium with a molar ratio of 1:1.

The computational details were similar to those used for PdH in section 3.3.3. The width of the Gaussian function replacing the δ-function was 10 meV. A summary of the other parameters required for convergence is given in table 4.2.

Table 4.2: Converged parameters for diffusion coefficient calculations.

	^{1}H	^{2}D	^{3}T
Size of grid used for wave function	48^3	64^3	72^3
Corresponding plane-wave cutoff [eV]	0.98	0.87	0.73
Number of states included in sum	800	800	1500

The diffusion coefficients are plotted over the full range of temperatures at which they were calculated in figure 4.3. The same data is plotted in figure 4.4 over a smaller temperature range of 200–1000 K.

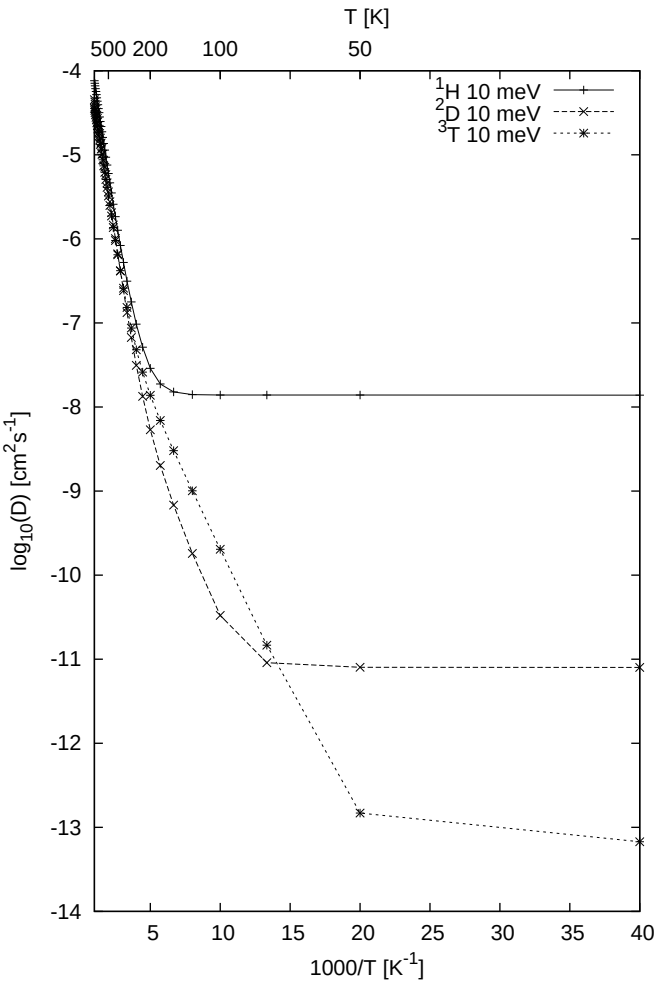

Figure 4.3: The diffusion coefficients of ^{1}H, ^{2}D and ^{3}T over a temperature range of 25 K – 1000 K

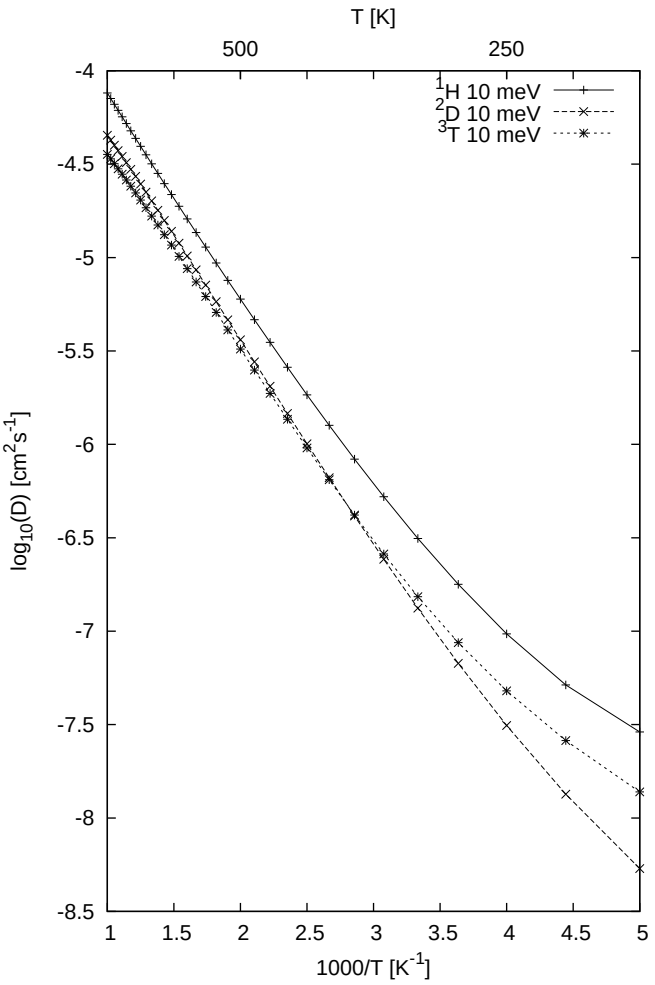

Figure 4.4: The diffusion coefficients of ^{1}H, ^{2}D and ^{3}T over a temperature range of 200 K – 1000 K

The temperature dependence of the diffusion coefficients of all three isotopes follow a roughly Arrhenius behaviour above room temperature. The results of Arrhenius fits of the diffusion coefficients between 300 K and 600 K are shown in table 4.3.

Table 4.3: Parameters of an Arrhenius fit of diffusion coefficients. between 300 K and 500 K

	^{1}H	^{2}D	^{3}T
D_0 [10^{-4} cm^{2}s^{-1}]	2.5	3.4	1.4
E_a [meV]	173	203	177

The Arrhenius fits of the calculated diffusion coefficients give higher activation energies than those found in experiments on the low concentration α-phase, but lower than the activation energy obtained for hydrogen diffusion in the β-phase. The rate of diffusion is certainly reduced as the concentration of hydrogen is increased.

Hydrogen is the fastest diffusing isotope at all temperatures, but tritium and deuterium are calculated to have very similar diffusion rates, deuterium diffusing faster at some temperatures and tritium at others. At very low temperatures the diffusion coefficient of deuterium is larger.

Below room temperature the diffusion coefficients are seen to deviate away from Arrhenius behaviour. Figure 4.3 shows that as the temperature is decreased the diffusion coefficients reach a plateau value. Hydrogen reaches this plateau first, then deuterium and finally tritium.

The temperature dependence of the diffusion coefficients can be analysed by plotting the contributions to diffusion arising from different sections of the energy spectrum. These plots are shown in figures 4.5 and 4.6.

Unlike in palladium, the hydrogen states in niobium lie in only one type of well. The pairs of states which contribute to diffusion at low energies are all pairs in which both states are in the tetrahedral sites.

At very low temperatures diffusion arises solely through tunnelling between ground states in different wells. There is no energy barrier to this process, and the plateau in the diffusion coefficients occurs when ground state tunnelling becomes the dominant process.

At higher temperatures the excited states become populated and tunnelling between excited states becomes important. As the excited states lie at lower energies for the heavier

isotopes these processes become important at lower temperatures for tritium and deuterium than they do for hydrogen. In the region that these processes dominate, diffusion occurs as an activated process, but the activation energy is lower than that predicted classically. The barrier in the potential between two tetrahedral sites, calculated using DFT, is roughly 230 meV.

Above 300 K processes involving transitions between states above the classical barrier become important and dominate at high temperatures. There is, however, still some contribution from tunnelling between lower lying excited states.

The diffusion of hydrogen and its isotopes in β-NbH seems to proceed by hops between neighbouring tetrahedral sites. These hops either occur by tunnelling at energies lower than the classical energy barrier or by transitions above this barrier.

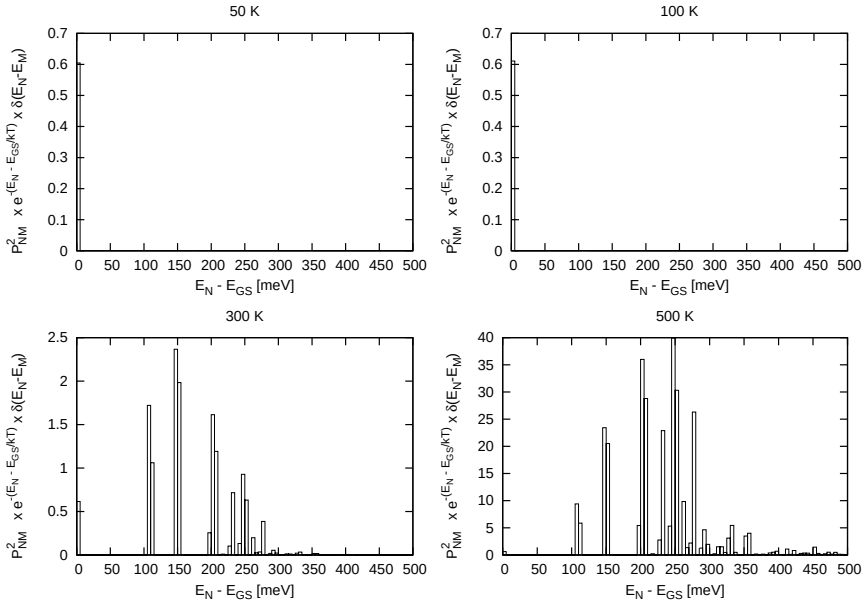

(a)

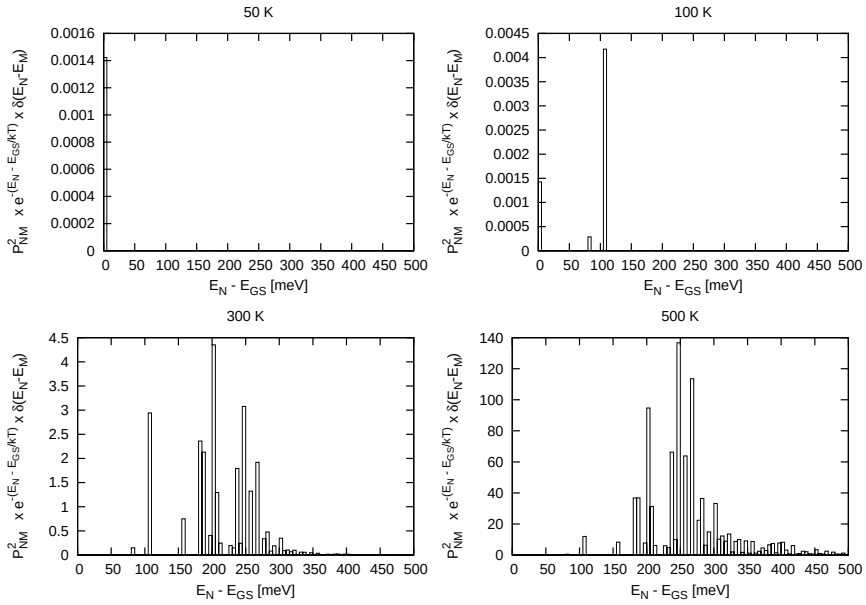

(b)

Figure 4.5: The contributions to the diffusion coefficient from different regions of the eigenspectrum below 500 meV above the ground state for (a) ^{1}H and (b) ^{2}D

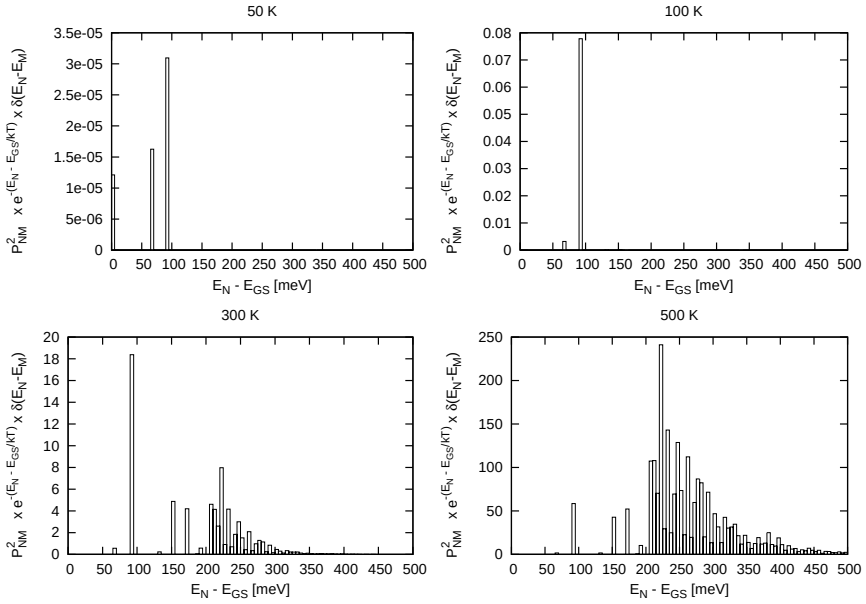

Figure 4.6: The contributions to the diffusion coefficient from different regions of the eigenspectrum below 500 meV above the ground state for ^{3}T

4.1.3 Conclusions

In contrast to the results for the face centred cubic (FCC) palladium hydride, hydrogen atoms in the body centred cubic (BCC) niobium hydride lattice only occupy one type of site. Quantum calculations have confirmed experimental predictions that the hydrogen atoms reside at the tetrahedral interstitial sites in the BCC niobium lattice. The excitation energies from this site show good agreement with those obtained by experiment and analysis of the corresponding excited state wave functions can be carried out to look at the properties of the excited states.

Diffusion of hydrogen and its isotopes in β-NbH(DT) occurs due to transitions between states in neighbouring tetrahedral sites. These transitions occur between states which are above and below the classical barrier to diffusion. Tunnelling between the ground states in neighbouring wells has a relatively higher contribution in niobium hydride than it does in palladium hydride, with some contribution from this process still important at 300 K for ^{1}H.

The relative diffusion rates of the different isotopes occur in the order predicted classically (^{1}H$>^{2}$D$>^{3}$T) over most temperature regions, although ^{3}T is predicted to diffuse at a faster rate than ^{2}D below roughly 350 K.

There has been little experimental research into the diffusion of different isotopes of hydrogen in the stoichiometric β-phase niobium hydride. The results of this study suggests that the diffusion coefficients measured in the β-phase will be considerably lower than those measured in the α-phase and show large deviations away from Arrhenius behaviour below room temperature.

4.2 Lithium Imide

It has been suggested that lithium imide (Li_2NH) is a potential hydrogen storage material[68]. Safe storage materials for hydrogen are necessary for the manufacture of practical hydrogen-based energy sources. Li_2NH was shown to be able to absorb 6.5 wt% of hydrogen by the reaction $Li_2NH + H_2 \leftrightarrow LiNH_2 + LiH$.

4.2.1 The Location of the Hydrogen Atoms

In order to control and improve the performance of hydrogen storage materials it is important to understand the fundamental properties of the storage material, such as its crystal structure and the location of the hydrogen atoms within it.

Early experimental evidence suggested a crystal structure in which the nitrogen atoms formed a face centred cubic (FCC) lattice with the lithium atoms at the tetrahedral interstitial sites and the hydrogen atoms at the octahedral interstitial sites[69]. A diagram of this structure can be seen in figure 4.7(a).

Although the position of the nitrogen atoms and lithium ions has not been disputed, the position of the hydrogen atoms has been questioned. Ohoyama *et al* argued that the nitrogen-hydrogen distance in the structure proposed by Juza and Opp was too large[70]. Following an investigation using neutron powder diffraction, two alternative structures were proposed. In both structures the hydrogen atoms could occupy one of several sites around the nitrogen atoms. The possible sites of the hydrogen atoms could be arranged in a tetrahedron, as in figure 4.7(b), or a truncated octahedron, as in figure 4.7(c). The structure in which one of the twelve sites per nitrogen atom shown in figure 4.7(c) is occupied, was also found to be the most likely by Noritake *et al*, who used precise X-ray diffraction to find the structure[71].

The wave functions and energies of hydrogen in Li_2NH were calculated using the same method as that used to find the hydrogen wave functions in palladium hydride and niobium hydride (sections 3.2 and 4.1.1).

The potential was calculated on a 32^3 real space grid using CASTEP to perform DFT calculations with the PBE functional. Ultrasoft pseudopotentials were used to model the ionic cores. The plane-wave cutoff was set to 330 eV and calculations performed on a 12^3 k-point grid.

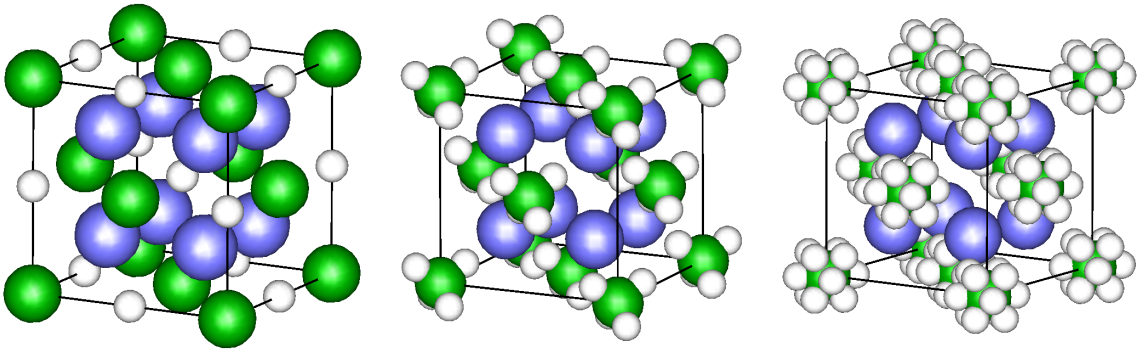

(a) (b) (c)

Figure 4.7: Crystal structures of Li_2NH proposed by (a) Juza and Opp [69] and (b),(c) Ohoyama *et al* [70] Nitrogen atoms are green, lithium blue and hydrogen white.

Once the potential was calculated it was interpolated onto an 88^3 grid and used to calculate the hydrogen wave functions and energies by solving a set of Bloch equations in a plane-wave basis. The plane-wave cutoff used for calculating the hydrogen wave functions was 1.1 eV.

By performing this calculation over a range of lattice parameters the lattice parameter with the lowest energy ground state was calculated to be 5.007 Å, in good agreement with the values of 5.047 Å[69], 5.0769 Å[70], and 5.0742 Å[71] found by experiment.

The hydrogen occupation in the ground state wave function did not match either of the possible structures described by Ohoyama *et al* and shown in figure 4.7. No low lying states were found with structures similar to those in figure 4.7.

Instead, the hydrogen atoms were found to have an equal probability of occupying six sites at the vertices of an octahedron centred at each nitrogen atom. The centres of these sites were separated from the nitrogen atoms by ≈ 1 Å. A schematic diagram and real space plot of the ground state wave function can be seen in figure 4.8. The ground state wave functions were found at ≈ 275 meV above the potential minimum.

In support of these findings, DFT calculations were performed in which the position of the hydrogen atoms in the unit cell was optimised with the hydrogen atoms initially placed in the sites suggested by Ohoyama *et al*. In both cases the hydrogen was found to have moved to the octahedral-type sites at the end of the optimisation.

Interestingly, the structure with hydrogen atoms at vertices of an octahedron was considered by Noritake *et al* and dismissed due to a slightly worse fit to the diffraction data than

the model shown in figure 4.7(c). Further experimental evidence is required to determine the correct location of the hydrogen atoms.

Rather than the classical picture of the sites being randomly filled with a probability of 1/6, in the quantum mechanical picture all six sites surrounding a nitrogen atom are partially occupied.

Since there are six sites around each of four distinct nitrogen atoms in the unit cell, there are 24 different linear combinations of the localised vibrational states in the ground state manifold. The bandwidth, J, of this manifold is significant, ≈ 4 meV, which suggests a tunnelling rate of $\tau \approx J/\hbar \approx 6$ ps^{-1}. Localised orbitals cannot be formed by combining different states in the manifold due to the significant gap in energy between the states.

The quantum tunnelling rate is several orders of magnitude larger than the classical kinetic rate constant predicted for transitions between the sites. The potential calculated using DFT gives a barrier of 477 meV between different sites around the same nitrogen. Estimating the zero point energies at the stable site and the transition state using a harmonic approximation, the expression for the rate constant from transition state theory (equation 1.12) gives an estimated classical rate constant of $\approx 6.0 \times 10^{-8}$ ps^{-1} at 300 K. This is much slower than the predicted quantum tunnelling rate, suggesting that quantum effects must be taken into account when considering the location of the hydrogen atoms in the Li_2NH lattice.

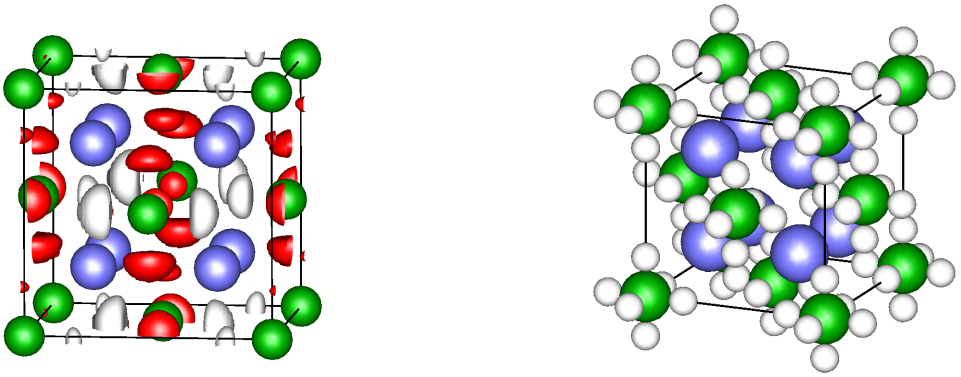

(a) (b)

Figure 4.8: (a) The ground state wave function. The nitrogen atom positions are shown in green, the lithium ions in blue. (b) Possible hydrogen sites predicted by calculating the ground state hydrogen wave function of the system, coloured as in figure 4.7.

4.2.2 Diffusion

For Li_2NH to be a practical hydrogen storage material it must be possible to absorb and desorb hydrogen from it at reasonable rates.

If the diffusion of hydrogen atoms in Li_2NH is considered classically, the barrier to hydrogen transport between different nitrogen atoms is very large. The potential used to calculate the wave functions previous section gives a barrier of 477 meV between different sites on the same nitrogen atom, and a barrier of 2.9 eV between sites on different nitrogen atoms.

The wave functions and energies calculated in the previous section can be used in equation 1.39 to calculate diffusion coefficients in the same way as for palladium hydride and niobium hydride. After performing this calculation, the temperature dependence of the diffusion coefficient of hydrogen from 300 K to 800 K could be fitted to an Arrhenius expression with an activation energy of just 260 meV. This is much lower than the classical barrier to diffusion, suggesting that quantum effects are very large in hydrogen diffusion in Li_2NH.

4.2.3 Conclusions

The location of the hydrogen atoms in Li_2NH is not well described by the classical description of randomly occupied sites around the nitrogen atoms. What is more, the sites predicted by diffraction experiments do not match the location of hydrogen calculated using quantum mechanics.

Quantum calculations find that the ground state hydrogen wave function in Li_2NH has partially occupied sites centred in an octahedral arrangement around each nitrogen atom.

The quantum tunnelling rate between the sites around a given nitrogen atom is much faster than that predicted classically. The classical barrier to diffusion between sites around different nitrogen sites is very high ($\approx$ 2.9 eV) suggesting that quantum effects are very large in hydrogen diffusion in Li_2NH.

Chapter 5

Transport in One Dimension

5.1 A model potential

A periodic potential in one dimension was chosen for preliminary studies of hydrogen diffusion.

$$V(x) = -\frac{1}{2}\left(E_{tet} - E_{oct}\right)\cos\left(\frac{2\pi x}{L}\right) + \frac{1}{2}\left(E_{tet} + E_{oct}\right)\cos\left(\frac{4\pi x}{L}\right) \tag{5.1}$$

The potential is periodic in L, the length of the box, and has two wells which can be chosen to have different depths, E_{oct} and E_{tet}, roughly modelling the potential along the pathway between octahedral and tetrahedral sites in a face centred cubic (FCC) lattice. E_{oct} is in general taken to be lower in energy than E_{tet}. The two wells can be chosen to have the same depth, modelling the potential between two equivalent sites in a lattice.

The single-particle wave functions and energies can be found by solving the usual time-independent single particle Schrödinger equation.

$$\hat{\mathcal{H}}\psi_n = \varepsilon_n\psi_n \tag{5.2}$$

As the potential is periodic, this is most sensibly done by solving the Bloch equations (2.33) in a plane-wave basis.

The Fourier components of $V(x)$, $\tilde{V}(g)$ are given by the following expression.

$$\tilde{V}(g) = \left\{ \begin{array}{cc} -\frac{1}{4}(E_{tet} - E_{oct}) & g = \pm 1 \\ \frac{1}{4}(E_{tet} + E_{oct}) & g = \pm 2 \\ 0 & otherwise \end{array} \right\} \tag{5.3}$$

The Fourier components of the Bloch functions at a given point in k-space, $\tilde{u}_{k,n}(g)$ are the eigenfunctions of a Hermitian matrix with elements given by equation 2.34, the eigenvalues giving the energies of the states.

Once the wave functions and energies have been obtained, the integral over the momentum operator can be calculated.

$$\left\langle \psi_m^k | \hat{p} | \psi_n^k \right\rangle = \sum_g \tilde{u}_{k,n}^*(g)\,(g+k)\,\tilde{u}_{k,m}(g) \tag{5.4}$$

For ease of notation the integral $\left\langle \psi_m^k | \hat{p} | \psi_n^k \right\rangle$ will be represented by P_{nm}^k.

The momentum integrals and the single-particle energies can then be used in equation 1.39 (reproduced here for convenience) to calculate the diffusion coefficient of the particle in this potential at a given temperature. It is necessary to perform an integral over sufficient k-points to give convergence in the diffusion coefficient.

$$D = \int dk\, \frac{\pi}{NQm_H^2} \sum_{n,m \neq n} e^{-\beta\varepsilon_n} |P_{nm}^k|^2\, \delta\left(\frac{\varepsilon_n}{\hbar} - \frac{\varepsilon_m}{\hbar}\right) \tag{5.5}$$

5.2 Computational Details

The required theory was programmed in FORTRAN, the diagonalisation of the Bloch matrix carried out using a QR algorithm provided by the LAPACK libraries.

The diffusion coefficient at different temperatures was calculated for the three hydrogen isotopes ^{1}H, ^{2}D, and ^{3}T in different potentials. For each calculation the measured diffusion coefficients were converged with respect to the number of plane-waves used as a basis set (limited by a kinetic energy cutoff) and the number of k-points over which the diffusion coefficient was integrated. The width of the Gaussian which replaced the δ-function in equation 5.5 was chosen such that the diffusion coefficient only varied slowly with the width.

5.3 Results and Discussion

5.3.1 An Asymmetric Double Well Potential

The results in this section were obtained using a plane-wave cutoff of 0.1 E_H, (2.7 eV), 2^{13} k-points, and a Gaussian of width 0.1 meV.

Calculations were carried out using a potential which repeated every 6.8 a_0 (3.6 Å) The shallow well minimum (E_{tet}) was kept at -0.002 E_H and the deeper well minimum (E_{oct}) varied between -0.0065 E_H and -0.01 E_H (figure 5.1). The dependence of the diffusion coefficients at 100 K, 400 K and 1000 K with the depth of the well can be seen in figure 5.2.

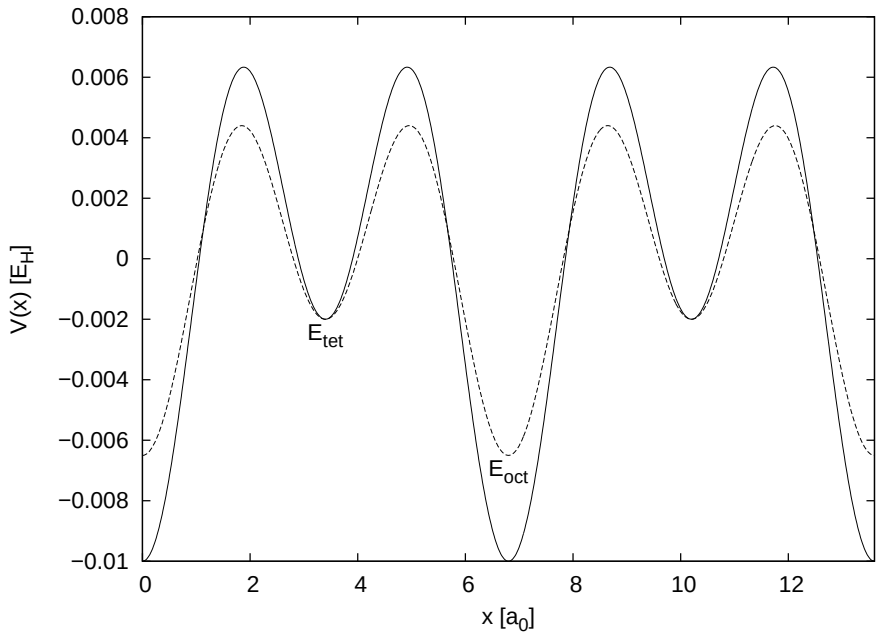

Figure 5.1: The potential curve used at the two extremes of the calculation.

The diffusion of hydrogen isotopes in this potential shows peaks as the minimum of the deeper well is varied (see figure 5.2). These peaks occur at -0.0081 E_H for ^{1}H, -0.0087 E_H for ^{2}D, and -0.007 E_H and -0.0096 E_H for ^{3}T. The isotope effect is not constant over the region. Each of the hydrogen isotopes diffuses more quickly in different regions of the curve.

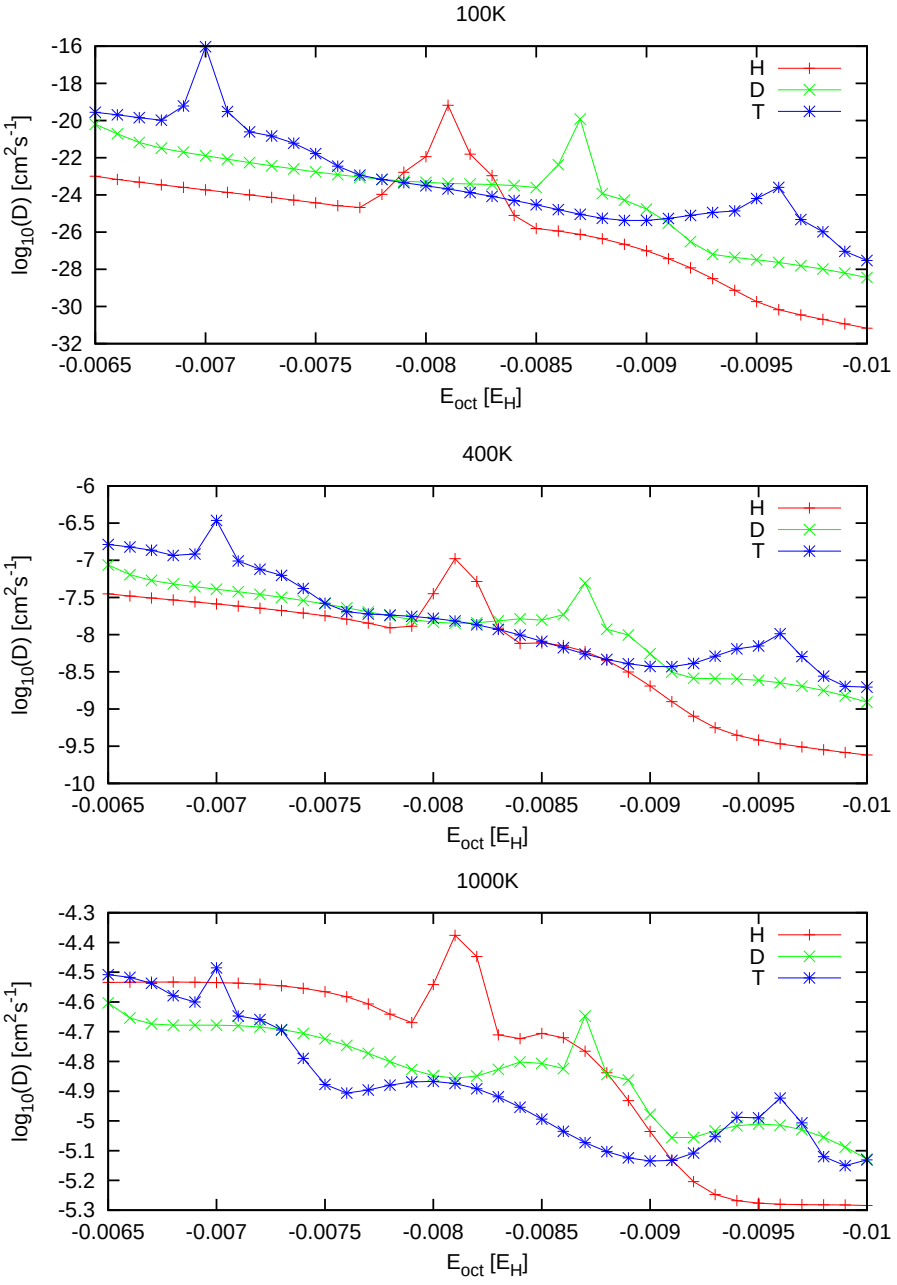

Figure 5.2: The diffusion coefficients of ^{1}H, ^{2}D and ^{3}T at different temperatures.

If the eigenstates at the ^{1}H at -0.0081 E_H (figure 5.3(a)) and those at -0.0075 E_H (figure 5.3(b)) are compared it can be seen that the bound states in the two wells (those below the classical inter-well barrier with little dispersion) become near degenerate when E_{oct} is -0.0081 E_H, whereas at -0.0075 E_H the states in different wells are well separated.

The near degenerate bound states with E_{oct} = -0.0081 E_H allow contributions to the diffusion coefficient at much lower energies than with E_{oct} = -0.0075 E_H where contributions only occur at the band edges of the continuum states above the classical barrier. As a result, diffusion in the potential with E_{oct} = -0.0081 E_H is faster than that with E_{oct} = -0.0075 E_H at all temperatures (figure 5.4). The classical barriers are shown in table 5.1.

The peaks in diffusion in figure 5.2 are caused when the eigenstates in the deep well and the eigenstates in the shallow well become close in energy.

The δ-function in equation 5.5 ensures that contributions to the diffusion coefficient only arise from matrix elements between degenerate or near degenerate states. Such pairs of states then contribute to the diffusion coefficient according to the magnitude of the momentum matrix element between them, P_{nm}, and a Boltzmann factor, $e^{-\beta\varepsilon_n}$.

The contributions to the diffusion coefficient arising from different regions of the eigenspectrum are plotted for different temperatures in figure 5.5 for the two potentials discussed above.

The relative rates of diffusion of the different isotopes of hydrogen in the same potential vary for similar reasons. The temperature dependence of the diffusion coefficents for ^{2}D and ^{3}T in a potential with E_{oct} = -0.0081 E_H are shown in figure 5.6, and the separate contributions to diffusion from parts of the eigenspectrum are shown in figure 5.7.

The contribution from states beneath the classical barrier with ^{1}H leads to much faster diffusion, especially at lower temperatures than with the heavier isotopes. The contributions to the diffusion of ^{2}D and ^{3}T only comes from states above the classical barrier.

Although tunnelling between states beneath the classical barrier has been shown to be important, the diffusion of hydrogen isotopes in this potential remains an activated process since in the cases in which bound states become close enough in energy to contribute, the states involved are excited states. As a result the temperature dependence of the diffusion coefficient remains largely Arrhenius, although at low temperatures the effective activation energy is seen to decrease as higher energy excited states are no longer thermally accessible.

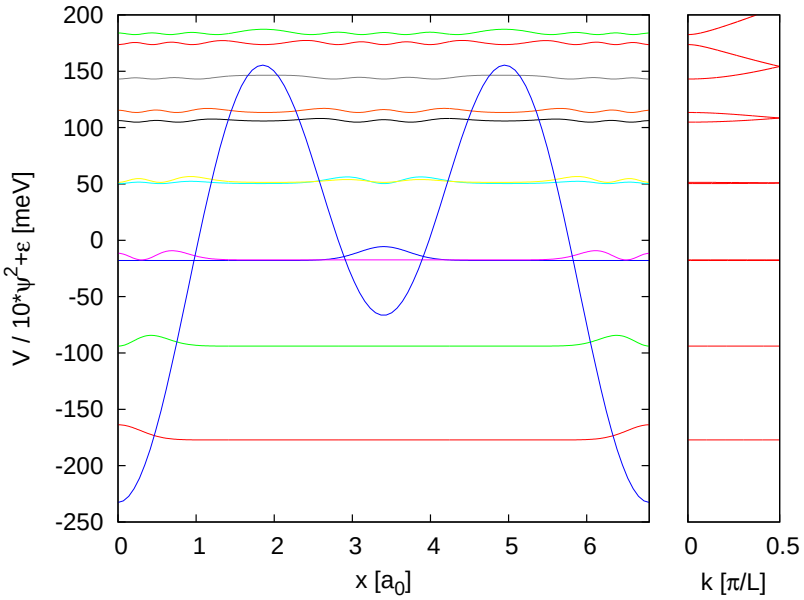

(a)

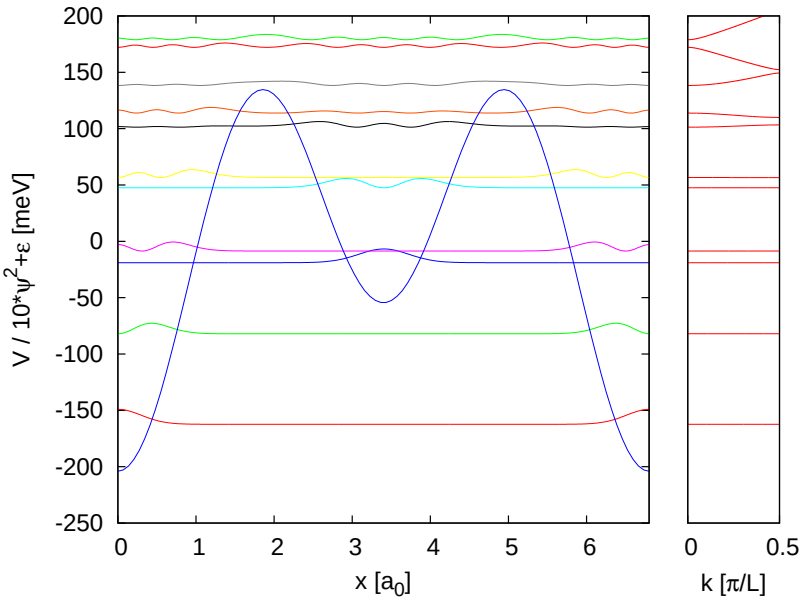

(b)

Figure 5.3: The proton densities and band structure of ^{1}H of the first 11 states with (a) E_{oct} = -0.0081 E_H, (b) E_{oct} = -0.0075 E_H. The potential energy curve is shown in blue.

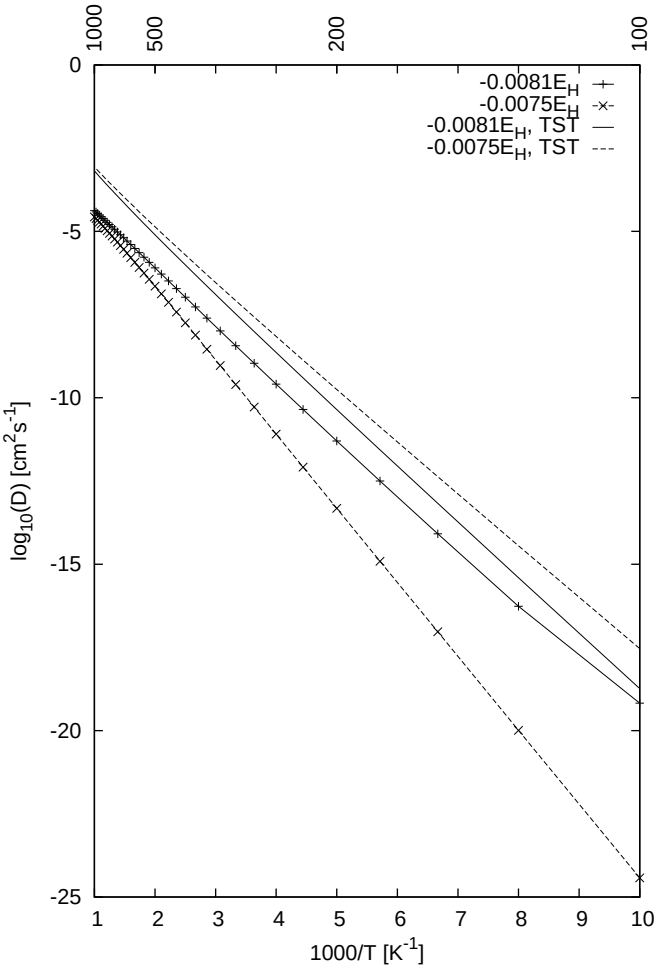

Figure 5.4: The diffusion coefficients of ^{1}H plotted against inverse temperature with E_{oct} = -0.0081 E_H and E_{oct} = -0.0075 E_H.

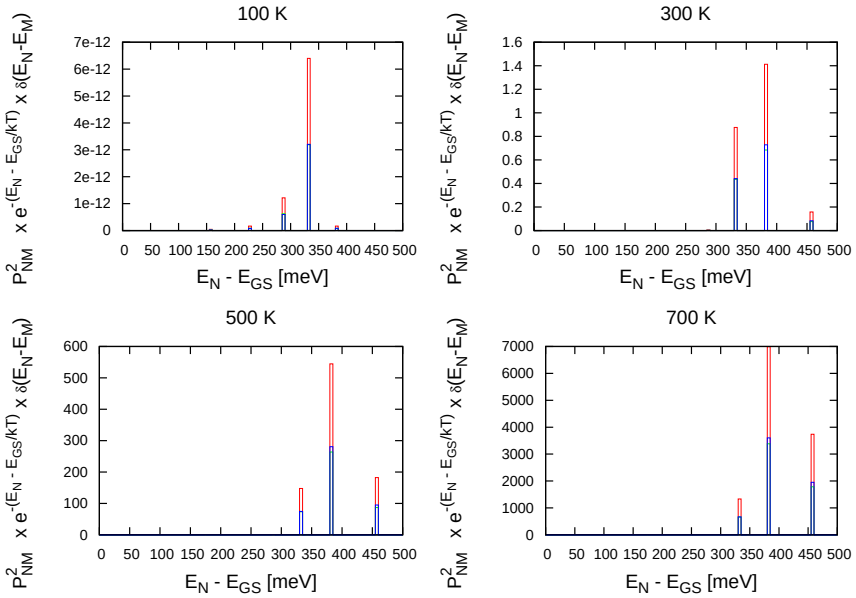

(a)

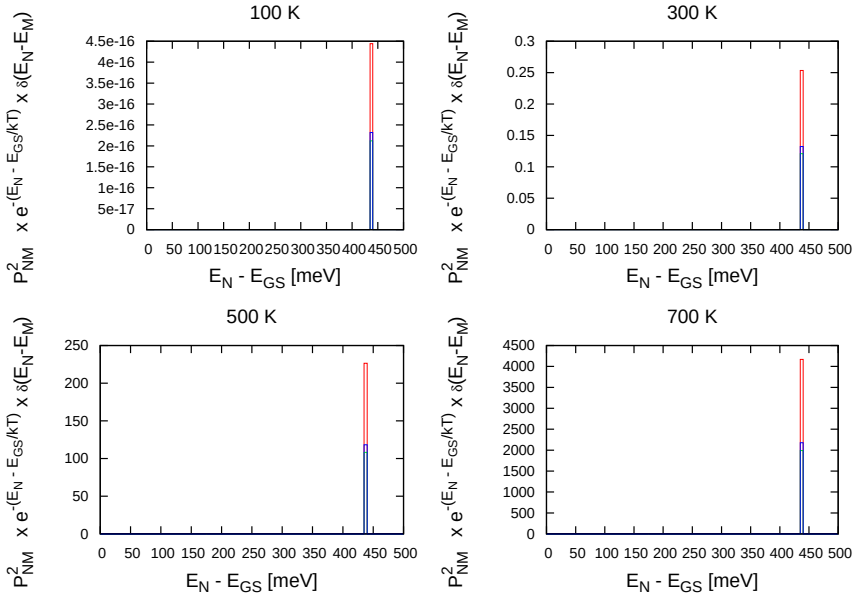

(b)

Figure 5.5: The contributions to the diffusion coefficient from different regions of the eigenspectrum below 500 meV above the ground state for ^{1}H (a) E_{oct} = -0.0081 E_H, (b) E_{oct} = -0.0075 E_H.

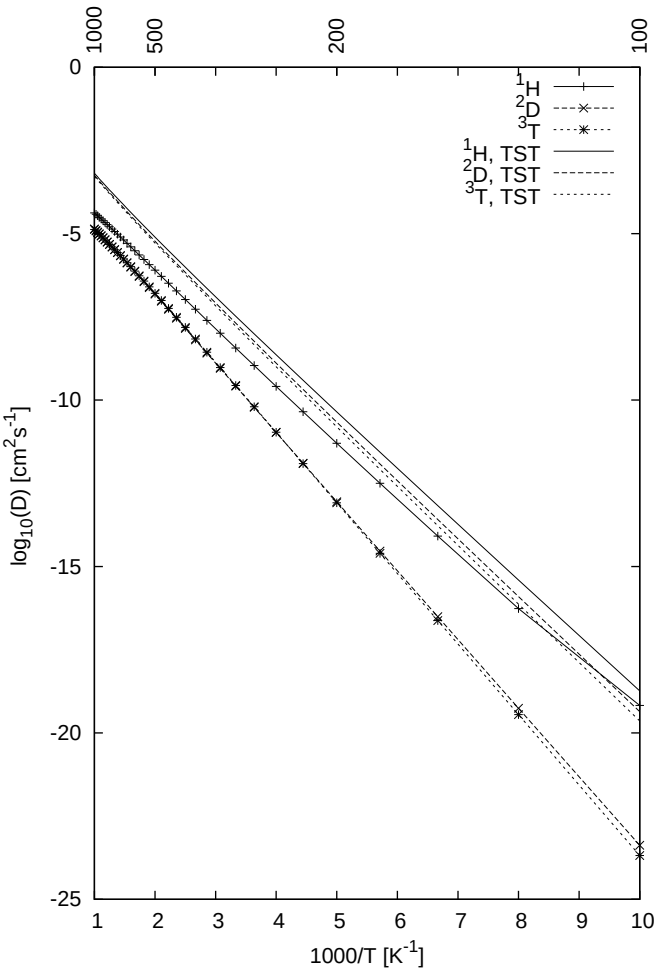

Figure 5.6: The diffusion coefficients of different hydrogen isotopes plotted against inverse temperature with E_{oct} = -0.0081 $\mathrm{E_H}$.

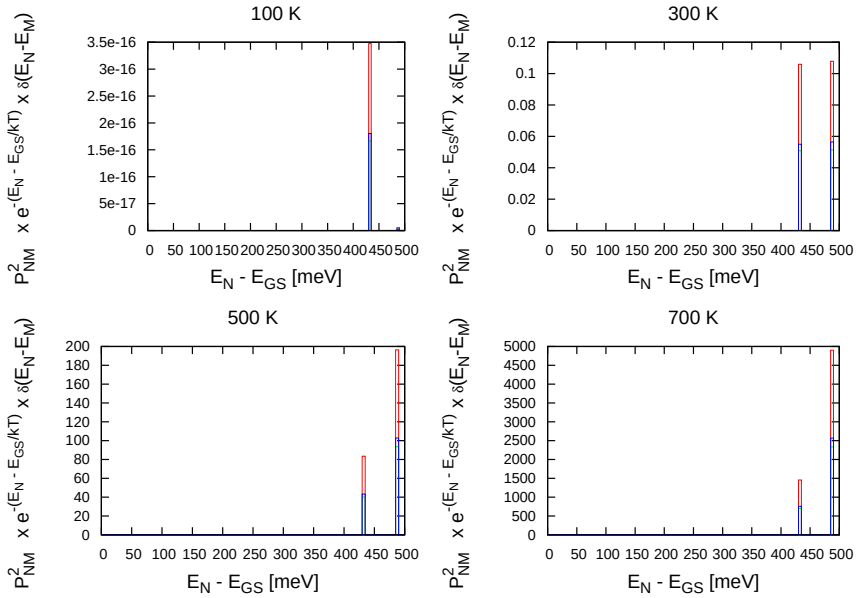

(a)

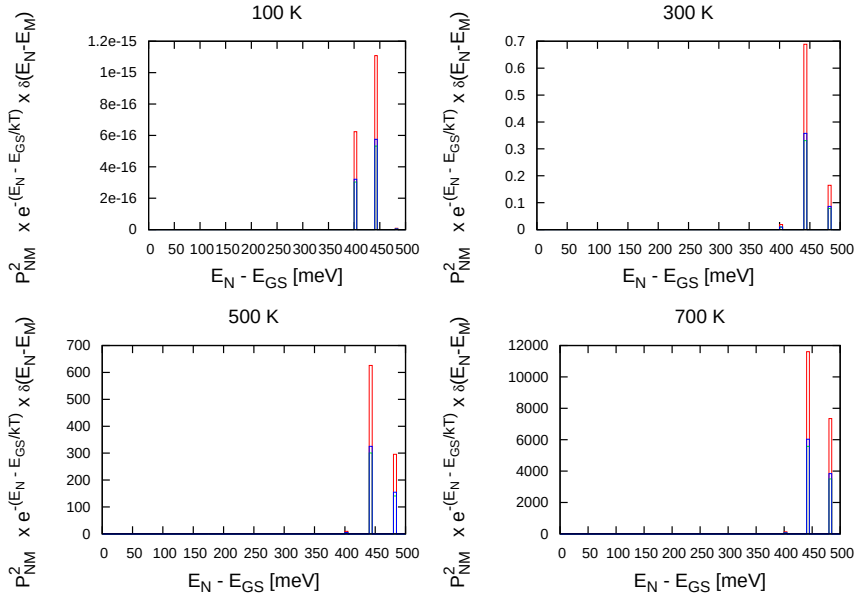

(b)

Figure 5.7: The contributions to the diffusion coefficient from different regions of the eigenspectrum below 500 meV above the ground state for (a) ^{2}D and (b) ^{3}T with E_{oct} = -0.0081 E_H.

5.3.2 Transition State Theory and Arrhenius Expressions

A comparison can be made between the diffusion coefficients calculated using equation 5.5 and those calculated using the following simple transition state theory (TST) expression discussed in section 1.1.2.

$$D_{TST} = \frac{l^2 k_B T}{h} e^{-\frac{E_{TS}-E_{GS}}{k_B T}} \tag{5.6}$$

where E_{TS} is the energy at the top of the barrier between the two wells and E_{GS} is the energy of the lowest eigenstate, and l is the distance between two neighbouring wells. Table 5.1 and figures 5.4 and 5.6 show the results of these calculations. The values in table 5.1 are the results of a fit to an Arrhenius expression of the form

$$D_{Arr} = D_0 e^{-\frac{E_a}{k_B T}} \tag{5.7}$$

Where D_0 is the diffusion coefficient in the finite temperature limit and E_a is an effective activation energy. The diffusion curves shown in figures 5.4 and 5.6 follow Arrhenius behaviour except at low temperatures (<200 K). The values of D_0 and E_a were calculated by fitting 13 points between 300 K and 600 K to an Arrhenius expression.

Table 5.1: A comparison of the parameters resulting from fitting the diffusion coefficients calculated using equation 5.5 and TST to an Arrhenius expression. D_0 in 10^{-3} cm^{2}s^{-1}, activation energies in meV.

Isotope	E_{oct}	Equation 5.5		TST		$E_{TS} - E_{oct}$	$E_{TS} - E_{GS}$
	[E$_H$]	D_0	E_a	D_0	E_a		
^{1}H	-0.0075	5.74	438	31.4	333	339	297
^{1}H	-0.0081	2.60	348	31.5	357	364	321
^{2}D	-0.0081	2.07	410	31.5	369	364	333
^{3}T	-0.0081	2.13	409	31.5	374	364	339

The diffusion coefficients calculated using TST do not agree with those calculated using equation 5.5. In general, the pre-exponential, D_0, is an order of magnitude too large, and the barrier to diffusion, E_a, too small. On the occasions in which diffusion is large because of bound state degeneracies the TST expression does not show any enhanced diffusion.

The dependence of diffusion on the mass of the isotope and the potential in TST comes solely from the $E_{TS} - E_{GS}$ term in equation 5.6. As a result, the TST diffusion coefficients have a simple dependence on both the isotope and E_{oct}. A normal isotope effect is always obtained when using TST, since ^{1}H has the highest ground state and therefore the lowest barrier of the isotopes. Similarly, a more negative value of E_{oct} gives a higher barrier and

hence a lower diffusion with TST. Hence TST cannot reproduce the peaks in diffusion at certain values of E_{oct} found using equation 5.5 and gives a different ordering of diffusion for the different isotopes.

TST only considers the ground state energy and the height of the barrier for diffusion, whereas it would appear necessary to consider both the energies of excited states and the momentum matrix elements or transition probabilities between states to give a more accurate representation of quantum diffusion in these systems.

A Quantum Correction to Transition State Theory

A large amount of work has been carried out attempting to derive expressions for rate constants in transition state theory which include quantum effects. A review of many of these attempts is given by Benderskii *et al*[6], including work by Garrett and Truhlar[72] and Miller[73].

A simple correction can be made to the classical transition state expression used in the previous section by including a scaling factor derived by Wigner[74]. Wigner's correction includes the effect of quantum tunnelling through a reaction barrier, assuming that it is parabolic. The corrected diffusion coefficient becomes

$$D_{QTST} = k_W D_{TST} \tag{5.8}$$

Where k_W is Wigner's correction given by

$$k_W = 1 + \frac{\left(\hbar \left|\omega^{\ddagger}\right|\right)^2}{24 \left(k_B T\right)^2} \tag{5.9}$$

$\omega^{\ddagger}$ is the imaginary frequency of the barrier found by calculating the second derivative of the potential at the transition state, $k^{\ddagger}$, and using the usual harmonic expression, $\omega^{\ddagger} = \sqrt{\left|k^{\ddagger}\right| / m}$ where m is the mass of the diffusing particle.

The potential used in these calculations is a sum of cosine curves, and as such is well modelled by a parabola close to the barrier to diffusion. The second derivative at the top of the barrier is given by

$$k^{\ddagger} = \frac{8\pi^2}{L^2} \left(E_{tet} + E_{oct}\right) - \frac{\pi^2}{2L^2} \frac{\left(E_{tet} - E_{oct}\right)^2}{\left(E_{tet} + E_{oct}\right)} \tag{5.10}$$

This expression was used to calculate the imaginary frequency and hence the diffusion coefficients with quantum corrections for ^{1}H, ^{2}D and ^{3}T in the potential with E_{oct} = -0.0081E_H and E_{tet} = -0.002E_H. The quantum correction caused a shift away from Arrhenius behaviour with a small increase in the estimated diffusion coefficients at low temperatures. The diffusion curves calculated for ^{1}H with and without the correction are shown in figure 5.8. The curves for ^{2}D and ^{3}T show similar behaviour and are left out of the figure for the sake of clarity.

The quantum correction to the transition state theory expression causes a decrease in the effective activation energy, and an increase in the calculated diffusion coefficients. As such it does not improve the agreement between transition state theory calculations and those carried out with the Kubo theory expression, equation 5.5.

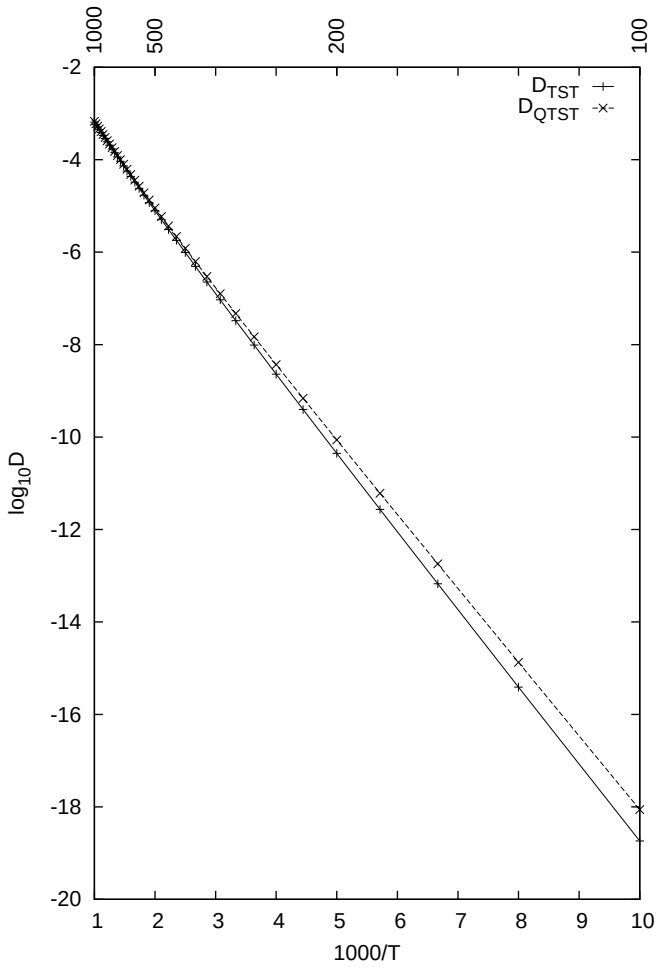

Figure 5.8: The diffusion coefficients of ^{1}H calculated using transition state theory plotted against inverse temperature with E_{oct} = -0.0081 E_H.

5.4 Conclusions

A one-dimensional potential was used to model the process of hydrogen diffusion in a potential with two different types of well, such as that of palladium hydride.

In this system diffusion only occurs due to transitions involving states above the classical barrier to diffusion, unless there are degenerate or near degenerate bound states in the two wells. As a result the rate of diffusion is very dependent on the potential. If the potential is altered so that two levels in different wells become coincident then diffusion is greatly enhanced.

This suggests that coupling the potential to an oscillator which could vary the relative depths of the two wells could have a large effect on the diffusion of hydrogen through the system as different levels were made coincident by the oscillator.

The isotope dependence of the diffusion coefficients also varies considerably with the shape of the potential, as the states of different isotopes are brought into coincidence with different potentials.

The strong dependence of diffusion on the shape of this model potential highlights the importance of building an accurate potential in studies of real systems such as those of palladium hydride, niobium hydride and lithium imide discussed in the previous chapters.

Even in this simple system in which most of the contributions to diffusion occur through processes at energies above the classical barrier to diffusion, transition state theory does not accurately reproduce the diffusion coefficients calculated using equation 1.39. It is unlikely that it will be any better at describing diffusion in generally more complicated real systems.

Chapter 6

Coupling to a Harmonic Oscillator

6.1 The Born-Huang Equations

The total Hamiltonian for a system which is periodic in the coordinates $\mathbf{x}$ and harmonic in the coordinate q is given by

$$\hat{\mathcal{H}} = -\frac{1}{2M_i}\nabla^2_{\mathbf{x}} - \frac{1}{2M_I}\nabla^2_q + \frac{1}{2}k_q\left(q-q_0\right)^2 + V\left(\mathbf{x}, q-q_0\right) \tag{6.1}$$

working in atomic units. M_i is the mass of the particle with coordinates $\mathbf{x}$ and M_I is the mass associated with the harmonic oscillator such that the harmonic frequency, $\omega = \sqrt{\frac{k_q}{M_I}}$. q_0 is the equilibrium position of the oscillator.

It is often sufficient to treat the q dependence of the potential V using a Taylor expansion to first order in q such that

$$V\left(\mathbf{x}, q-q_0\right) = V\left(\mathbf{x}, q_0\right) + \frac{\partial}{\partial q}V\left(\mathbf{x}, q\right)\Big|_{q=q_0}\left(q-q_0\right) + \mathcal{O}\left(\left(q-q_0\right)^2\right) \tag{6.2}$$

From this point onwards the expression $\frac{\partial}{\partial q}V\left(\mathbf{x}, q\right)\Big|_{q=q_0}$ will be written $V_0'(\mathbf{x})$. Making the Taylor expansion, and setting $q_0 = 0$ for convenience, the terms in the Hamiltonian which depend on q can be gathered to give:

$$\hat{\mathcal{H}}_q = -\frac{1}{2M_I}\nabla^2_q + \frac{1}{2}k_q q^2 + V_0'(\mathbf{x})q \tag{6.3}$$

Ignoring the $\mathbf{x}$ dependence of the $V_0'(\mathbf{x})$ term for the time being, this Hamiltonian is that

of a simple forced Harmonic oscillator.

$$\hat{\mathcal{H}}_q = -\frac{1}{2M_I}\nabla_q^2 + \frac{1}{2}k_q\left(q + \frac{1}{k_q}V_0'(\mathbf{x})\right)^2 - \frac{1}{2k_q}\left|V_0'(\mathbf{x})\right|^2 \tag{6.4}$$

The time-independent Schrödinger equation $\hat{\mathcal{H}}_q\phi_\nu = \varepsilon_\nu\phi_\nu$ then has solutions similar to a simple harmonic oscillator in q, but in which the wave functions and eigenvalues are shifted by $\mathbf{x}$ dependent terms.

$$\phi_\nu(q;\mathbf{x}) = N_\nu e^{-\frac{Q(\mathbf{x})^2}{2}} H_\nu(Q(\mathbf{x})) \tag{6.5}$$

$$\varepsilon_\nu(\mathbf{x}) = \left(\nu + \frac{1}{2}\right)\omega - \frac{1}{2k_q}\left|V_0'(\mathbf{x})\right|^2 \tag{6.6}$$

Where $Q(\mathbf{x})$ is a scaled harmonic oscillator coordinate given by

$$Q(\mathbf{x}) = \frac{\beta_q}{\sqrt{2}}\left(q + \frac{1}{k_q}V_0'(\mathbf{x})\right) \tag{6.7}$$

β_q is a constant given by

$$\beta_q = \sqrt{2\omega M_I} \tag{6.8}$$

N_ν is the usual normalisation constant

$$N_\nu = \sqrt{\frac{\beta_q}{2^\nu\sqrt{2\pi}\nu!}} \tag{6.9}$$

and H_ν is the νth order Hermite polynomial.

The orbitals ϕ_ν can be used as part of a basis set which is used to solve for the Hamiltonian of the whole system. The one-particle orbitals of the coupled system at a given point in k-space $\Psi_{N,k}$ are expressed as sums of ϕ_ν with an $\mathbf{x}$ dependent coefficient, $\psi_\nu^{N,k}$.

$$\Psi_{N,k}(\mathbf{x},q) = \sum_\nu \psi_\nu^{N,k}(\mathbf{x})\phi_\nu(q;\mathbf{x}) \tag{6.10}$$

Inserting this expression into the time-independent Schrödinger equation for the coupled system the following expression is obtained

$$\left(-\frac{1}{2M_i}\nabla_{\mathbf{x}}^2 + V(\mathbf{x},0) - \frac{1}{2M_I}\nabla_q^2 + \frac{1}{2}k_q q^2 + V_0'(\mathbf{x})q - E_N\right)\sum_\nu \psi_\nu^{N,k}(\mathbf{x})\phi_\nu(q;\mathbf{x}) = 0 \tag{6.11}$$

where E_N is the total energy of the coupled system.

The functions $\phi_\nu(q;\mathbf{x})$ are solutions to the Schrödinger equation, $\hat{\mathcal{H}}_q\phi_\nu(q;\mathbf{x}) = \varepsilon_\nu(\mathbf{x})\phi_\nu(q;\mathbf{x})$. As a result the previous expression can be simplified to

$$\left(-\frac{1}{2M_i}\nabla^2_{\mathbf{x}} + V(\mathbf{x},0) + \varepsilon_\nu(\mathbf{x}) - E_N\right)\sum_\nu \psi^{N,k}_\nu(\mathbf{x})\phi_\nu(q;\mathbf{x}) = 0 \tag{6.12}$$

Multiplying by $\phi_{\nu'}(q;\mathbf{x})$ and integrating over q the orthonormality of the functions $\phi_{\nu'}$ can be used to obtain the following expression

$$-\frac{1}{2M_i}\sum_\nu \int_{-\infty}^{\infty} \phi_{\nu'}(q;\mathbf{x})\,\nabla^2_{\mathbf{x}}\phi_\nu(q;\mathbf{x})\,\psi^{N,k}_\nu(\mathbf{x})dq + \left(V(\mathbf{x},0) + \varepsilon_\nu(\mathbf{x}) - E_N\right)\psi^{N,k}_{\nu'}(\mathbf{x}) = 0 \tag{6.13}$$

Both ϕ_ν and $\psi^{N,k}_\nu$ depend on $\mathbf{x}$, so the $\mathbf{x}$ derivatives in the above expression have to be carried out carefully. Using the usual product rule the following is obtained

$$\begin{aligned} -\frac{1}{2M_i}\sum_\nu \int_{-\infty}^{\infty} \phi_{\nu'}\left(\phi_\nu\nabla^2_{\mathbf{x}}\psi^{N,k}_\nu + 2\nabla_{\mathbf{x}}\phi_\nu.\nabla_{\mathbf{x}}\psi^{N,k}_\nu + \psi^{N,k}_\nu\nabla^2_{\mathbf{x}}\phi_\nu\right)dq & \\ + \left(V(\mathbf{x},0) + \varepsilon_\nu(\mathbf{x}) - E_N\right)\psi^{N,k}_{\nu'} &= 0 \end{aligned} \tag{6.14}$$

Which can be simplified to give

$$\begin{aligned} -\frac{1}{M_I}\sum_\nu \int_{-\infty}^{\infty} \phi_{\nu'}\nabla_{\mathbf{x}}\phi_\nu.\nabla_{\mathbf{x}}\psi^{N,k}_\nu dq - \frac{1}{2M_I}\sum_\nu \psi^{N,k}_\nu \int_{-\infty}^{\infty} \phi_{\nu'}\nabla^2_{\mathbf{x}}\phi_\nu dq & \\ + \left(-\frac{1}{2M_i}\nabla^2_{\mathbf{x}} + V(\mathbf{x},0) + \varepsilon_\nu(\mathbf{x}) - E_N\right)\psi^{N,k}_{\nu'} &= 0 \end{aligned} \tag{6.15}$$

These equations for the $\mathbf{x}$ dependent orbitals $\psi^{N,k}_\nu$ and the energies E_N are coupled-channel or Born-Huang equations[75]. The remaining integrals over q can be carried out by using the chain rule and finding the Q derivatives of the functions ϕ_ν.

$$\nabla_{\mathbf{x}}\phi_\nu(q;\mathbf{x}) = \nabla_{\mathbf{x}}Q(\mathbf{x})\frac{\partial}{\partial Q}\phi_\nu(q;\mathbf{x}) \tag{6.16}$$

To find the Q derivative of ϕ_ν it is necessary to use two properties of the Hermite polynomials. The derivative of a Hermite polynomial is given by $\frac{d}{dQ}H_\nu(Q) = 2\nu H_{\nu-1}(Q)$.

Another useful relation is that $QH_\nu(Q) = \frac{1}{2}\left(2\nu H_{\nu-1}(Q) + H_{\nu+1}(Q)\right)$.

$$\frac{\partial}{\partial Q}\phi_\nu(q;\mathbf{x}) = N_\nu\left(-Qe^{-\frac{Q^2}{2}}H_\nu(Q) + 2\nu e^{-\frac{Q^2}{2}}H_{\nu-1}(Q)\right) \tag{6.17}$$

$$= \sqrt{\frac{\nu}{2}}\phi_{\nu-1} - \sqrt{\frac{\nu+1}{2}}\phi_{\nu+1} \tag{6.18}$$

This expression can then be used with the $\mathbf{x}$ derivative of $Q(\mathbf{x})$ to give a final expression for $\nabla_\mathbf{x}\phi_\nu(q;\mathbf{x})$:

$$\nabla_\mathbf{x}Q(\mathbf{x}) = \frac{\beta_q}{k_q\sqrt{2}}\nabla_\mathbf{x}V_0'(\mathbf{x}) \tag{6.19}$$

$$\nabla_\mathbf{x}\phi_\nu(q;\mathbf{x}) = \frac{\beta_q}{k_q\sqrt{2}}\nabla_\mathbf{x}V_0'(\mathbf{x})\left(\sqrt{\frac{\nu}{2}}\phi_{\nu-1} - \sqrt{\frac{\nu+1}{2}}\phi_{\nu+1}\right) \tag{6.20}$$

The first term in equation 6.15 is then given by

$$-\frac{1}{M_I}\sum_\nu\int_{-\infty}^{\infty}\phi_{\nu'}\nabla_\mathbf{x}\phi_\nu.\nabla_\mathbf{x}\psi_\nu^{N,k}dq = -\frac{1}{M_I}\frac{\beta_q}{k_q\sqrt{2}}\nabla_\mathbf{x}V_0'(\mathbf{x}).\left(\sqrt{\frac{\nu'+1}{2}}\nabla_\mathbf{x}\psi_{\nu'+1}^{N,k} - \sqrt{\frac{\nu'}{2}}\nabla_\mathbf{x}\psi_{\nu'-1}^{N,k}\right) \tag{6.21}$$

To derive a similar expression for the second term in equation 6.15 is is necessary to find $\nabla_\mathbf{x}^2\phi_\nu$. In a similar way to that used for the first term it can be shown that

$$\nabla_\mathbf{x}^2\phi_\nu = \frac{\beta_q}{k_q\sqrt{2}}\nabla_\mathbf{x}^2V_0'(\mathbf{x})\left(\sqrt{\frac{\nu}{2}}\phi_{\nu-1} - \sqrt{\frac{\nu+1}{2}}\phi_{\nu+1}\right) + \frac{\beta_q^2}{4k_q^2}\left|\nabla_\mathbf{x}V_0'(\mathbf{x})\right|^2\left(\sqrt{\nu(\nu-1)}\phi_{\nu-2} - (2\nu+1)\phi_\nu + \sqrt{(\nu+2)(\nu+1)}\phi_{\nu+2}\right) \tag{6.22}$$

Which gives the following for the second term in equation 6.15

$$-\frac{1}{2M_I}\sum_\nu\psi_\nu^{N,k}\int_{-\infty}^{\infty}\phi_{\nu'}\nabla_\mathbf{x}^2\phi_\nu dq = -\frac{1}{2M_I}\frac{\beta_q}{k_q\sqrt{2}}\nabla_\mathbf{x}^2V_0'(\mathbf{x})\left(\sqrt{\frac{\nu'+1}{2}}\psi_{\nu'+1}^{N,k} - \sqrt{\frac{\nu'}{2}}\psi_{\nu'-1}^{N,k}\right) - \frac{1}{2M_I}\frac{\beta_q^2}{4k_q^2}\left|\nabla_\mathbf{x}V_0'(\mathbf{x})\right|^2\left(\sqrt{(\nu'+2)(\nu'+1)}\psi_{\nu'+2}^{N,k} - (2\nu'+1)\psi_{\nu'}^{N,k} + \sqrt{\nu'(\nu'-1)}\psi_{\nu'-2}^{N,k}\right) \tag{6.23}$$

Performing the integrals over q in equation 6.15 a set of equations for $\psi_\nu^{N,k}(\mathbf{x})$ are obtained. These equations couple together $\psi_\nu^{N,k}$ functions with values of ν which differ by up to two.

$$\begin{aligned}
&-\frac{1}{2M_I}\frac{\beta_q^2}{4k_q^2}\left|\nabla_{\mathbf{x}}V_0'(\mathbf{x})\right|^2\sqrt{(\nu+2)(\nu+1)}\psi_{\nu+2}^{N,k}(\mathbf{x})\\
&-\frac{1}{2M_I}\frac{\beta_q}{k_q\sqrt{2}}\sqrt{\frac{\nu+1}{2}}\left(2\nabla_{\mathbf{x}}V_0'(\mathbf{x}).\nabla_{\mathbf{x}}+\nabla_{\mathbf{x}}^2V_0'(\mathbf{x})\right)\psi_{\nu+1}^{N,k}(\mathbf{x})\\
&+\left(\frac{1}{2M_I}\frac{\beta_q^2}{4k_q^2}\left|\nabla_{\mathbf{x}}V_0'(\mathbf{x})\right|^2(2\nu+1)-\frac{\nabla_{\mathbf{x}}^2}{2M_i}+V(\mathbf{x},0)+\varepsilon_\nu(\mathbf{x})\right)\psi_\nu^{N,k}(\mathbf{x})\\
&+\frac{1}{2M_I}\frac{\beta_q}{k_q\sqrt{2}}\sqrt{\frac{\nu}{2}}\left(2\nabla_{\mathbf{x}}V_0'(\mathbf{x}).\nabla_{\mathbf{x}}+\nabla_{\mathbf{x}}^2V_0'(\mathbf{x})\right)\psi_{\nu-1}^{N,k}(\mathbf{x})\\
&-\frac{1}{2M_I}\frac{\beta_q^2}{4k_q^2}\left|\nabla_{\mathbf{x}}V_0'(\mathbf{x})\right|^2\sqrt{\nu(\nu-1)}\psi_{\nu-2}^{N,k}(\mathbf{x}) \;=\; 0 \quad (6.24)
\end{aligned}$$

The functions $\psi_\nu^{N,k}$ and other $\mathbf{x}$ dependent terms in these equations can be expressed as Fourier transforms in reciprocal $\mathbf{x}$ space, as functions of the reciprocal lattice vectors $\mathbf{g}$. This results in a set of Bloch equations which can be solved to give the Fourier components of $\psi_\nu^{N,k}$ and the energies of the total Hamiltonian, E_N. The total number of coupled states obtained will be the product of the number of plane-waves used in the finite Fourier transforms and the number of forced harmonic oscillator functions included in the sum in equation 6.10.

The resulting orbitals are built from a combined basis set of plane-waves and solutions to the forced harmonic oscillator Hamiltonian.

$$\Psi_{n,k}(\mathbf{x},q)=\sum_\nu\sum_{\mathbf{g}}\tilde{u}_\nu^{N,k}(\mathbf{g})e^{-i\mathbf{g}.\mathbf{x}}\phi_\nu(q;\mathbf{x}) \quad (6.25)$$

The momentum matrix element $P_{N,M}^k$ can be calculated in this basis as

$$\begin{aligned}
P_{N,M}^k &= -i\int\int\Psi_{N,k}^*(\mathbf{x},q)\,\nabla_{\mathbf{x}}\Psi_{M,k}(\mathbf{x},q)\,d\mathbf{x}dq & (6.26)\\
&= -i\int\int\sum_\nu\sum_{\mathbf{g}}\tilde{u}_\nu^{N,k,*}(\mathbf{g})e^{i(\mathbf{g}+\mathbf{k}).\mathbf{x}}\phi_\nu\sum_{\nu'}\sum_{\mathbf{g}'}\tilde{u}_{\nu'}^{M,k}(\mathbf{g}')\,\nabla_{\mathbf{x}}e^{-i(\mathbf{g}'+\mathbf{k}).\mathbf{x}}\phi_{\nu'}d\mathbf{x}dq & (6.27)\\
&= -\int\int\sum_{\nu,\nu'}\sum_{\mathbf{g},\mathbf{g}'}\tilde{u}_\nu^{N,k,*}(\mathbf{g})\tilde{u}_{\nu'}^{M,k}(\mathbf{g}')(\mathbf{g}'+\mathbf{k})\,e^{i(\mathbf{g}-\mathbf{g}').\mathbf{x}}\phi_\nu\phi_{\nu'}d\mathbf{x}dq\\
&\quad -i\int\int\sum_{\nu,\nu'}\sum_{\mathbf{g},\mathbf{g}'}\tilde{u}_\nu^{N,k,*}(\mathbf{g})\tilde{u}_{\nu'}^{M,k}(\mathbf{g}')\,e^{i(\mathbf{g}-\mathbf{g}').\mathbf{x}}\phi_\nu\nabla_{\mathbf{x}}\phi_{\nu'}d\mathbf{x}dq & (6.28)
\end{aligned}$$

The integral over q can be carried out using the expression given in equation 6.20 and the orthogonality of the functions ϕ_ν:

$$\int \phi_\nu \nabla_{\mathbf{x}} \phi_{\nu'} dq = \frac{\beta_q}{k_q\sqrt{2}} \nabla_{\mathbf{x}} V_0'(\mathbf{x}) \int \phi_\nu \left(\sqrt{\frac{\nu'}{2}} \phi_{\nu'-1} - \sqrt{\frac{\nu'+1}{2}} \phi_{\nu'+1} \right) dq \quad (6.29)$$

$$= \frac{\beta_q}{k_q\sqrt{2}} \nabla_{\mathbf{x}} V_0'(\mathbf{x}) \left(\sqrt{\frac{\nu'}{2}} \delta_{\nu,\nu'-1} + \sqrt{\frac{\nu'+1}{2}} \delta_{\nu,\nu'+1} \right) \quad (6.30)$$

The expression for the momentum matrix elements then becomes

$$\begin{aligned} P^k_{N,M} = & -\sum_\nu \sum_{\mathbf{g}} \tilde{u}^{N,k,*}_\nu(\mathbf{g}) \tilde{u}^{M,k}_\nu(\mathbf{g}) (\mathbf{g}+\mathbf{k}) \\ & - i \frac{\beta_q}{k_q\sqrt{2}} \sum_\nu \sum_{\mathbf{g},\mathbf{g}'} \tilde{u}^{N,k,*}_\nu(\mathbf{g}) \tilde{u}^{M,k}_{\nu+1}(\mathbf{g}') \sqrt{\frac{\nu+1}{2}} \int e^{i(\mathbf{g}-\mathbf{g}').\mathbf{x}} \nabla_{\mathbf{x}} V_0'(\mathbf{x}) d\mathbf{x} \\ & - i \frac{\beta_q}{k_q\sqrt{2}} \sum_\nu \sum_{\mathbf{g},\mathbf{g}'} \tilde{u}^{N,k,*}_\nu(\mathbf{g}) \tilde{u}^{M,k}_{\nu-1}(\mathbf{g}') \sqrt{\frac{\nu}{2}} \int e^{i(\mathbf{g}-\mathbf{g}').\mathbf{x}} \nabla_{\mathbf{x}} V_0'(\mathbf{x}) d\mathbf{x} \end{aligned} \quad (6.31)$$

Once the energies, E_N, and the momentum matrix elements, $P^k_{N,M}$ have been calculated they can be used in the relation derived from non-equilibrium statistical mechanics (equation 1.39) to calculate the diffusion coefficient for a particle in the coupled potential.

6.2 An Uncoupled Basis

An alternative method to that of section 6.1 is to work in a basis set of the eigenfunctions of the following two uncoupled Hamiltonians.

$$\hat{\mathcal{H}}_{\mathbf{x}} = -\frac{1}{2M_i} \nabla^2_{\mathbf{x}} + V(\mathbf{x}, q_0) \quad (6.32)$$

$$\hat{\mathcal{H}}_q = -\frac{1}{2M_I} \nabla^2_q + \frac{1}{2} k_q (q - q_0)^2 \quad (6.33)$$

The eigenfunctions of the $\mathbf{x}$ dependent Hamiltonian are the same as those calculated in section 2.3. The same method can be used to calculate the Fourier components of the Bloch functions, and hence the wave functions and energies at any given point in $\mathbf{k}$ space.

The eigenfunctions are then expressed in a plane-wave basis:

$$\psi_{\mathbf{k},\mathbf{n}}(\mathbf{x}) = \sum_{\mathbf{g}} \tilde{u}_{\mathbf{k},\mathbf{n}}(\mathbf{g}) e^{-i(\mathbf{g}+\mathbf{k}).\mathbf{x}} \tag{6.34}$$

The eigenstates of the q dependent Hamiltonian are the wave functions and energies of a simple harmonic oscillator with mass M_I and spring constant k_q.

$$\phi_\nu(q) = N_\nu e^{-\frac{Q^2}{2}} H_\nu(Q) \tag{6.35}$$

where Q is a scaled harmonic oscillator coordinate given by

$$Q = \frac{\beta_q}{\sqrt{2}}(q - q_0) \tag{6.36}$$

β_q is a constant given by

$$\beta_q = \sqrt{2\omega M_I} \tag{6.37}$$

N_ν is the usual normalisation constant

$$N_\nu = \sqrt{\frac{\beta_q}{2^\nu \sqrt{2\pi}\nu!}} \tag{6.38}$$

and H_ν is the νth order Hermite polynomial.

The full Hamiltonian for the coupled system can be approximated with a Taylor expansion as in the last section. It then becomes

$$\hat{\mathcal{H}} = \hat{\mathcal{H}}_{\mathbf{x}} + \hat{\mathcal{H}}_q + V_0'(\mathbf{x})(q - q_0) \tag{6.39}$$

The wave functions of the time-independent Schrödinger equation for the coupled system are then expressed in a basis of the product of $\psi_{\mathbf{k},\mathbf{n}}$ and ϕ_ν.

$$\Psi_{N,\mathbf{k}}(\mathbf{x}, q) = \sum_{\mathbf{n},\nu} c_{\mathbf{n},\nu}^{N,\mathbf{k}} \psi_{\mathbf{k},\mathbf{n}}(\mathbf{x}) \phi_\nu(q) \tag{6.40}$$

Such that $\hat{\mathcal{H}}\Psi_{N,\mathbf{k}} = E_{N,\mathbf{k}}\Psi_{N,\mathbf{k}}$.

A set of simultaneous equations for the coefficients $c_{\mathbf{n},\nu}^{N,\mathbf{k}}$ and the energies $E_{N,\mathbf{k}}$ can be obtained by multiplying the Schrödinger equation by a specific state $\Psi_{M,\mathbf{k}*}$ and integrating over all space (the integrals over states with different values of $\mathbf{k}$ are zero).

$$\int\int \sum_{\mathbf{n}',\nu'} c^{M,\mathbf{k}*}_{\mathbf{n}',\nu'} \psi^*_{\mathbf{k},\mathbf{n}'} \phi_{\nu'} \left(\hat{\mathcal{H}}_{\mathbf{x}} + \hat{\mathcal{H}}_q + (q-q_0)\, V_0'(\mathbf{x}) - E_{N,\mathbf{k}} \right) \sum_{\mathbf{n},\nu} c^{N,\mathbf{k}}_{\mathbf{n},\nu} \psi_{\mathbf{k},\mathbf{n}} \phi_\nu d\mathbf{x} dq = 0 \quad (6.41)$$

The integrals over the Hamiltonians $\hat{\mathcal{H}}_{\mathbf{x}}$ and $\hat{\mathcal{H}}_q$ are performed in the usual manner:

$$\sum_{\mathbf{n}',\nu'} \sum_{\mathbf{n},\nu} c^{M,\mathbf{k}*}_{\mathbf{n}',\nu'} c^{N,\mathbf{k}}_{\mathbf{n},\nu} \left(\varepsilon_{\mathbf{n},\mathbf{k}} + \omega_q \left(\nu + \frac{1}{2} \right) - E_{N,\mathbf{k}} \right) \delta_{\mathbf{n}',\mathbf{n}} \delta_{\nu',\nu} + \sum_{\mathbf{n}',\nu'} \sum_{\mathbf{n},\nu} c^{M,\mathbf{k}*}_{\mathbf{n}',\nu'} c^{N,\mathbf{k}}_{\mathbf{n},\nu} \int\int \psi^*_{\mathbf{k},\mathbf{n}'} \phi_{\nu'} \, (q-q_0)\, V_0'(\mathbf{x}) \psi_{\mathbf{k},\mathbf{n}} \phi_\nu d\mathbf{x} dq = 0 \quad (6.42)$$

The integrals over q can be carried out leaving only integrals over $\mathbf{x}$:

$$\sum_{\mathbf{n}',\nu'} c^{M,\mathbf{k}*}_{\mathbf{n}',\nu'} c^{N,\mathbf{k}}_{\mathbf{n}',\nu'} \left(\varepsilon_{\mathbf{n}',\mathbf{k}} + \omega_q \left(\nu' + \frac{1}{2} \right) - E_{N,\mathbf{k}} \right) + \sum_{\mathbf{n}',\nu'} \sum_{\mathbf{n},\nu} c^{M,\mathbf{k}*}_{\mathbf{n}',\nu'} c^{N,\mathbf{k}}_{\mathbf{n},\nu} \int \phi_{\nu'} \, (q-q_0)\, \phi_\nu dq \int \psi^*_{\mathbf{k},\mathbf{n}'} V_0'(\mathbf{x}) \psi_{\mathbf{k},\mathbf{n}} d\mathbf{x} = 0 \quad (6.43)$$

$$\sum_{\mathbf{n}',\nu'} c^{M,\mathbf{k}*}_{\mathbf{n}',\nu'} c^{N,\mathbf{k}}_{\mathbf{n}',\nu'} \left(\varepsilon_{\mathbf{n}',\mathbf{k}} + \omega_q \left(\nu' + \frac{1}{2} \right) - E_{N,\mathbf{k}} \right) + \sum_{\mathbf{n}',\nu'} \sum_{\mathbf{n}} c^{M,\mathbf{k}*}_{\mathbf{n}',\nu'} \left(c^{N,\mathbf{k}}_{\mathbf{n},\nu'-1} \frac{\sqrt{\nu'}}{\beta_q} + c^{N,\mathbf{k}}_{\mathbf{n},\nu'+1} \frac{\sqrt{\nu'+1}}{\beta_q} \right) \int \psi^*_{\mathbf{k},\mathbf{n}'} V_0'(\mathbf{x}) \psi_{\mathbf{k},\mathbf{n}} d\mathbf{x} = 0 \quad (6.44)$$

The remaining integral over $\mathbf{x}$ is can be performed in Fourier space and the coefficients and energies can then be obtained by diagonalising a matrix with elements

$$H_{\mathbf{n}'\nu',\mathbf{n}\nu} = \left(\varepsilon_{\mathbf{n}',\mathbf{k}} + \omega_q \left(\nu' + \frac{1}{2} \right) - E_{N,\mathbf{k}} \right) \delta_{\mathbf{n}',\mathbf{n}} \delta_{\nu',\nu} + \frac{\sqrt{\nu+1}}{\beta_q} \delta_{\nu',\nu+1} \int \psi^*_{\mathbf{k},\mathbf{n}'} V_0'(\mathbf{x}) \psi_{\mathbf{k},\mathbf{n}} d\mathbf{x} + \frac{\sqrt{\nu}}{\beta_q} \delta_{\nu',\nu-1} \int \psi^*_{\mathbf{k},\mathbf{n}'} V_0'(\mathbf{x}) \psi_{\mathbf{k},\mathbf{n}} d\mathbf{x} \quad (6.45)$$

The number of wave functions, $\Psi_{N,k}$, and their energies found using this method, is the product of the number of periodic wave functions, $\psi_{\mathbf{n},\mathbf{k}}$, and the number of harmonic oscillator wave functions, ϕ_ν, included in the basis.

Since the functions ϕ_ν have no $\mathbf{x}$ dependence, the momentum matrix elements of the coupled wave functions, $\Psi_{N,k}$, are easily calculated in terms of the integrals over the

functions $\psi_{\mathbf{n},k}$ discussed in section 2.3.

$$\langle \Psi_{M,k} | \hat{p}_{\mathbf{x}} | \Psi_{N,k} \rangle = \sum_{\mathbf{n}',\nu'} \sum_{\mathbf{n},\nu} c^{M,\mathbf{k}*}_{\mathbf{n}',\nu'} c^{N,\mathbf{k}}_{\mathbf{n},\nu} \langle \psi_{\mathbf{n}',k} | \hat{p}_{\mathbf{x}} | \psi_{\mathbf{n},k} \rangle \langle \phi_{\nu'} | \phi_{\nu} \rangle \quad (6.46)$$

$$= \sum_{\mathbf{n}',\nu'} \sum_{\mathbf{n}} c^{M,\mathbf{k}*}_{\mathbf{n}',\nu'} c^{N,\mathbf{k}}_{\mathbf{n},\nu'} \langle \psi_{\mathbf{n}',\mathbf{k}} | \hat{p}_{\mathbf{x}} | \psi_{\mathbf{n},\mathbf{k}} \rangle \quad (6.47)$$

Although this method requires an extra diagonalisation step compared to the Born-Huang method described in section 6.1 it can be more efficient for larger systems. It is often the case that the number of periodic wave functions, $\psi_{\mathbf{n},k}$, that need to be included in this basis to give converged results is lower than the number of plane-waves needed to correctly describe these wave functions. In such a case the matrix given by 6.45 is considerably smaller than that given by the Born-Huang equations, which can become prohibitively large for some systems.

6.3 A Model Potential

The model potential used in part 5.1 was extended to include coupling to a harmonic oscillator. The positions of the bottoms of the two wells were made to vary with the harmonic oscillator coordinate q such that $E_{oct}(q) = E^0_{oct} + \alpha q$ and $E_{tet}(q) = E^0_{tet} - \alpha q$.

As the oscillator moved in the positive direction the two wells became closer together in energy until the "tetrahedral" well became the deepest. In the negative direction the two wells got further apart in energy. α is a measure of the strength of coupling between the two potentials. The harmonic oscillator has a characteristic force constant, k_q and mass, M_I. The form of this potential can be seen in figure 6.1.

$$V(x,q) = \frac{k_q}{2} q^2 - \frac{1}{2} \left(E_{tet}(q) - E_{oct}(q) \right) \cos\left(\frac{2\pi x}{L} \right) + \frac{1}{2} \left(E_{tet}(q) + E_{oct}(q) \right) \cos\left(\frac{4\pi x}{L} \right) \quad (6.48)$$

$$= \frac{k_q}{2} q^2 - \frac{1}{2} \left(E^0_{tet} - E^0_{oct} \right) \cos\left(\frac{2\pi x}{L} \right) + \frac{1}{2} \left(E^0_{tet} + E^0_{oct} \right) \cos\left(\frac{4\pi x}{L} \right) + \alpha q \cos\left(\frac{2\pi x}{L} \right) \quad (6.49)$$

$$= V(x,0) + \frac{k_q}{2} q^2 + \alpha q \cos\left(\frac{2\pi x}{L} \right) \quad (6.50)$$

This potential may give rise to the so-called "polaron" effect, in which the position of the hydrogen atom in a lattice alters the potential such that the hydrogen atom becomes

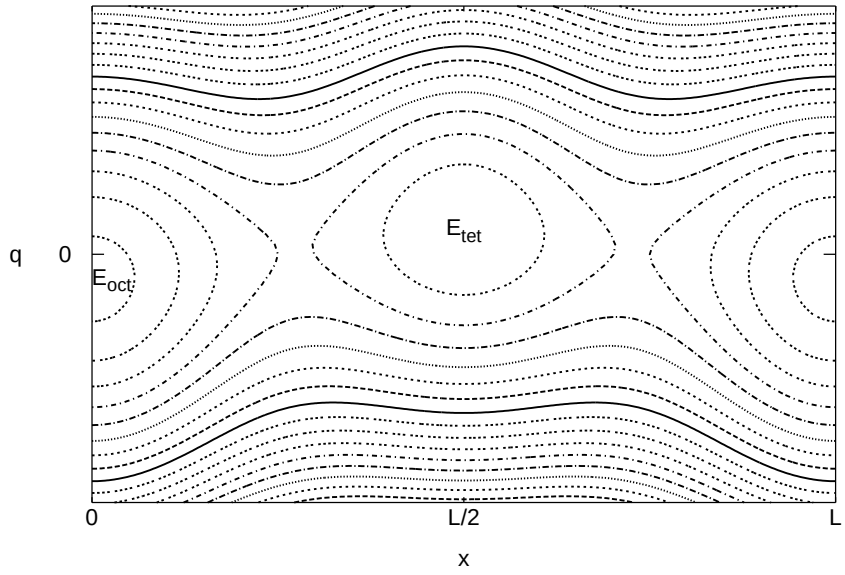

Figure 6.1: A contour plot of the dependence of the coupled potential on the harmonic oscillator coordinate, q, and the periodic coordinate, x.

trapped in whichever well it currently resides.

The q and x derivatives of this potential can be carried out analytically and all x dependent terms have an analytic Fourier transform. As a result the Born-Huang equations (6.24) can be used to form a set of Bloch equations which can be solved by diagonalisation as in part 5.1.

The resulting wave functions and energies can then be used in equation 5.5 to calculate the diffusion coefficient of a particle with mass m_H travelling in the x direction at a given temperature.

6.3.1 Results and Discussion

Varying the Well Depths

For comparison with the results for an uncoupled system, a similar investigation to that in part 5.3.1 was made. The value of E_{tet} at the equilibrium position of q, E^0_{tet} was kept at

at -0.002 E_H and the deeper well minimum (E^0_{oct}) varied between -0.0075 E_H and -0.009 E_H. The potential was periodic with a box length of 6.8 a_0, (3.6 Å). The plane-wave cutoff necessary to obtain convergence remained at 0.1 E_H, (2.7 eV), and the width of the Gaussian modelling the δ-function in equation 1.39 was kept at 0.1 meV. It was found that only 2^8 k-points were required to converge the diffusion coefficients.

The harmonic oscillator had a frequency of 200 cm^{-1} and the mass of a palladium atom. The coupling constant between the periodic potential and the harmonic oscillator, α, was kept at 10^{-3}. Twenty harmonic oscillator states were included in the calculation. The results can be seen in figure 6.2.

It can be seen that the coupling to the harmonic oscillator increases diffusion at both high and low temperatures. If the polaron effect was causing particles to be trapped in wells, then the diffusion coefficients would be expected to decrease upon coupling to the oscillator. There must be other more important factors present which cause diffusion to be increased.

The peaks found in the curves in section 5.3.1 are still present in figure 6.2 (for example the peak in the ^{2}D curve at E_{oct} = -0.0087 E_H). In addition a new peak has appeared in the ^{1}H curve at E_{oct} = -0.0077 E_H.

To investigate the effect of coupling further, the diffusion of ^{1}H at three points on the curve will be considered: at E_{oct} = -0.0081 E_H, the peak seen in the uncoupled system; at E_{oct} = -0.0077 E_H, the new peak; and at E_{oct} = -0.0075 E_H. The diffusion curves for ^{1}H in the three potentials are shown in figure 6.3 along with the curves for the uncoupled potential with the same values of E_{oct}.

In all three cases the diffusion at high temperatures is higher than in the uncoupled case. The effective activation energies (the gradients in figure 6.3) are smaller for E^0_{oct} = -0.0075 E_H and -0.0077 E_H, leading to much increased diffusion at low temperatures. This is not seen at E^0_{oct} = -0.0081 E_H.

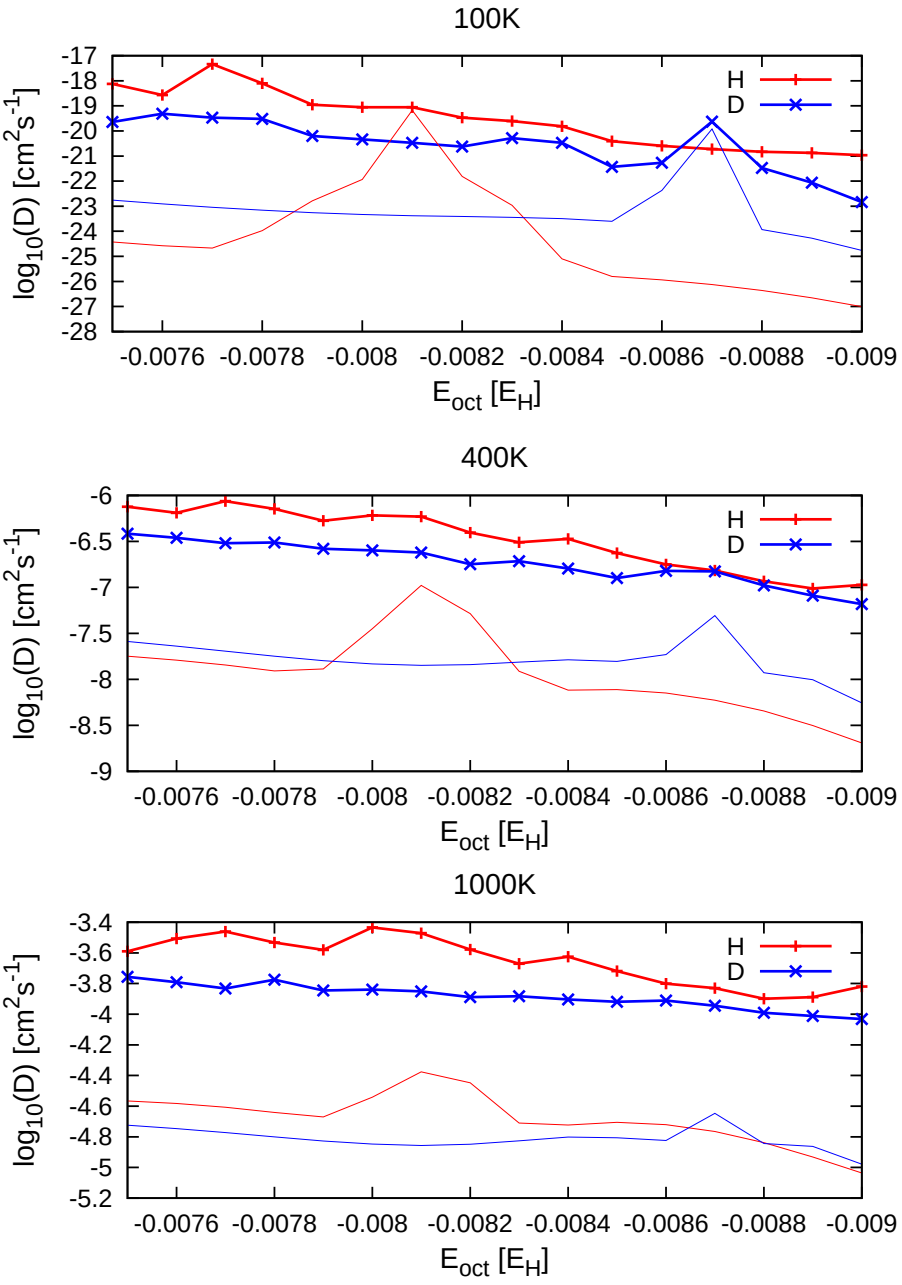

Figure 6.2: The diffusion coefficients of ^{1}H and ^{2}D at different temperatures. The lines without points are those calculated in part 5.3.1 included for comparison.

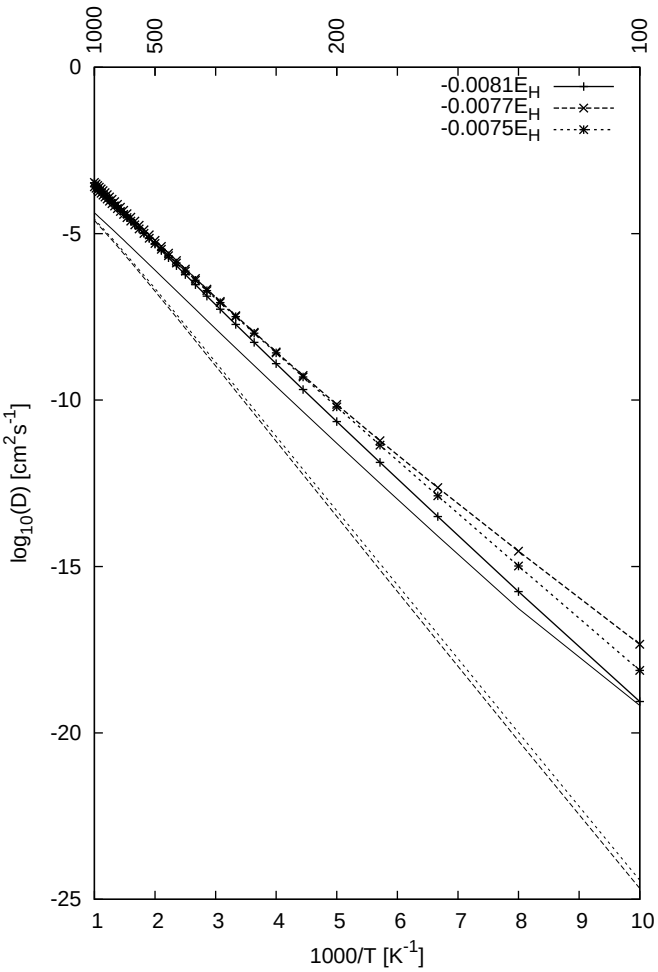

Figure 6.3: The diffusion curves for ^{1}H in three potentials. The lines without points are those calculated in part 5.3.1 included for comparison.

The contributions to diffusion from different regions of the eigenspectrum are plotted in figures 6.4 and 6.5. The band structures of the systems are shown in 6.6. The positions of the main peaks in figures 6.4 and 6.5 are marked on the band structures with arrows, along with the energy of the classical barriers (E_{TS}).

The contributions to diffusion for E^0_{oct} = -0.0075 E_H shown in figure 6.4(a) should be compared with those seen in figure 5.5(b). Whereas the lowest energy contribution was at around 440 meV in the uncoupled system, there are large contributions coming from just above 300 meV in the coupled system. By comparing with figure 6.6(a) these can be seen to be coming from states just above the classical barrier.

In the uncoupled potential contributions in this region could only come at the band edges, where two states became close in energy. There are now many more states in this region. States with a large amount of dispersion cross over other dispersive states which are shifted due to having a different phonon quantum number, ν. These crossing points give rise to contributions to diffusion at many different energies above the barrier, leading to both a lower activation energy and more diffusion at high temperatures.

The two peaks at E^0_{oct} = -0.0077 E_H and -0.0081 E_H occur due to contributions to diffusion from states below the classical barrier.

Figure 6.4(b) shows the contributions to diffusion when E^0_{oct} = -0.0081 E_H. Comparison with the band structure in figure 6.6(c) shows contributions at low temperatures from states which are considerably below the classical barrier. These are contributions from states which are in different wells, but which have the same phonon quantum number ν.

This can be seen by looking at the states contributing to the peak at 160 meV, the 12-th and 13-th states shown in figure 6.7. The 12-th state is the ground state in the tetrahedral well, whilst the 13-th state is the second excited state in the octahedral well. Neither state has nodes in the harmonic oscillator coordinate, q, so both must have large contributions from the $\nu = 0$ harmonic oscillator state. Such processes, which involve hops between different proton states whilst conserving the value of ν, can be called "coherent" processes.

The largest contributions at E^0_{oct} = -0.0081 E_H now come from above the barrier processes, even at low temperatures. The increase in contributions from the processes discussed above for the E^0_{oct} = -0.0075 E_H potential, leads to these processes dominating diffusion, rather than the coherent processes below the barrier.

The contributions to diffusion when E^0_{oct} = -0.0077 E_H are shown in figure 6.5. At low

temperatures the largest contribution occurs from states at around 272 meV above the ground state. Figure 6.6(b) shows that this contribution occurs at the crossing of a state with very little dispersion and one with slightly more. These two states, the 35-th and 36-th, are shown in figure 6.7.

The 35-th state looks like the third excited state in the octahedral well, with two nodes in the q dimension (ν=2). The 36-th state is more diffuse and centred in the tetrahedral well. It has no nodes in the q direction and looks like a ν=0 state. Contributions are also seen to occur at 297 meV and 322 meV. These are repetitions of the same states separated by $\hbar\omega$ which is 25 meV for a 200 cm^{-1} harmonic oscillator. Below the barrier processes which involve a change in the phonon quantum number, ν can be called "incoherent" processes. The incoherent processes which contribute to diffusion when E^0_{oct} = -0.0077 E_H lead to increased diffusion and a lower activation energy than would otherwise be the case, leading to a peak in the diffusion coefficients with this potential.

At higher temperatures, above 300K, the diffusion is once again dominated by contributions arising from transitions between dispersive states above the classical barrier with a change in phonon number, as in the two other potentials. The diffusion coefficients of hydrogen in all three potentials are very similar in the high temperature limit.

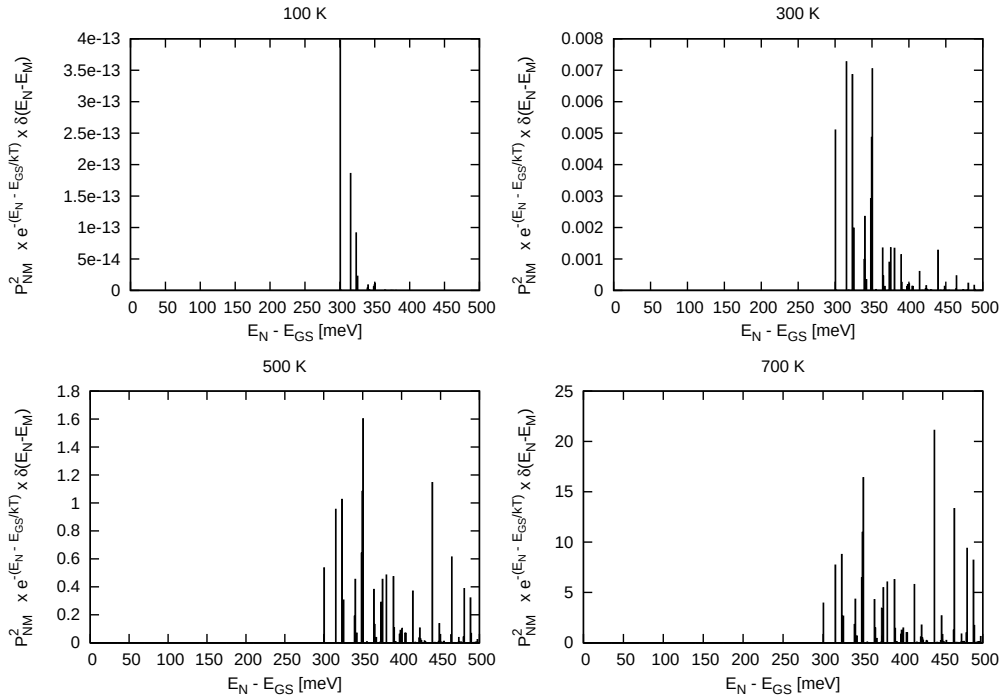

(a)

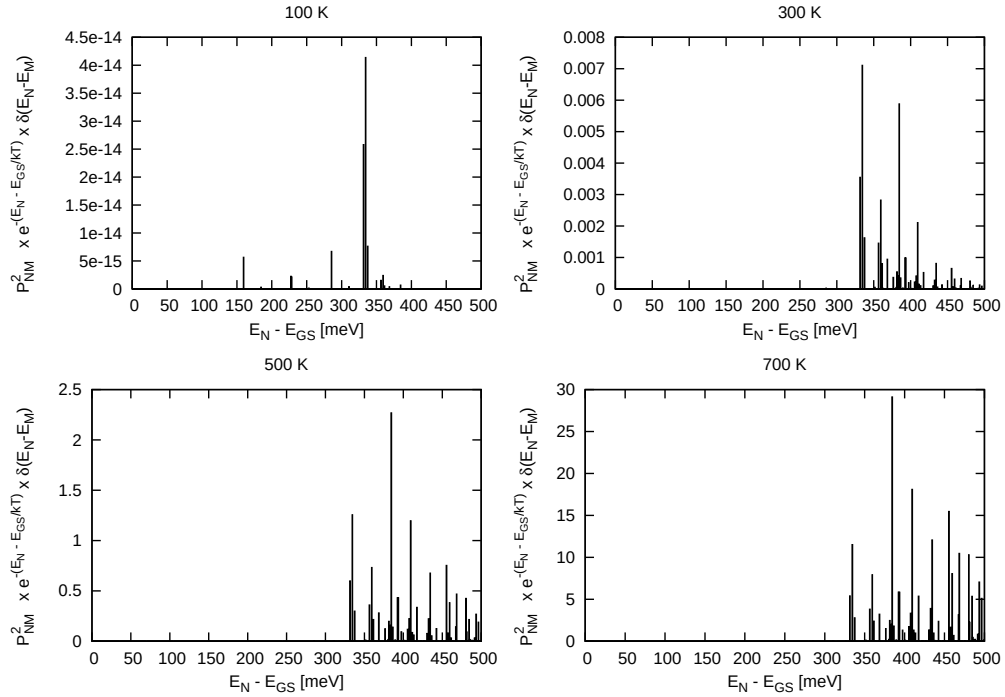

(b)

Figure 6.4: The contributions to the diffusion coefficient from different regions of the eigenspectrum below 500 meV above the ground state for ^{1}H (a)E_{oct} = -0.0075 E_H, (b)E_{oct} = -0.0081 E_H.

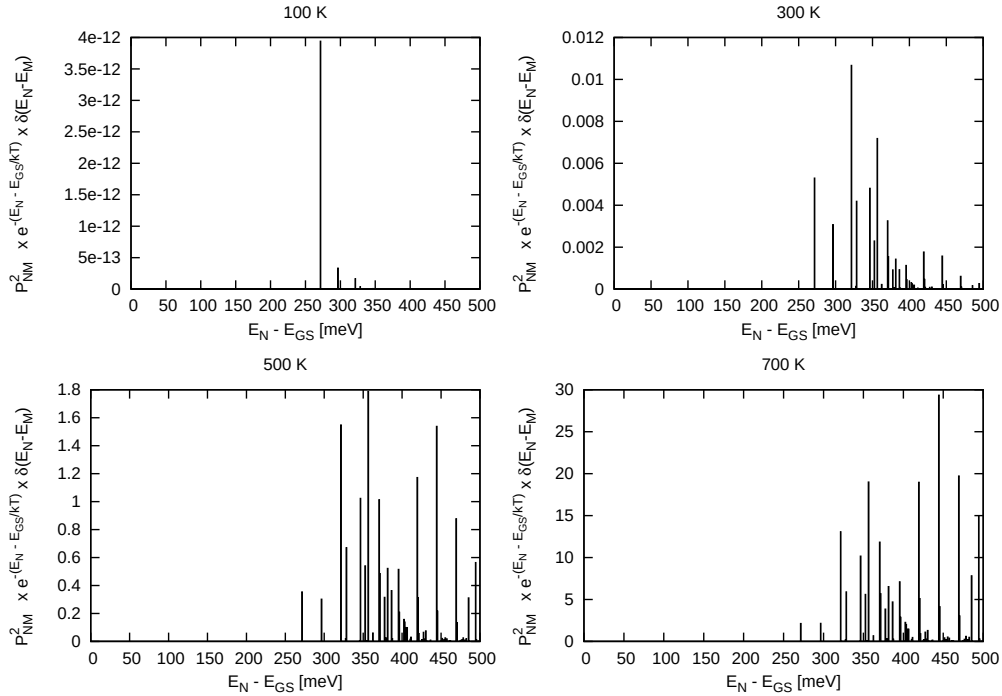

Figure 6.5: The contributions to the diffusion coefficient from different regions of the eigenspectrum below 500 meV above the ground state for ^{1}H, E_{oct} = -0.0077 E_H.

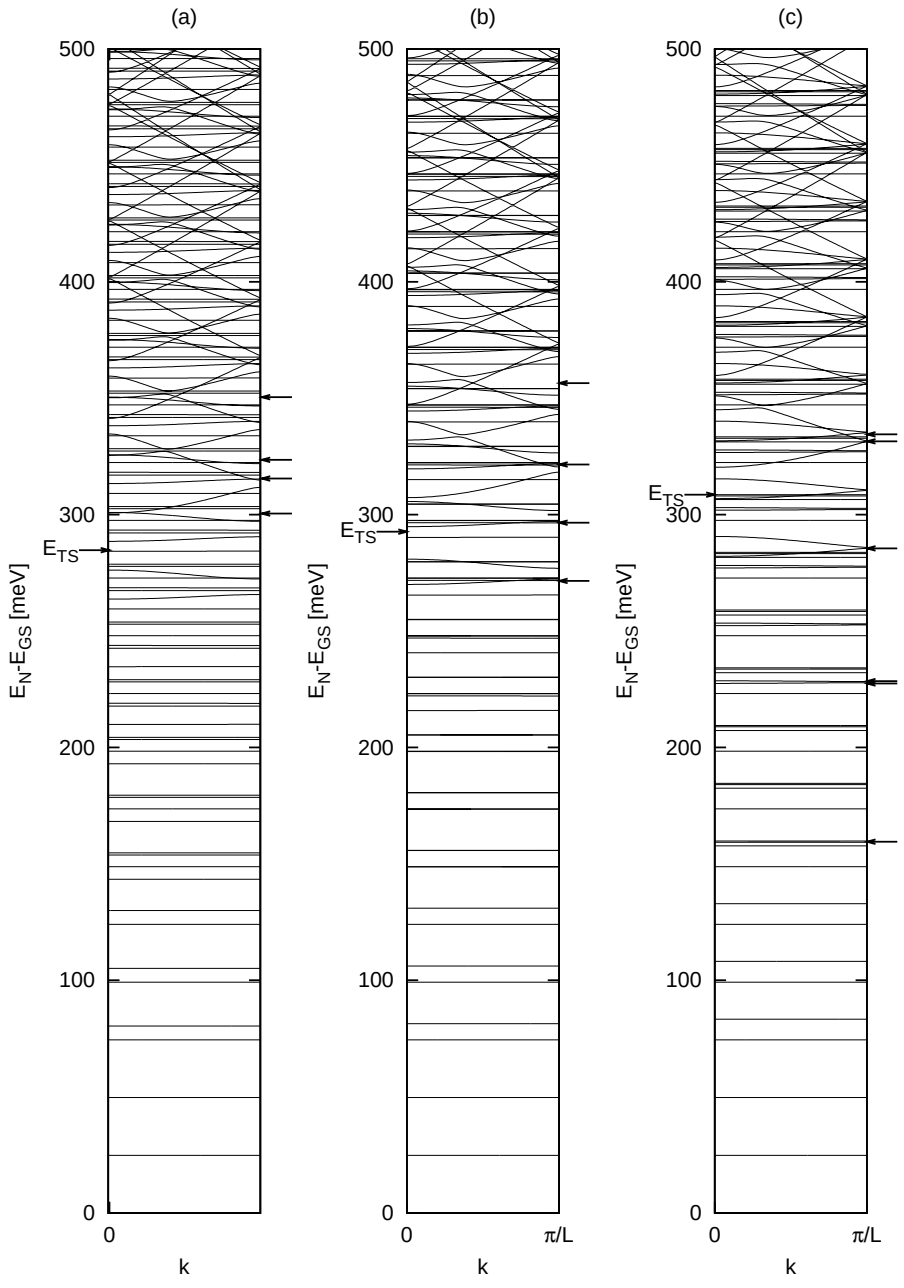

Figure 6.6: The band structure for ^{1}H states in three potentials (a) E_{oct} = -0.0075 E_H, (b)E_{oct} = -0.0077 E_H, (c) E_{oct} = -0.0081 E_H.

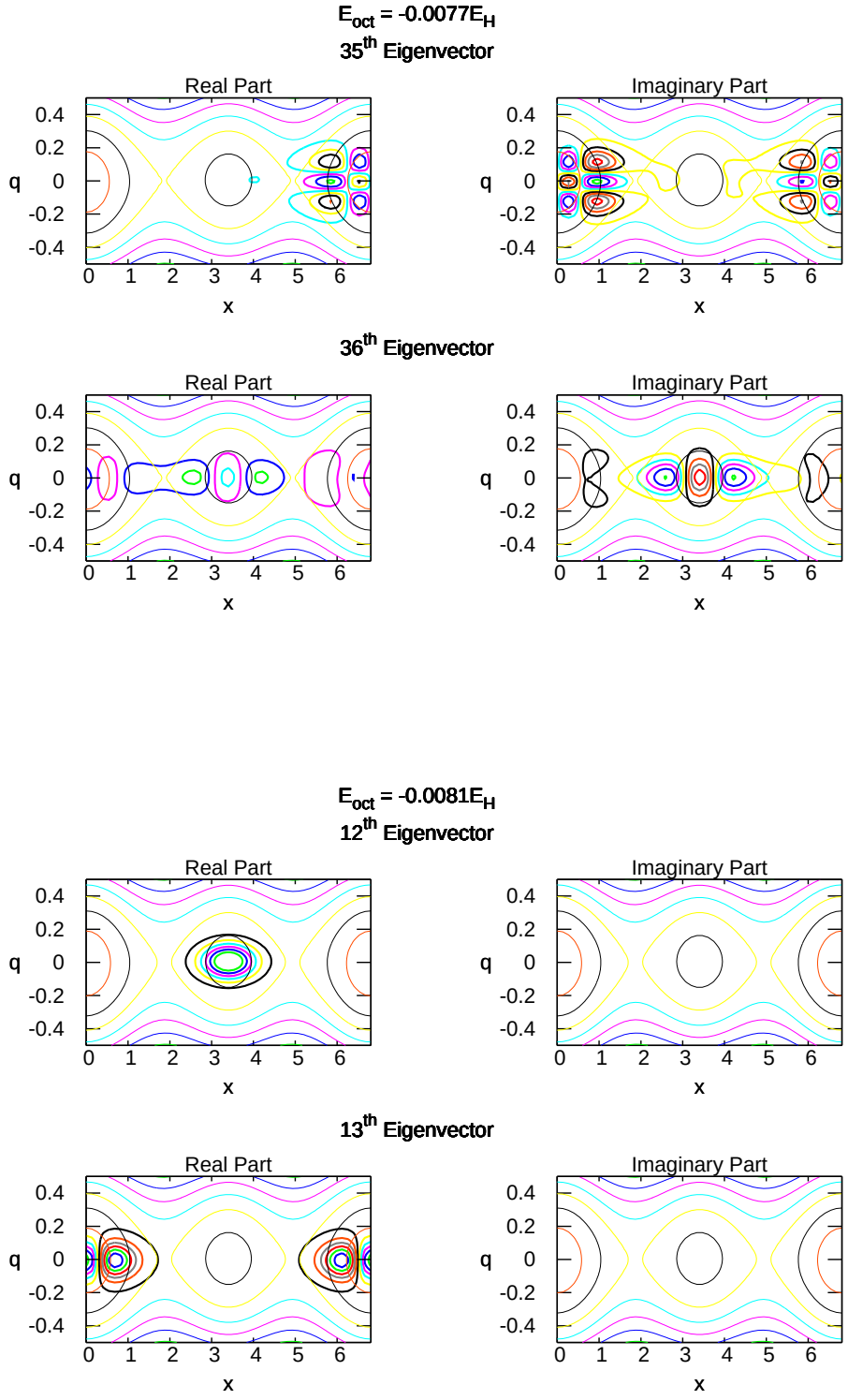

Figure 6.7: Contour plots of the ^{1}H wave functions which make low temperature contributions to diffusion in two different potentials, E_{oct} = -0.0077 E_H and E_{oct} = -0.0081 E_H. The wave functions are in bold and are plotted on top of the underlying potential.

Tuning the Frequency of the Oscillator

The incoherent processes described in the previous section (6.3.1) rely on there being a gap in between two hydrogen states which are an integer multiple of $\hbar\omega$ apart. It ought to be possible to vary the oscillator frequency, ω, and cause an increase in diffusion when incoherent processes become possible.

Diffusion coefficients were calculated using a potential similar to that in section 6.3.1, in which below the barrier incoherent processes were shown to contribute to diffusion. (E^0_{tet} = -0.002 E_H, E^0_{oct} = -0.0077 E_H, and α = 0.001). The frequency of the oscillator was varied about 200 cm^{-1} and the results can be seen in figure 6.8.

At 100K the only significant contribution is that described in the previous section between the 35-th and 36-th states of the system. As the frequency is altered, the relative position of the two states changes at a rate of approximately $2\hbar\omega$ as there is a difference of two in the phonon quantum numbers of the two states. The more diffuse state has a width of 2.3 meV, 18.6 cm^{-1}, approximately twice the width of the peak seen at 100 K in figure 6.8. The peak occurs when the two states cross each other.

At higher temperatures other processes contribute to diffusion and the dependence of diffusion on frequency is more complicated.

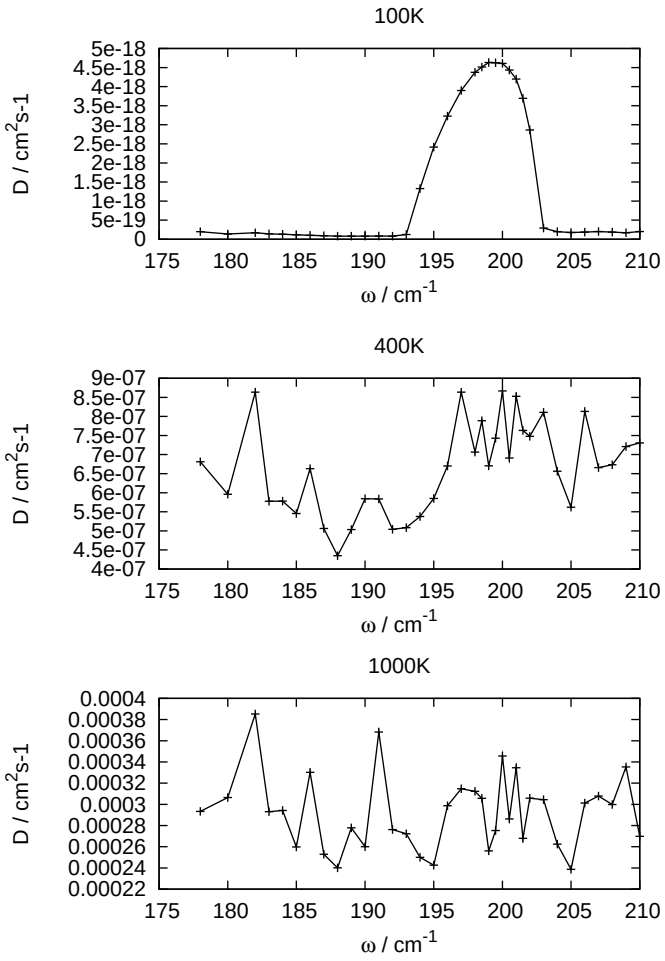

Figure 6.8: The diffusion coefficient for ^{1}H in a potential with E^0_{oct} = -0.0077 E_H, E^0_{tet} = -0.002 E_H and a coupling constant, α = 0.001 as the frequency of the oscillator was varied.

6.4 Approximations to Exact Coupling Calculations

Although it may appear that similar results could be obtained by using a set of wave functions which were purely the product of an eigenvector of the periodic system and one of the harmonic oscillator, this is not the case. The integral over the momentum operator of two states with different ν is zero. The diffusion calculated would be the same as in the periodic potential without the harmonic oscillator.

$$\langle \psi_n(x)\phi_\nu(q)|\hat{p}_x|\psi_m(x)\phi_{\nu'}(q)\rangle = \langle \psi_n(x)|\hat{p}_x|\psi_m(x)\rangle\, \delta_{\nu,\nu'} \tag{6.51}$$

To alter the diffusion it is necessary to have coupled wave functions which contain contributions from states with different ν.

6.4.1 Franck-Condon Factors

A simple approximation can be made along the lines of the methods proposed by Franck and Condon [76][77][78] to calculate electronic transition probabilities. It was assumed that electronic transitions occurred instantaneously with respect to nuclear motion. As a result the transition probability could be estimated by separating out the electronic and nuclear degrees of freedom and including an integral over the nuclear wave functions for the initial and final state. The nuclear wave function for the initial state was calculated in a potential assuming the electron was in its initial state, and the nuclear wave function for the final state was calculated using a different potential assuming the electron was in its final state.

Transitions between hydrogen states rather than electronic states are needed to make approximate calculations of the diffusion coefficients found in the previous sections. It is hoped that the mass difference between hydrogen and that of the coupled harmonic oscillator (or in a more realistic system, the mass of metal atoms through which the hydrogen is diffusing) is large enough that the assumption that hydrogen transitions occur without a change in the harmonic oscillator coordinate, q, is still valid. If this is the case, then the hydrogen atom can be assumed to be in the same potential in both the initial and final states. Only the harmonic oscillator potential will change.

A further assumption is made that the harmonic oscillator potential has only three different equilibrium positions and frequencies. These represent potentials when the hydrogen nucleus is in the deeper (octahedral) well, the shallower (tetrahedral) well, or spread

between the two. The equilibrium positions and frequencies of the oscillators can be calculated by varying q and calculating hydrogen states in the resulting periodic potential

$$V(x;q) = \frac{1}{2}\left(E_{tet}(q) - E_{oct}(q)\right)\cos\left(\frac{2\pi x}{L}\right) + \frac{1}{2}\left(E_{tet}(q) + E_{oct}(q)\right)\cos\left(\frac{4\pi x}{L}\right) \quad (6.52)$$

Where $E_{oct}(q) = E^0_{oct} + \alpha q$ and $E_{tet}(q) = E^0_{tet} - \alpha q$.

The energies of the eigenstates, $\varepsilon(q)$, were then plotted after adding the harmonic potential $\frac{1}{2}k_q q^2$. States were identified as belonging to the octahedral or tetrahedral well, or both, by integration of the hydrogen wave functions. Results of this procedure can be seen in figure 6.9.

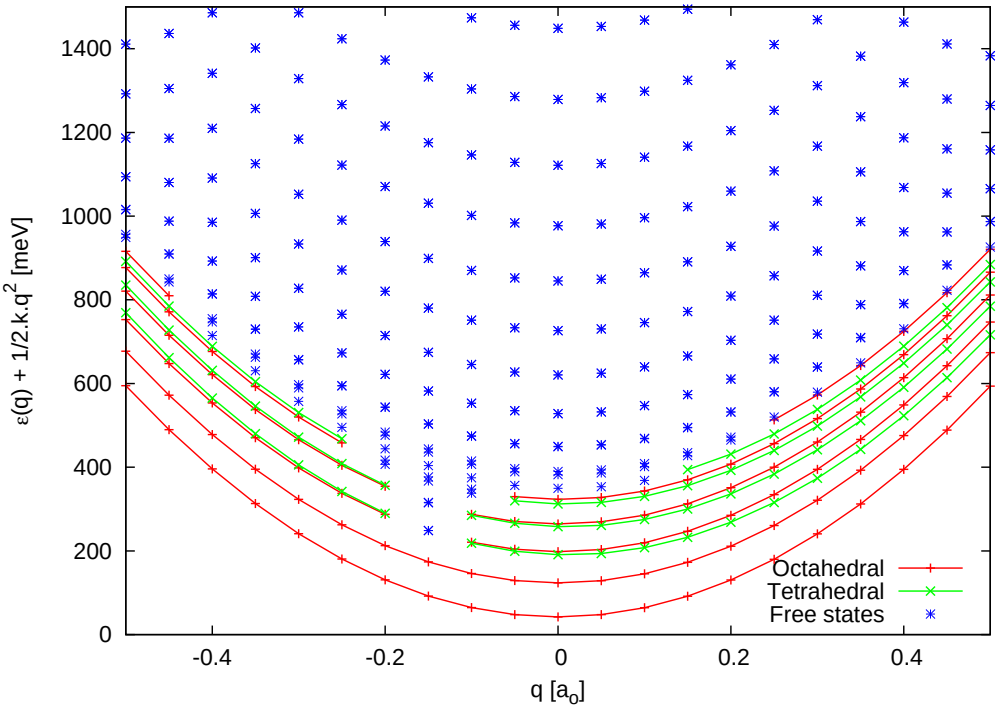

Figure 6.9: A plot of the energies of the hydrogen atom ε against q with E^0_{tet} = -0.002 E_H, E^0_{oct} = -0.0077 E_H, ω = 200 cm^{-}1, and α = 0.001.

The curves for the three potentials were then fitted to quadratic functions of q to give the frequencies and equilibrium positions of the three harmonic potentials.

Using the potential defined in this chapter (equation 6.50), it can be shown that the q

dependent part of the potential is a forced harmonic oscillator.

$$V(x,q) = V(x,0) + \frac{k_q}{2}q^2 + \alpha q \cos\left(\frac{2\pi x}{L}\right) \tag{6.53}$$

$$= V(x,0) + \frac{k_q}{2}\left(q + \frac{\alpha}{k_q}\cos\left(\frac{2\pi x}{L}\right)\right)^2 - \frac{\alpha^2}{2k_q}\cos^2\left(\frac{2\pi x}{L}\right) \tag{6.54}$$

$$= V'(x) + \frac{k_q}{2}\left(q - q_0(x)\right)^2 \tag{6.55}$$

Where $q_0(x) = -\frac{\alpha}{k_q}\cos\left(\frac{2\pi x}{L}\right)$. This potential has the same frequency as the uncoupled harmonic potential. However, the equilibrium position depends on the value of x. The equilibrium positions should be roughly $q_0 = -\frac{\alpha}{k_q}$ when $x = 0$ (at the bottom of the deepest well), $q_0 = \frac{\alpha}{k_q}$ when $x = \frac{L}{2}$ (at the bottom of the shallower well), and $q_0 = 0$ for states which are not bound in any one well. The frequencies should be the same in each case. A comparison of these parameters with those calculated using the fitting technique discussed above can be seen in table 6.1.

Table 6.1: Parameters for different potentials when E^0_{tet} = -0.002 E_H, E^0_{oct} = -0.0077 E_H, $\omega = 200$ cm^{-1}, and $\alpha = 0.001$.

	Octahedral		Tetrahedral		Unbound	
	ω [cm^{-1}]	q_0 [a_0]	ω [cm^{-1}]	q_0 [a_0]	ω [cm^{-1}]	q_0 [a_0]
Fit	200.0	-5.93×10^{-3}	200.0	5.88×10^{-3}	200.0	3.54×10^{-4}
Calc.	200	-6.16×10^{-3}	200	6.16×10^{-3}	200	0

Once the parameters for the three harmonic potentials have been found, the diffusion coefficient can be approximated by calculating the integral of two states over the momentum operator. The states are given by the product of a wave function of the uncoupled periodic potential, $\psi^k_n(x)$, and a wave function of the harmonic potential chosen depending on whether $\psi^k_n(x)$ is bound in the deeper well, the shallower well, or unbound.

$$\left\langle \psi^k_m \phi_{\nu'}(\omega', q - q'_0) \left| \hat{p}_x \right| \psi^k_n \phi_\nu(\omega, q - q_0) \right\rangle$$

$$= \left\langle \phi_{\nu'}(\omega', q - q'_0) \middle| \phi_\nu(\omega, q - q_0) \right\rangle \left\langle \psi^k_m \middle| \hat{p}_x \middle| \psi^k_n \right\rangle \tag{6.56}$$

$$= S_{\nu'\nu} \left\langle \psi^k_m \middle| \hat{p}_x \middle| \psi^k_n \right\rangle \tag{6.57}$$

$S_{\nu'\nu}$ are Franck-Condon factors, an overlap integral over two harmonic oscillator states which arise from potentials with different frequencies, ω and ω', and equilibrium positions, q_0 and q'_0. They can be accurately and efficiently calculated numerically using Gauss-Hermite quadrature. The second factor in equation 6.57 is simply the integral P^k_{nm}

discussed in section 5.1.

The diffusion coefficient can then be calculated using the usual formula and summing over enough harmonic oscillator states to converge the calculation.

$$D = \int dk \, \frac{\pi}{NQm_H^2} \sum_{n,m\neq n,\nu,\nu'} e^{-\beta\left(\varepsilon_n+\hbar\omega\left(\nu+\frac{1}{2}\right)\right)} S_{\nu'\nu} |P_{nm}^k|^2 \times \delta\left(\frac{\varepsilon_n}{\hbar} - \frac{\varepsilon_m}{\hbar} + \omega\left(\nu+\frac{1}{2}\right) - \omega'\left(\nu'+\frac{1}{2}\right)\right) \quad (6.58)$$

Results and Discussion

The diffusion coefficients of ^{1}H were calculated using the Franck-Condon approximations and using the exact diagonalisation technique discussed at the start of this chapter. The calculations were carried out with E_{tet}^0 = -0.002 E_H, E_{oct}^0 = -0.0077 E_H, ω = 200 cm^{-1} and α = 0.001 and 0.0001. The results can be seen in figure 6.10

Enhancement of diffusion over that calculated in the uncoupled system is only seen at low temperatures. A plot of the separate contributions to diffusion from different points in the eigenspectrum (see figure 6.11) shows that at low temperatures diffusion comes from contributions arising from the same states as in the exact calculation in figure 6.5. The magnitude of the contributions from these states is, however, underestimated by about two orders of magnitude.

At higher temperatures the contributions from states between 300 meV and 400 meV above the ground state are largely missing in the calculations using Franck-Condon factors. Instead the contributions from above the classical barrier occur at the band edges where the uncoupled proton wave functions become degenerate, hence the rate of diffusion is that of the uncoupled system.

It has been assumed that states which are not bound in one well or the other, which in general are states above the classical barrier, have the same harmonic potential. Contributions are only allowed from these states if the quantum number ν is the same in both. The exact calculations in section 6.3.1 show that contributions from incoherent processes above the classical barrier, which are missing using this approximate method, are important at higher temperatures.

At lower temperatures the important contributions arise from states which are bound in different wells and have different values of ν. These contributions are included using the

Franck-Condon factors but are severely underestimated.

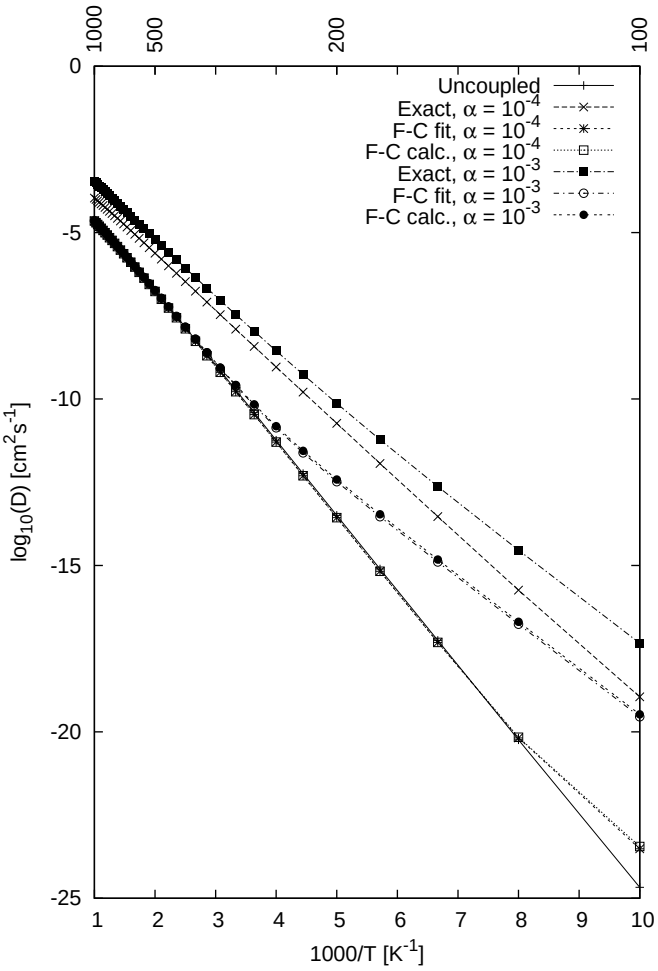

Figure 6.10: A plot of the diffusion coefficients of ^{1}H E^0_{tet} = -0.002 E_H, E^0_{oct} = -0.0077 E_H, ω = 200 cm$^-$1.

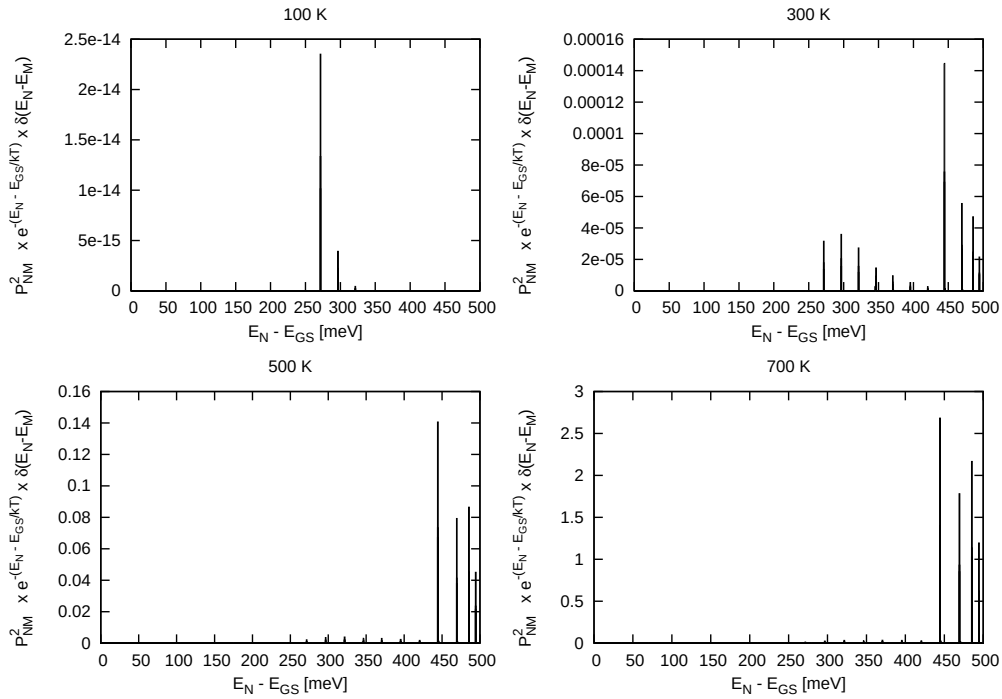

Figure 6.11: The contributions to the diffusion coefficient from different regions of the eigenspectrum below 500 meV above the ground state for ^{1}H, E^0_{tet} = -0.002 E_H, E^0_{oct} = -0.0077 E_H, ω = 200 cm$^-$1 and α = 0.001, using Franck-Condon factors.

6.4.2 Perturbation Theory

Perturbation theory could be used to generate wave functions and energies for the coupled system, starting from states which were products of the solutions for the uncoupled periodic potential and harmonic oscillator. These wave functions and energies could then be used to calculate diffusion coefficients for the coupled system as before.

$$\hat{\mathcal{H}}^{(0)} = -\frac{1}{2m_x}\nabla_x^2 - \frac{1}{2m_q}\nabla_q^2 + V(x,0) + \frac{k_q}{2}q^2 \tag{6.59}$$

$$\Psi_{n\nu}^{k(0)} = \psi_n^k(x)\phi_\nu(q) \tag{6.60}$$

$$E_{n\nu}^{k(0)} = \varepsilon_n^k + \hbar\omega\left(\nu + \frac{1}{2}\right) \tag{6.61}$$

Where $\psi_n(x)$ is the hydrogen wave function in the potential $V(x,0)$ and $\phi_\nu(q)$ is a harmonic oscillator wave function. The perturbation to this system is taken as the coupling part of the full Hamiltonian

$$\hat{\mathcal{H}}^{(1)} = \alpha q \cos\left(\frac{2\pi x}{L}\right) \tag{6.62}$$

The first order correction to the energies, $E_{n\nu}^{k(1)}$, is given by the integral $\left\langle \psi_n^k\phi_\nu|\hat{\mathcal{H}}^{(1)}|\psi_n^k\phi_\nu \right\rangle$. This integral is zero, since $\langle\phi_\nu|q|\phi_\nu\rangle$ is zero for all ν. Instead, the first order correction to the wave functions and the second order correction to the energies are calculated. It is important to use perturbation theory suitable for systems with degenerate states, since only transitions between degenerate states, or states close in energy, contribute to diffusion.

For degenerate states, it is necessary to use a set of secular equations to obtain the first order corrections to the energies, $E_{n\nu i}^{(1)}$, and the optimal choice for the zeroth order wave functions, $\Phi_{n\nu i}^{k(0)} = \sum_l c_{il}\Psi_{n\nu l}^{k(0)}$ (where the third index in these expressions distinguishes between formerly degenerate states).

$$\sum_l c_{il}\left(E_{n\nu i}^{k(1)}\delta_{ml} - \left\langle \Psi_{n\nu m}^{k(0)}|\hat{\mathcal{H}}^{(1)}|\Psi_{n\nu l}^{k(0)} \right\rangle\right) = 0 \tag{6.63}$$

In the case of degenerate states the first order correction to the energies may be non-zero.

Once this process has been carried out, the first order corrections to the wave functions, $\Psi_{n\nu}^{k(1)}$, and the second order corrections to the energies, $E_{n\nu}^{k(2)}$, can be calculated using the familiar expressions from Rayleigh-Schrödinger perturbation theory [79][80] in which the corrections to the wave functions are expressed as a linear combination of the zeroth order

wave functions.

$$\Psi_{n\nu}^{k(1)} = \sum_{m\nu'}{}' \frac{\left\langle \Psi_{m\nu'}^{k(0)} | \hat{\mathcal{H}}^{(1)} | \Psi_{n\nu}^{k(0)} \right\rangle}{E_{n\nu}^{k(0)} - E_{m\nu}^{k(0)}} \Psi_{m\nu'}^{k(0)} \tag{6.64}$$

$$E_{n\nu}^{k(2)} = \sum_{m\nu'}{}' \frac{|\left\langle \Psi_{m\nu'}^{k(0)} | \hat{\mathcal{H}}^{(1)} | \Psi_{n\nu}^{k(0)} \right\rangle|^2}{E_{n\nu}^{k(0)} - E_{m\nu}^{k(0)}} \tag{6.65}$$

The sums over m and ν' do not include terms in which $m = n$ and $\nu' = \nu$ or terms where $\Psi_{m\nu'}^{k(0)}$ and $\Psi_{n\nu}^{k(0)}$ are degenerate or near-degenerate wave functions.

The wave functions and energies of the perturbed system are then given by

$$\Psi_{n\nu}^{k} = \Psi_{n\nu}^{k(0)} + \Psi_{n\nu}^{k(1)} \tag{6.66}$$

$$E_{n\nu}^{k} = E_{n\nu}^{k(0)} + E_{n\nu}^{k(1)} + E_{n\nu}^{k(2)} \tag{6.67}$$

They can be used in the expression for the diffusion coefficients to give an estimate of the diffusion coefficients of the coupled system.

The diffusion coefficients of ^{1}H were calculated using perturbation theory to find the coupled wave functions and energies. The calculations were carried out with E_{tet}^0 = -0.002 E_H, E_{oct}^0 = -0.0077 E_H, ω = 200 cm^{-1} and α = 0.001 and 0.0001. The results can be seen in figure 6.12

The rates of diffusion calculated using perturbation theory underestimate those calculated from the exact wave functions and energies. Calculation of the wave functions using equation 6.64 gives wave functions with contributions from the original wave function with quantum number ν and wave functions with $\nu' = \nu \pm 1$. Using these wave functions to calculate diffusion coefficients includes contributions from states with up to $\nu \pm 2$, but no larger. Some of the extra contributions to diffusion in the coupled system are captured, but not all leading to an underestimate of the diffusion rates.

Separate contributions to diffusion from different points on the energy spectrum for the calculations with $\alpha = 0.001$ can be seen in figure 6.13. Comparing with the results from the calculations using the exact wave function in figure 6.5 it can be seen that contributions occur from interactions between states at the same places in the energy spectrum, but that some of the contributions are missing (for example those at around 330 meV), the relative contributions from different regions are different, and the magnitude of the contributions throughout the energy spectrum are a lot lower at a given temperature.

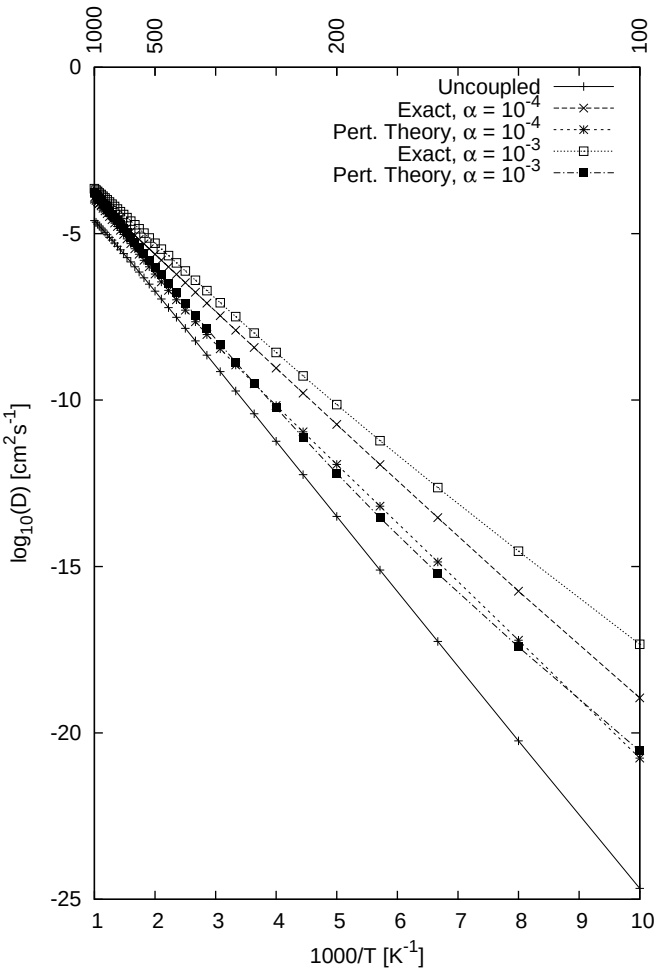

Figure 6.12: A plot of the diffusion coefficients of ^{1}H. E^0_{tet} = -0.002 E_H, E^0_{oct} = -0.0077 E_H, and ω = 200 cm$^-$1.

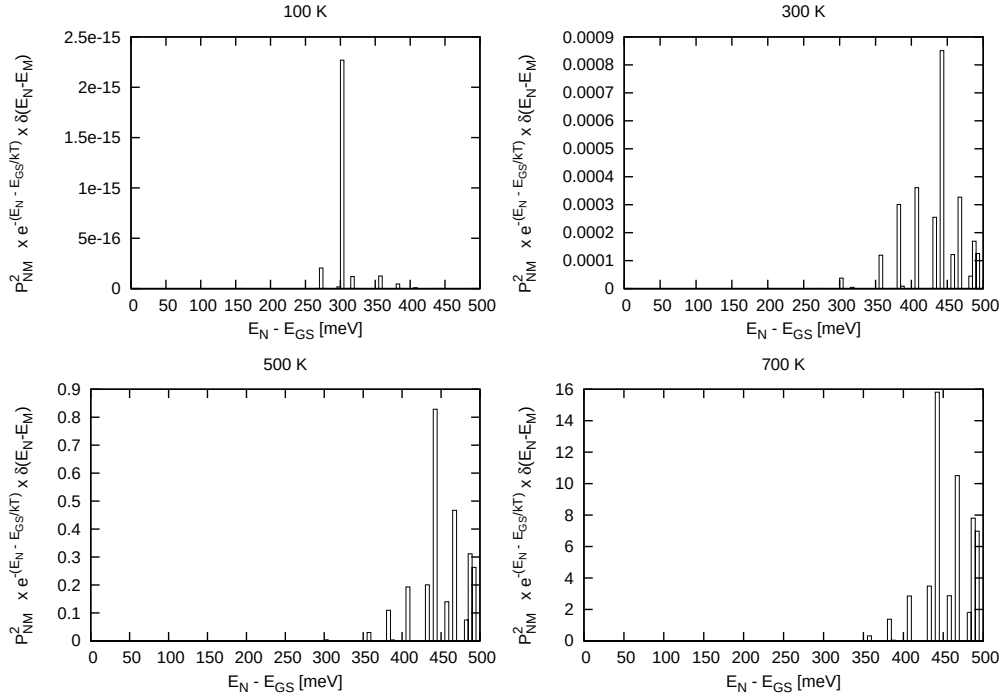

Figure 6.13: The contributions to the diffusion coefficient from different regions of the eigenspectrum below 500 meV above the ground state for ^{1}H, E^0_{tet} = -0.002 E_H, E^0_{oct} = -0.0077 E_H, ω = 200 cm$^-$1, and α = 0.001, using perturbation theory to find the wave functions and energies.

6.5 Conclusions

The one-dimensional well described in the previous chapter was coupled to a harmonic oscillator such that the depths of the two wells varied according to the harmonic oscillator coordinate. Coupling to the harmonic oscillator had a large effect on the diffusion coefficients calculated for hydrogen and deuterium.

The inclusion of harmonic oscillator states allowed for contributions to diffusion through a different type of process, so called "incoherent" processes. In incoherent processes transitions can be made between hydrogen states which were previously not coincident by gaining or losing phonons. The inclusion of incoherent processes at energies above and below the classical diffusion barrier led to a general increase in the rate of diffusion.

The diffusion coefficients of the coupled system did not vary as much with the equilibrium depths of the two wells as the diffusion coefficients of the uncoupled system. In general a smooth decrease in diffusion was seen as the wells were made deeper, with some variation caused by the inclusion of coherent or incoherent tunnelling processes below the classical barrier energy.

Similarly the isotope effect was less dependent on the potential, deuterium almost always diffusing at a slower rate than hydrogen.

Two methods were used to find approximate values for the diffusion coefficients of the coupled system. An attempt was made to include the effect of the harmonic oscillator by including Franck-Condon factors and by using perturbation theory. Neither method gave accurate results.

The method used to find the diffusion coefficients of this simple system could be used to look at coupling between hydrogen diffusion in a metal lattice and the phonon modes of the lattice. The increase in diffusion seen due to the inclusion of incoherent tunnelling in this system may also be seen in real systems such as palladium hydride.

Chapter 7

Concluding Remarks

This thesis has shown that new insights into materials containing hydrogen can be gained by calculating the single-particle wave functions and energies of hydrogen in the material. It is often necessary to use quantum mechanics when describing both the location and diffusion of hydrogen and its isotopes in metal hydrides and similar materials.

An accurate potential was necessary for the calculation of the hydrogen wave functions and energies. Density functional theory (DFT) in a plane-wave basis has been shown to be a computationally efficient way to perform accurate calculations of the electronic energies of periodic systems, and was used in this study to calculate the potential energy of a hydrogen atom within a host lattice.

The calculated vibrational energy levels of hydrogen and its isotopes in palladium hydride and niobium hydride were close to the values provided by experiments, suggesting that the potentials calculated using DFT were accurate enough to give meaningful results.

It was shown that quantum effects are important in determining the position of the hydrogen atom in palladium hydride and lithium imide.

The zero point energy of the hydrogen atom at the octahedral interstitial site of the palladium lattice is much lower than that at the tetrahedral site. This leads to a considerable increase in stability of the octahedral site over the tetrahedral site.

Hydrogen in lithium imide was found to occupy a different site to that predicted by X-ray and neutron diffraction experiments. The hydrogen atoms were found to occupy sites which formed an octahedron around the nitrogen atoms. The quantum tunnelling rate

between these sites is fast, so a delocalised picture of the hydrogen atoms is found to be more accurate than the classical idea of random occupation of the possible sites.

As well as providing a way to analyse the quantum effects on hydrogen location in materials, the wave functions and energies were used look at quantum effects in the diffusion of hydrogen and its isotopes in materials. An expression for the diffusion coefficient can be derived from the statistical mechanics of non-equilibrium systems and the wave functions and energies used in this expression to calculate the diffusion coefficient.

This method was used to calculate the diffusion coefficients of hydrogen, deuterium, and tritium in stoichiometric palladium and niobium hydrides. An inverse isotope effect was found in the activation energies to diffusion in palladium, as seen in experiment.

The processes which take place in hydrogen diffusion were investigated by considering which pairs of states contributed to diffusion in the expression used to calculate the diffusion coefficient.

It was found that diffusion in palladium hydride was dominated by processes which involved states in both the octahedral and tetrahedral sites. Some of the processes were at energies below the classical barrier and could be classified as activated tunnelling processes. Others were at energies above the classical energy barrier. Tunnelling between the ground states and lower excited states in neighbouring octahedral wells only became important at low temperatures.

The relative rates of diffusion for different isotopes was found to depend on the energy of the pairs of states which contribute to diffusion and how much each pair contributes. The heavier isotopes, deuterium and tritium, have a higher density of states at low energies, which favours diffusion, but also have more tightly bound states, which leads to less diffusion. The balance of these effects determines the isotope effect observed in the diffusion coefficients.

The diffusion of hydrogen in niobium hydride is much more dominated by tunnelling between the ground states and low energy excited states in neighbouring sites than in palladium hydride. This leads to an onset of non-Arrhenius behaviour in the diffusion coefficients at higher temperatures than is seen for palladium hydride. No second site is found to be important for diffusion in niobium hydride.

A model potential of a one-dimensional periodic potential coupled to a harmonic oscillator was used to investigate the possible effect of coupling between phonon modes and hydrogen

wave functions on diffusion in metal hydrides.

It was found that coherent and incoherent processes could contribute to diffusion when coupling was present. Coherent processes involve transitions between pairs of states with the same phonon occupation numbers, whereas incoherent processes involve transitions in which the phonon occupation numbers change. Both coherent and incoherent processes were seen to contribute at energies above and below the classical energy barrier to diffusion.

Coupling to a harmonic oscillator was found to increase the rates of diffusion of hydrogen and deuterium through the one-dimensional periodic potential. This was due to the increase in pairs of states which could contribute to diffusion as incoherent processes were included.

It was also found that including coupling to the harmonic oscillator reduced the strong dependence of the diffusion coefficients to the shape of the potential which was found when considering diffusion in the uncoupled one-dimensional potential.

The method used to calculate the diffusion coefficient of hydrogen and its isotopes in the coupled potential could be used to calculate the diffusion coefficient in a metal hydride, including coupling between some of the phonon modes of the lattice and the hydrogen wave functions.

If the rate of diffusion was increased by this coupling, then the calculated diffusion coefficients may be closer to experiment than in the case when coupling was neglected, and the diffusion coefficients were, in general, underestimated.

As well as extending this research to include coupling in real systems, studies could be made into the diffusion of hydrogen and its isotopes at different concentrations in palladium and niobium, and into diffusion of hydrogen in other systems. These applications would require a different potential to be calculated using DFT or some other method. The diffusion of other particles with small mass such as muonium could also be calculated.

Acknowledgements

The author would like the thank the following:

- Dr Ali Alavi, for all his guidance and support as my supervisor.
- Dr Changjun Zhang, for his work on the niobium hydride and lithium imide systems.
- The Engineering and Physical Sciences Research Council, for funding.
- Paul Webster, for proof reading.
- Christopher Rayson and Dr Mark Miller, for obtaining literature.
- Dr Catherine Pitt, for computer support.
- The other members of Dr Alavi's research group and the Cambridge University Centre for Computational Chemistry, for helpful discussion.
- My family, MethSoc, Naomi, Paul, Bert, Ian and Jess, my church and God for general support and guidance throughout my studies.

Bibliography

[1] J.-P. Hansen and I. R. McDonald. *Theory of Simple Liquids*. Academic Press, London, Second ed. (1986).

[2] P. W. Atkins. *Physical Chemistry*. Oxford University Press, Oxford, Sixth ed. (1998).

[3] A. Einstein. Ann. d. Physik **17**, 549–560 (1905).

[4] H. Eyring. J. Chem. Phys. **4**, 283–291 (1936).

[5] H. Eyring. J. Chem. Phys. **3**, 107–115 (1935).

[6] V. A. Benderskii, D. E. Makarov, and C. A. Wight. *Chemical Dynamics at Low Temperatures*. Wiley, New York (1994).

[7] A. O. Caldeira and A. J. Leggett. Ann. of Phys. **149**, 374–456 (1983).

[8] A. J. Leggett, S. Chakravarty, A. T. Dorsey, M. P. A. Fisher, A. Gang, and W. Zwerger. Rev. Mod. Phys. **59**, 1–85 (1987).

[9] D. Borgis, S. Lee, and J. T. Hynes. Chem. Phys. Lett. **162**, 19–26 (1989).

[10] D. Borgis and J. T. Hynes. J. Chem. Phys. **94**, 3619–3628 (1991).

[11] C. P. Flynn and A. M. Stoneham. Phys. Rev. B **1**, 3966–3978 (1970).

[12] P. G. Sundell and G. Wahnström. Phys. Rev. Lett. **92**, 155901 (2004).

[13] J. G. Kirkwood. J. Chem. Phys. **14**, 180–201 (1946).

[14] R. Kubo. J. Phys. Soc. Japan **12**, 570–586 (1957).

[15] H. Mori. J. Phys. Soc. Japan **11**, 1029–1044 (1956).

[16] M. S. Green. J. Chem. Phys. **19**, 1036–1046 (1951).

[17] M. S. Green. J. Chem. Phys. **22**, 398–413 (1954).

[18] D. A. Greenwood. Phys. Proc. **71**, 585–596 (1958).

[19] R. Car and M. Parrinello. Phys. Rev. Lett. **55**, 2471–2474 (1985).

[20] M. D. Segall, P. L. D. Lindan, M. J. Probert, C. J. Pickard, P. J. Hasnip, S. J. Clark, and M. C. Payne. J. Phys.: Condens. Matter **14**, 2717–2743 (2002).

[21] M. Born and R. Oppenheimer. Ann. d. Physik **84**, 457–484 (1927).

[22] W. Kohn and L. J. Sham. Phys. Rev. **140**, 1133–1138 (1965).

[23] J. P. Perdew, K. Burke, and M. Ernzerhof. Phys. Rev. Lett. **77**, 3865–3868 (1996).

[24] A. Alavi, J. Kohanoff, M. Parrinello, and D. Frenkel. Phys. Rev. Lett. **73**, 2599–2602 (1994).

[25] N. D. Mermin. Phys. Rev. **137**, A1441–A1443 (1965).

[26] P. Hohenberg and W. Kohn. Phys. Rev. **136**, B864–B871 (1964).

[27] N. Troullier and J. L. Martins. Phys. Rev. B **43**, 1993–2006 (1991).

[28] D. Vanderbilt. Phys. Rev. B **41**, 7892–7895 (1990).

[29] F. Bloch. Z. f. Phys. **52**, 555–600 (1928).

[30] L. Brillouin. *Wave propagation in periodic structures*. Dover (1953).

[31] F. A. Lewis. *The Palladium Hydrogen System*. Academic Press, London (1967).

[32] J. Völkl and G. Alefeld. *Hydrogen in Metals I*. Springer-Verlag, Berlin (1978).

[33] T. B. Flanagan and W. A. Oates. Annu. Rev. Mater. Sci. **21**, 269–304 (1991).

[34] C. N. Rao and K. K. Rao. Can. J. Phys. **42**, 1336–1342 (1964).

[35] A. C. Switendick. In J. Völkl and G. Alefeld, eds., *Hydrogen in Metals I*, chap. 5, pp. 106–107. Springer-Verlag, Berlin (1978).

[36] D. K. Ross, V. E. Antonov, E. L. Bokhenkov, A. I. Kolesnikov, E. G. Ponyatovsky, and J. Tomkinson. Phys. Rev. B **58**, 2591–2595 (1998).

[37] A. M. James and M. P. Lord. *Macmillan's chemical and physical data*. Macmillan, London (1992).

[38] L. A. Nygren and R. G. Leisure. Phys. Rev. B **37**, 6482–6485 (1988).

[39] R. B. Schwarz, H. T. Bach, U. Harms, and D. Tuggle. Acta Meter. **53**, 569–580 (2005).

[40] J. E. Schirber and B. Morosin. Phys. Rev. B **12**, 117–118 (1975).

[41] J. M. Rowe, J. J. Rush, L. A. de Graaf, and G. A. Ferguson. Phys. Rev. Lett. **29**, 1250–1253 (1972).

[42] J. J. Rush, J. M. Rowe, and D. Richter. Z. Phys. B - Condensed Matter **55**, 283–286 (1984).

[43] M. Kemali, J. E. Totolici, D. K. Ross, and I. Morrison. Phys. Rev. Lett. **84**, 1531–1534 (2000).

[44] C. Elsässer, K. M. Ho, C. T. Chan, and M. Fähnle. Phys. Rev. B **44**, 10377–10380 (1991).

[45] C. Elsässer, K. M. Ho, C. T. Chan, and M. Fähnle. J. Phys.: Condens. Matter **4**, 5207–5226 (1992).

[46] J. Völkl and G. Alefeld. In *Hydrogen in Metals I*, chap. 12, pp. 321–348. Springer-Verlag, Berlin (1978).

[47] G. Sicking and H. Buchold. Z. Naturforsch. A **26**, 1973–1980 (1971).

[48] D. A. Cornell and E. F. W. Seymour. J. Less-Common Met. **39**, 43–54 (1975).

[49] G. Bohmholdt and E. Wicke. Z. Phys. Chem. N. F. **56**, 133–154 (1967).

[50] E. F. W. Seymour, R. M. Cotte, and W. D. Williams. Phys. Rev. Lett. **35**, 165–167 (1975).

[51] M. M. Beg and D. K. Ross. J. Phys. C: Solid. St. Phys. **3**, 2487–2500 (1970).

[52] M. Kuballa and B. Baranowski. Ber. Bunsenges. Phys. Chem. **78**, 335–338 (1974).

[53] S. Majorowski and B. Baranowski. J. Phys. Chem. Solids **43**, 1119–1127 (1982).

[54] G. Holleck and E. Wicke. Z. Phys. Chem. N. F. **56**, 155–172 (1967).

[55] J. Völkl, G. Wollenweber, K.-H. Klatt, and G. Alefeld. Z. Naturforsch. A **26**, 922–923 (1971).

[56] H. Katsuta, R. J. Farraro, and R. B. McLellan. Acta Metall. **27**, 1111–1114 (1979).

[57] M. Dyer, C. Zhang, and A. Alavi. Chem. Phys. Chem. **6**, 1–6 (2005).

[58] C. Zhang, M. Dyer, and A. Alavi. J. Phys. Chem. B **109**, 22089 (2005).

[59] B. J. Makenas and H. K. Birnbaum. Acta Metall. **30**, 469–481 (1982).

[60] U. Köbler and J.-M. Welter. J. Less-Common Met. **84**, 225–235 (1982).

[61] M. A. Pick and R. Bausch. J. Phys. F: Met. Phys. **6**, 1751–1763 (1976).

[62] D. Richter and S. M. Shapiro. Phys. Rev. B **22**, 599–605 (1980).

[63] J. J. Rush, A. Magerl, J. M. Rowe, J. M. Harris, and J. L. Provo. Phys. Rev. B **24**, 4903–4905 (1981).

[64] J. Eckert, J. A. Goldstone, D. Tonka, and D. Richter. Phys. Rev. B **27**, 1980–1990 (1983).

[65] B. Hauer, R. Hempelmann, T. J. Udovic, J. J. Rush, E. Jansen, W. Kockelmann, W. Schäfer, and D. Richter. Phys. Rev. B **57**, 11115–11123 (1998).

[66] H.-J. Tao, K.-M. Ho, and X.-Y. Zhu. Phys. Rev. B **34**, 8394–8400 (1986).

[67] J. Engelhard. J. Phys. F: Met. Phys. **9**, 2217–2229 (1979).

[68] P. Chen, Z. Xiong, J. Luo, J. Lin, and K. L. Tan. Nature **420**, 302–304 (2002).

[69] V. R. Juza and K. Opp. Z. Anorg. Allg. Chem. **266**, 325–330 (1951).

[70] K. Ohoyama, Y. Nakamori, S. Orimo, and K. Yamada. J. Phys. Soc. Japan **483**, 483–487 (2005).

[71] T. Noritake, H. Nozaki, M. Aoki, S. Towata, G. Kitahara, Y. Nakamori, and S. Orimo. J. Alloys Compounds **393**, 264–268 (2005).

[72] B. C. Garrett and D. G. Truhlar. J. Phys. Chem. **83**, 1079–1112 (1979).

[73] W. H. Miller. J. Chem. Phys. **61**, 1823–1834 (1974).

[74] E. Wigner. Z. Phys. Chem. B. **19**, 203–216 (1932).

[75] M. Born and K. Huang. *Dynamical Theory of Crystal Lattices*, pp. 406–407. Oxford University Press, Oxford (1954).

[76] J. Franck. Trans. Faraday Society **21**, 536–542 (1926).

[77] E. U. Condon. Phys. Rev. **28**, 1182–1201 (1926).

[78] E. U. Condon. Phys. Rev. **32**, 858–872 (1928).

[79] L. Rayleigh. *The Theory of Sound*, vol. 1, pp. 115–118. Macmillan, London, Second ed. (1894).

[80] E. Schrödinger. Ann. d. Physik **80**, 437–490 (1926).